

# **Assessing Structure and Function in Glaucoma**

Nicolaas J. Reus

ISBN-10: 909019908X

ISBN-13: 9789090199085

Assessing Structure and Function in Glaucoma

PhD thesis, Erasmus University Rotterdam, The Netherlands, 2005

Nicolaas J. Reus

Cover: 'The Glaucoma Puzzle' by N.J. Reus, 2005

© N.J. Reus, 2005. All rights reserved. No part of this book may be reproduced or transmitted in any form or by any means, without permission of the author.

Design, illustrations and layout by N.J. Reus

Printed by Febodruk b.v., Enschede

# **Assessing Structure and Function in Glaucoma**

Bepalen van structuur en functie in glaucoom

## **Proefschrift**

ter verkrijging van de graad van doctor aan de  
Erasmus Universiteit Rotterdam op gezag van de rector magnificus

**Prof.dr. S.W.J. Lamberts**

en volgens besluit van het College voor Promoties.

De openbare verdediging zal plaatsvinden  
op woensdag 16 november 2005 om 11:45 uur

door  
Nicolaas Johannes Reus  
geboren te Uithoorn.

## **Promotiecommissie**

Promotor: Prof.dr. G. van Rij

Overige leden: Prof.dr. C.J.J. Avezaat  
Prof.drs. C.C. Sterk  
Prof.dr. C.I. de Zeeuw

Copromotor: Dr. H.G. Lemij





## **Acknowledgment**

The studies presented in this thesis were supported by The Rotterdam Eye Hospital Research Foundation (Stichting Wetenschappelijk Onderzoek Het Oogziekenhuis [SWOO] Prof.dr. H.J. Flieringa, Rotterdam) and by Stichting Glaucoomfonds (Leiden).

Publication of this thesis was supported by The Rotterdam Eye Hospital Research Foundation (SWOO Prof.dr. H.J. Flieringa, Rotterdam), Carl Zeiss Meditec, Inc. (Dublin, CA, USA), Carl Zeiss Meditec AG (Jena, Germany), Carl Zeiss bv (Sliedrecht), Visio Landelijke Stichting Slechtzienden en Blinden (Huizen), Pfizer bv (Capelle aan den IJssel), Alcon Nederland bv (Gorinchem), Allergan bv (Nieuwegein), Landelijke stichting voor blinden en slechtzienden (Utrecht), Laservision Instruments bv (Rouveen), Medical Workshop bv (Groningen), Tramedico bv (Weesp), D.O.R.C. International bv (Zuidland), Merck Sharp & Dohme bv (Haarlem), Théa Pharma sa (Wetteren, België), Nico Reus Consultancy bv (Deventer).

## Contents

<b>Abbreviations</b>	<b>viii</b>
<b>1. Introduction</b>	<b>1</b>
<b>2. Developments in scanning laser polarimetry</b>	<b>23</b>
2.1 Visualization of localized retinal nerve fiber layer defects with the GDx with individualized and with fixed compensation of anterior segment birefringence <i>NJ Reus, TP Colen, and HG Lemij. Ophthalmology 2003;110:39-43</i>	25
2.2 Effects of inadequate anterior segment compensation on measurements with scanning laser polarimetry <i>NJ Reus, LME van Koolwijk, and HG Lemij. Ophthalmic Surgery, Lasers &amp; Imaging. In press.</i>	35
2.3 Enhanced imaging algorithm for scanning laser polarimetry with variable corneal compensation <i>NJ Reus, Q Zhou, and HG Lemij. Invest Ophthalmol Vis Sci. Submitted.</i>	41
<b>3. Diagnostic accuracies for glaucoma</b>	<b>59</b>
3.1 Diagnostic accuracy of the GDx VCC for glaucoma <i>NJ Reus and HG Lemij. Ophthalmology 2004;110:1860-1865</i>	61
3.2 Accuracy of GDx VCC, HRT I, and clinical assessment of stereoscopic optic nerve head photographs for diagnosing glaucoma <i>NJ Reus and HG Lemij. Am J Ophthalmol. Submitted.</i>	75
<b>4. The relationship between function and structure</b>	<b>89</b>
4.1 The relationship between standard automated perimetry and GDx VCC measurements <i>NJ Reus and HG Lemij. Invest Ophthalmol Vis Sci 2004;45:840-845</i>	91
4.2 Relationships between standard automated perimetry, HRT confocal scanning laser ophthalmoscopy, and GDx VCC scanning laser polarimetry <i>NJ Reus and HG Lemij. Invest Ophthalmol Vis Sci. In press.</i>	105
<b>5. Scanning laser polarimetry of the retinal nerve fiber layer in perimetrically unaffected eyes of glaucoma patients</b>	<b>125</b>
<i>NJ Reus and HG Lemij. Ophthalmology 2004;111:2199-2203</i>	
<b>6. The prevalence of glaucomatous defects with short-wavelength automated perimetry in patients with elevated intraocular pressures</b>	<b>139</b>
<i>NJ Reus, TP Colen, and HG Lemij. J Glaucoma 2005;14:26-29</i>	
<b>7. General discussion</b>	<b>149</b>
<b>8. Summary / Samenvatting</b>	<b>165</b>
8.1 Summary	167
8.2 Samenvatting	171
<b>Dankwoord</b>	<b>177</b>
<b>Curriculum Vitae</b>	<b>181</b>

## Abbreviations

AUC	area under the ROC curve
BCVA	best-corrected visual acuity
CA	California
CI	confidence interval
CPA	corneal polarization axis
CPM	corneal polarization magnitude
CPSD	corrected pattern standard deviation
CSLO	confocal scanning laser ophthalmoscopy
dB	decibel
DLS	differential light sensitivity
ECC	enhanced variable corneal compensation
F(C)C	fixed (corneal) compensation
FDT	frequency-doubling technology perimetry
FT	full threshold
GHT	glaucoma hemifield test
HFA	Humphrey Field Analyzer
HRP	high-pass resolution perimetry
HRT	Heidelberg Retina Tomograph
IC	individualized compensation
IL	Illinois
IN	inferonasal
IOP	intraocular pressure
ISNT	inferior-superior-nasal-temporal
IT	inferotemporal
$k$	kappa
LDF	linear discriminant function
LR	likelihood ratio
LWS	long-wavelength sensitive
MD	mean deviation
MRA	Moorfields Regression Analysis
MWS	medium-wavelength sensitive
N	nasal
NA	not applicable
ND	nasally downward
NFA	Nerve Fiber Analyzer

NFI	Nerve Fiber Indicator
OCT	optical coherence tomography
OD	oculo dextra
OH	ocular hypertension
ONH	optic nerve head
OS	oculo sinistra
<i>P</i>	<i>P</i> value
PI	prediction interval
POAG	primary open-angle glaucoma
PSD	pattern standard deviation
PS-OCT	polarization-sensitive OCT
$R^2$	Coefficient of determination
$r_s$	Spearman's rank correlation coefficient
RGC	retinal ganglion cell
RNFL	retinal nerve fiber layer
RZVL	retinale zenuwvezellaag
ROC	receiver operating characteristic
SAP	standard automated perimetry
SD	standard deviation
SE	standard error
SITA	Swedish interactive threshold algorithm
SLP	scanning laser polarimetry
SN	superonasal
ST	superotemporal
SWAP	short-wavelength automated perimetry
SWS	short-wavelength sensitive
T	temporal
USA	United States of America
VCC	variable corneal compensation
WA	Washington



# 1

## **An introduction to glaucoma and its detection**





**G**laucoma is a heterogeneous group of optic nerve diseases that share an accelerated degeneration of retinal ganglion cells (RGCs), resulting in a distinct appearance of the optic nerve head (ONH; Fig 1.1) and a matching pattern of visual field loss (Fig. 1.2).<sup>1-3</sup> Traditionally, the various types of glaucoma are classified into primary and secondary. Whereas primary glaucomas have no etiological basis in other ocular or systemic disorders, secondary forms may be caused by ophthalmological or extraocular disease(s), drugs, and treatments.<sup>4</sup> Glaucoma is further classified based on the anatomy of the anterior chamber angle, i.e., open versus closed.<sup>4</sup> Subsequent classification is based on the onset of the disease, i.e., developmental versus late-onset.<sup>4</sup>

### **Blindness**

If untreated, all glaucomas lead to progressive loss of visual function. In 2002, glaucoma was the second leading cause of blindness worldwide (blindness defined as a visual acuity of less than 3/60 or a corresponding visual field loss to less than 10° in the better eye with best possible correction): an estimated 12.3% (corresponding to approximately 4.6 million people) of all blindness is due to glaucoma.<sup>5</sup> The leading causes of blindness in underdeveloped and in developed countries were cataract and age-related macular degeneration, respectively.<sup>5</sup>

### **Primary open-angle glaucoma**

Of the many types of glaucoma, primary open-angle glaucoma (POAG) is probably the most common type of glaucoma in Western countries.<sup>6-8</sup> The disease typically has its onset in adults. Typical signs are an open anterior chamber angle of normal appearance and a characteristic atrophy of the optic nerve that cannot be attributed to any other cause. Traditionally, an elevated level of intraocular pressure (IOP) is associated with POAG. An elevated IOP is defined as an IOP higher than the upper 97.5% probability level in healthy subjects, i.e., 21 mmHg.<sup>9</sup> However, up to 50% of patients with POAG have been estimated to have an IOP within normal limits.<sup>10,11</sup> Therefore, POAG is often, arbitrarily, subdivided in high pressure and normal pressure (i.e., normal tension) glaucoma.

The prevalence of POAG in Western Europe is approximately 1.6% (0.8%-2.1%).<sup>7,11,12</sup> This would suggest that there are more than 260,000 people with POAG in The Netherlands. In developed countries, probably less than half of all people who have the disease are aware of it.<sup>13,14</sup> Most patients with POAG have no or only few symptoms until the later stages of the disease, when they may lose their central vision.<sup>15</sup> Any loss of vision by glaucoma is irreversible.

### **Risk factors**

Several risk factors have been found to be associated with the development and progression of POAG. Probably the most important one is the level of IOP: the relative risk of POAG rises with

increasing levels of IOP.<sup>10</sup> Subjects with an elevated IOP but without signs of glaucomatous damage are referred to as having ocular hypertension (OH).<sup>4</sup> Other risk factors include increasing age, a family history of glaucoma, African descent, high myopia, a thinner cornea, and a horizontal or vertical cup-to-disc ratio of  $\geq 0.4$ .<sup>3,15</sup> Furthermore, fellow eyes of patients with glaucoma with unilateral field loss have an increased risk of developing glaucomatous damage.<sup>16-18</sup> Systemic hypertension, cardiovascular disease, diabetes mellitus, migraine headache, and peripheral vasospasm have been suggested as risk factors as well, but so far, the evidence is inconclusive.<sup>3,15</sup>

### **Pathophysiology**

The pathophysiology of the neurodegeneration in POAG is not fully understood.<sup>3</sup> Of the various theories that have been proposed, two distinct ones are based on an elevated IOP and a reduction in ocular blood supply, respectively.<sup>19</sup> Although no obstruction of the trabecular meshwork can be seen by gonioscopy in patients with POAG, the resistance to aqueous outflow is increased, often associated with a high IOP.<sup>3</sup> When IOP increases above physiological levels, the lamina cribrosa, a series of perforated connective tissue sheets through which the optic nerve fibers traverse to form the optic nerve, deforms which may mechanically damage the traversing optic nerve fibers.<sup>3</sup> In addition, an increased IOP may lead to a blockade of axonal protein transport in the optic nerve axons at the level of the lamina cribrosa.<sup>3</sup> Independently or in addition to IOP, a reduced retinal blood supply may lead to local ischemia and/or hypoxia and subsequent death of RGCs and optic nerve fibers in glaucoma.<sup>3</sup>

Other proposed factors that may contribute include poorly functioning cellular pumps and glutamate transporters, oxidative stress, inflammatory cytokines (e.g., nitric oxide), an aberrant immunity, and apoptosis of RGCs secondary to initial optic nerve injury.<sup>3,19</sup>

### **Treatment of glaucoma**

As stated by the European Glaucoma Society, the goal of glaucoma treatment is 'to preserve visual function adequate to the individual needs with minimal or no side effects, for the expected lifetime of the patient, without any disruption of his/her normal activities, at a sustainable cost'.<sup>4</sup> At the moment, lowering of the IOP, either with medication or surgical intervention, is the only factor that has been shown to slow down the development and progression of glaucoma.<sup>20,21</sup> It is, however, unclear which patients to treat and how vigorously and when to initiate treatment in patients with ocular hypertension.<sup>22</sup> To this end, a risk assessment of all patients to determine how prone they are to becoming blind may be useful.<sup>23</sup> In addition, more sensitive and precise assessment of early, i.e. little, axonal loss may be advantageous.

### **Clinical detection of glaucoma**

In clinical practice, both structural losses (i.e., atrophy of RGCs and their axons) and functional

losses (i.e., impairment of the visual field) are evaluated in the diagnosis of glaucoma. Traditionally, structural losses are evaluated by assessing the appearance of the ONH and the retinal nerve fiber layer (RNFL); functional losses are usually assessed with standard automated perimetry (SAP).

### The optic nerve head

The ONH (also referred to as optic disc) is usually examined with a magnified stereoscopic view at the slit lamp biomicroscope with an indirect or a contact lens in a dilated pupil.<sup>3,15</sup> In healthy eyes, the neuroretinal rim is thickest in the inferior region, followed by the superior, nasal, and temporal regions. The rim is therefore said to follow the ISNT-rule (e.g., Fig. 1.1, *left*).<sup>24</sup> Characteristic glaucomatous ONH changes are increased cupping or excavation, notching, or thinning of the neuroretinal rim, disc hemorrhages, asymmetry of the amount of optic-nerve cupping between the two eyes of the patient, and barring of circumlinear vessels.<sup>3,4,15</sup>

In contrast to other optic neuropathies, glaucoma leads to thinning of the ONH's neuroretinal rim without marked loss of the color of the rim. Other optic neuropathies usually result in pallor of the ONH but, for unknown reasons, rarely show enlargement of the optic disc cup.<sup>3</sup> Discriminating between healthy and glaucomatous ONHs has been shown to be difficult for clinicians, as even glaucoma experts do not classify all optic discs correctly.<sup>25-29</sup> Nonetheless, the subjective assessment of the ONH's appearance remains a cornerstone for diagnosing glaucoma in clinical practice.

### The retinal nerve fiber layer

The RNFL may be observed with red-free (green) light through a well-dilated pupil. The green light is reflected in the superficial parts of the retina, thereby only outlining the nerve fibers. In healthy eyes, the retinal nerve fibers are detectable as bright and fine striations in the inner retinal layer fanning off the optic disc to the retinal periphery (Fig. 1.3, *left*).<sup>24</sup> These fine striations represent tissue canals, in which processes of the Müller cells keep the axons together.<sup>24</sup> In normal eyes, the nerve fiber bundles are most visible inferotemporally to the ONH, followed by the temporal superior area, the nasal superior region, and finally inferionasally. It is least visible in the superior, inferior, temporal horizontal, and nasal horizontal regions.<sup>30</sup>

In glaucoma, RNFL loss may be diffuse, local, or both.<sup>31-33</sup> Localized defects are visible as wedge-shaped, well-demarcated defects of the RNFL that run toward or touch the optic disc border (Fig. 1.3, *right*).<sup>34</sup> Diffuse loss of retinal nerve fibers leads to a decreased visibility of the RNFL. With ophthalmoscopy, localized RNFL defects are therefore easier to detect than diffuse loss.

Red-free fundus photography allows a better view of RNFL appearance than does clinical ophthalmoscopy. However, it is infrequently used in clinical practice because high quality photographs are difficult to obtain in eyes with opaque media, a yellow lens, and a low degree of

pigmentation of the retinal pigment epithelium, which are all quite common in a Caucasian glaucoma population.<sup>24</sup> In addition, even interpretation of nerve fiber loss in photographs is difficult, although some attempts have been made to quantify the analysis.<sup>35,36</sup>

### **The visual field**

Both in clinical practice and in clinical trials visual field testing (also referred to as perimetry) is often performed with the Humphrey Field Analyzer (HFA; Carl Zeiss Meditec, Inc., Dublin, CA, USA). With this instrument, visual function is usually assessed by determining the retinal differential light sensitivity (DLS) to white light at various locations in the central retina within 30° of fixation. In the commonly used 24-2 test paradigm, DLS is assessed in 54 locations, which are compared with age-corrected normative data.

In glaucoma, visual field abnormalities typically follow a nerve-fiber bundle pattern (e.g., Fig. 1.2, *right*).<sup>37</sup> Common glaucomatous visual field defects are paracentral scotomas, arcuate (Bjerrum) scotomas, nasal steps, altitudinal defects, and temporal wedges.<sup>37,38</sup> Glaucoma may also produce a more generalized decrease in sensitivity. However, purely generalized functional loss is rare in glaucoma and more frequently caused by media opacities and miosis.<sup>37</sup> In far advanced glaucoma, only a central island of vision may be apparent.<sup>38</sup>

There are, however, no generally approved and used criteria for glaucomatous visual field defects.<sup>39</sup> In addition, perimetry is highly dependent on a patient's response, which varies both during and between tests,<sup>40-42</sup> limiting the reproducibility of measurements with standard automated perimetry (SAP). In one study, 85.9% of abnormal visual fields were not confirmed upon retesting.<sup>42</sup> Furthermore, various studies have suggested that structural losses may precede functional losses assessed with SAP.<sup>32,33,43,44</sup>

### **New techniques for glaucoma detection**

In summary, a clinical diagnosis of glaucoma integrates all the available information about the patient, including assessment of the ONH, RNFL, visual field, and anterior chamber angle as well as the various risk factors.<sup>45</sup> There is, however, no consistent and generally approved acceptance of the diagnostic criteria.<sup>39,46</sup> In addition, the techniques that are being used in clinical practice are subjective (e.g., ONH and RNFL assessment), have a poor reproducibility of measurements (e.g., SAP), and may not detect glaucoma at an early stage (e.g., SAP).

Various techniques have been developed to better detect glaucomatous optic neuropathy. For example, scanning laser polarimetry (SLP), optical coherence tomography (OCT), and confocal scanning laser ophthalmoscopy (CSLO) have been developed to allow a more objective, repro-

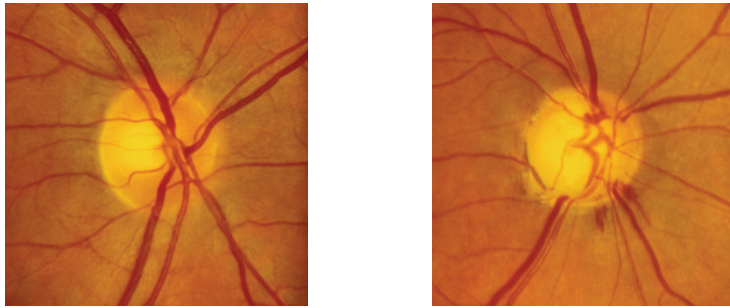


Figure 1.1. A healthy (*left*) and a glaucomatous (*right*) optic nerve head.

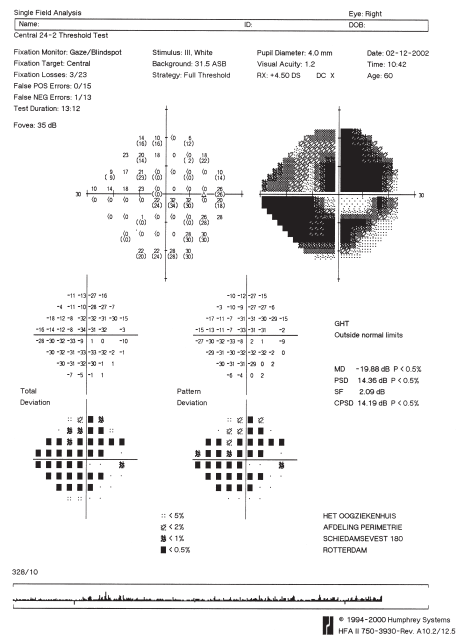
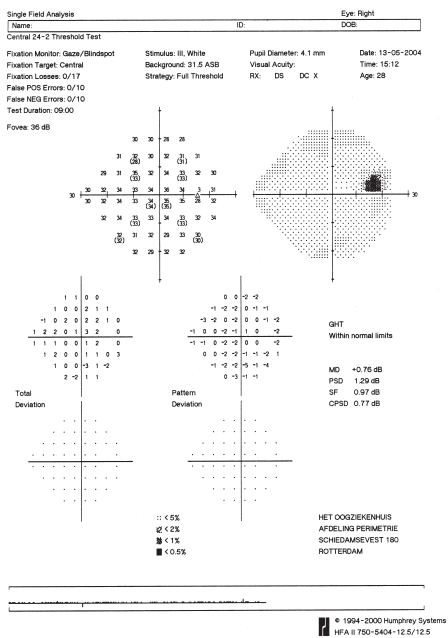


Figure 1.2. A healthy (*left*) and a glaucomatous (*right*) visual field.

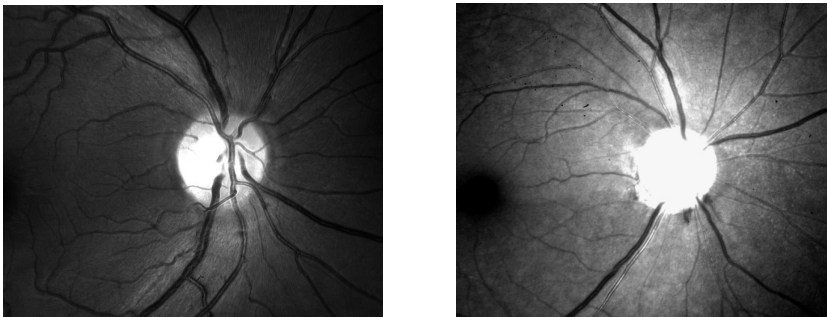


Figure 1.3. Red-free photographs of a healthy (*left*) and a glaucomatous (*right*) retinal nerve fiber layer.

ducible, and quantitative assessment of structural losses of the RNFL (SLP and OCT) and ONH (CSLO and OCT).<sup>47</sup> Similarly, various psychophysical tests, such as short-wavelength automated perimetry (SWAP), frequency-doubling technology perimetry (FDT), and high-pass resolution perimetry (HRP), have been developed to allow earlier detection of glaucomatous functional losses than with SAP.<sup>48</sup> Of these techniques, SLP, CSLO, and SWAP have been studied in this thesis and, therefore, will be discussed hereafter.

### Scanning laser polarimetry

SLP is a technique that allows evaluation of the RNFL.<sup>49-51</sup> SLP is based on the presumed form birefringence of the microtubules.<sup>52</sup> Microtubules are cylindrical structures with a diameter of 25 nm that support the axons in the RNFL.<sup>53</sup> Because SLP uses a near-infrared laser with a wavelength (approximately 785 nm) that is significantly larger than that of the diameter of the microtubules, the RNFL exhibits form birefringence.<sup>54</sup> Birefringence can be described in terms of polarization axis and polarization magnitude (i.e., amount of retardation). The parallel arrangement of microtubules results in a net change in the retardation of passing polarized light (Fig. 1.4). In SLP, the back of the eye is scanned with a polarized laser beam and the retardation of the backscattered light that has double passed the RNFL is determined.

The amount of retardation exhibited by the RNFL is proportional to its thickness:<sup>55</sup> the greater the number of microtubules, the greater the retardation of the polarized laser light, indicating the presence of more tissue. SLP thus gives an indirect assessment of the thickness of the layer. The amount of retardation is often expressed in micrometers of thickness, based on a conversion factor of 0.67 nm/ $\mu\text{m}$ .<sup>56</sup>

The first commercial SLP instrument was known as the Nerve Fiber Analyzer (NFA) and became available in 1993. Extensive hard- and software changes resulted in the NFA II. The third generation was marketed as the GDx NFA, which included a normative database and a neural network algorithm (i.e., The Number). This parameter discriminated fairly well between healthy and glaucomatous eyes with a sensitivity and specificity of 76.8% and 89.1%, respectively.<sup>57</sup> Of note, the term GDx is used by American ophthalmologists to denote the diagnosis (Dx) of glaucoma (G).

Two structures in the anterior segment, i.e. the cornea and, to a lesser extent, the lens, are also birefringent.<sup>58-60</sup> In order to assess retardation exhibited by the RNFL, anterior segment retardation needs to be neutralized.<sup>61,62</sup> The NFA I, NFA II, and the GDx NFA were equipped with a fixed corneal compensator (FCC) that cancelled a fixed amount of birefringence reflecting the median values in the general population.<sup>61</sup> However, in 2000 and 2002, Greenfield et al<sup>61</sup> and Knighton and Huang,<sup>63</sup> respectively, reported that anterior segment birefringence varied considerably between subjects. Fixed compensation of anterior segment birefringence was suggested to

be inadequate in many subjects, leading to erroneous RNFL measurements and an increase in variability in assessment of the RNFL between eyes.<sup>61,64</sup> The ability of various GDx NFA parameters to discriminate between healthy and glaucomatous eyes increased when they were corrected mathematically for uncompensated corneal birefringence.<sup>65,66</sup> A similar approach was taken by Tjon-Fo-Sang and Lemij<sup>67</sup> who mathematically corrected for an observed offset, of which the origin was unknown at the time.

In 2002, Zhou and Weinreb<sup>68</sup> reported results obtained with a modified GDx that used variable corneal compensation (VCC). In this prototype instrument, both the axis and magnitude of anterior segment birefringence that had to be compensated could be adjusted manually.<sup>68</sup>

The birefringence of the anterior segment was assessed in each individual eye by acquiring an image of the macular region with the retardation of the compensator set to zero. The combination of the birefringence of the radially oriented axons of the photoreceptors that constitute Henle's fiber layer in the macula and the birefringence of the anterior segment resulted in a bow-tie like retardation pattern in the macula (Fig 1.5, *middle*).<sup>68</sup> The anterior segment birefringence was assessed by determining the orientation of the retardation maxima in the macula, which correspond with the slow axis of the anterior segment.<sup>68</sup> The birefringence magnitude was determined by the average of the retardation profile if the retardation of the anterior segment was higher than that of Henle's fiber layer and by half of the modulation of the retardation profile if the retardation of the anterior segment was lower than that of Henle's fiber layer.<sup>68</sup>

RNFL measurements obtained with SLP-VCC in monkey eyes with and without glaucoma, reflected the expected appearance of the RNFL observed with stereoscopic optic disc photographs.<sup>69</sup> Moreover, SLP-VCC measurements were shown to have an improved ability to discriminate between healthy and glaucomatous eyes over measurements with SLP-FCC.<sup>70,71</sup>

At the end of 2002, automated VCC was incorporated into an SLP instrument called the GDx VCC (Laser Diagnostic Technologies, Inc., Dublin, CA, USA; now, Carl Zeiss Meditec, Inc., Dublin, CA, USA) (Fig. 1.6). This instrument is a user-friendly and compact device. The measured subject rests his head in a facemask and looks at an internal fixation light. Pupils preferably are not dilated and the room lights are left on. A laser scans the fundus at a 40° x 20° scanning angle. Two imaging trials per eye are run successively, the first to determine anterior segment birefringence, the second to image the area of interest with adjusted compensation. Image acquisition takes approximately 0.7 seconds per trial. Because of the laser wavelength (785 nm), mild to moderate cataract does not degrade the images. The printout of the images includes a 20° x 20° reflectance image of the disc and peripapillary area, a color coded retardation map, a probability map (in which areas of retardation are compared to those of a normative database and abnormally low retardation areas are color flagged at various probability levels), and several



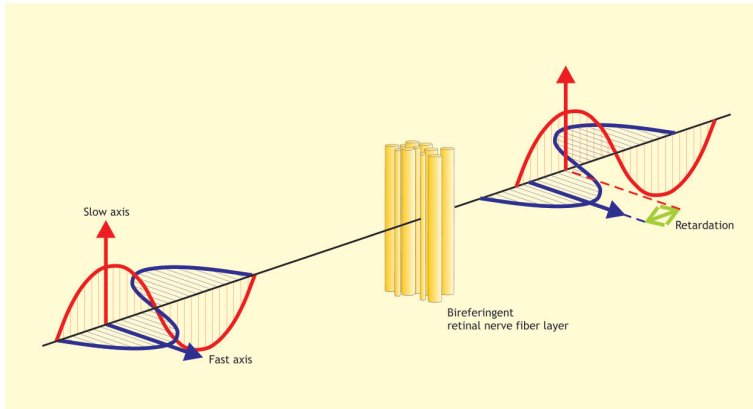


**Figure 1.4.** Cartoon of the working principle of SLP.

graphs and parameters (Fig. 1.7). In the retardation map, measurements are color coded: bright, warm colors represent thicker areas; dark, cool colors represent thinner areas.<sup>72</sup>

Typically, in healthy eyes, larger amounts of retardation are apparent next to the blood vessels superior and inferior to the ONH (Fig. 1.7, *left*). The amount of retardation decreases with increasing distance from the ONH. In glaucomatous eyes, the loss of nerve fibers is visible as a localized and/or diffuse decrease in the amount of retardation, which is apparent as a loss of bright, warm colors (Fig. 1.7, *right*).

The GDx VCC features several parameters, one of which, the Nerve Fiber Indicator (NFI), has been trained specifically to discriminate between healthy and glaucomatous eyes. The NFI provides a single number (range, 1-100) representing the overall integrity of the RNFL.<sup>73</sup> The score is the output of a machine learning classifier based on a linear support vector machine. The higher the score, the more likely the RNFL measurement represents a glaucomatous eye. The NFI has been trained on a large group of 540 healthy subjects and 271 glaucoma patients with varying degrees of disease severity.<sup>73</sup>

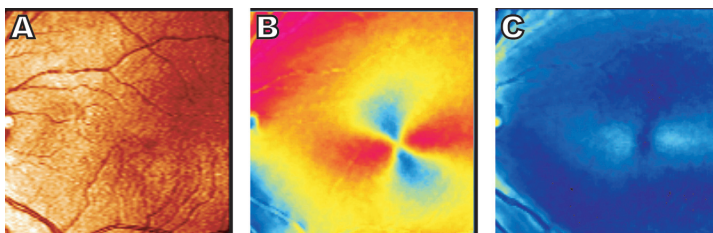


**Figure 1.5.** Macular images of a healthy subject's eye. (A): Reflection image. (B): Retardation image without any compensation of anterior segment birefringence (50 nm and 19.6° nasally downward [ND]). (C): Retardation image compensated with VCC (13 nm and -78.3° ND).





Figure 1.6. The GDx VCC.

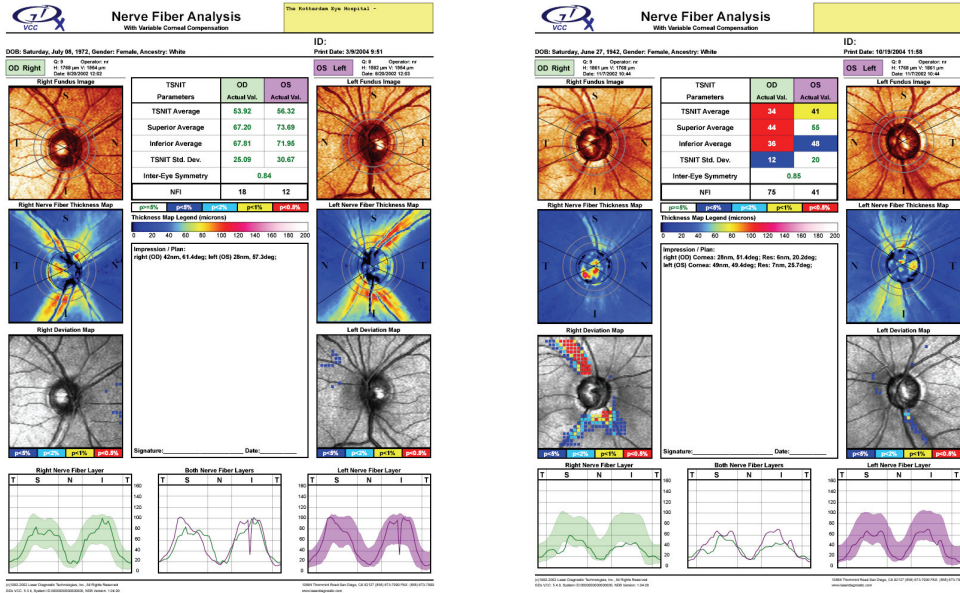


Figure 1.7. GDx VCC printout of a healthy (left) and a glaucoma (right) subject.

### Confocal scanning laser ophthalmoscopy

CSLO allows clinical assessment of ONH topography.<sup>74</sup> This technique is commercially available in the Heidelberg Retina Tomograph (HRT; Heidelberg Engineering GmbH, Dossenheim, Germany) (Fig. 1.8). CSLO uses a laser diode with a wavelength of 670 nm to scan the papillary region. CSLO is based on the reflectivity of the retinal surface. To estimate the position of the retinal surface, CSLO measures the intensity of light reflected off the retinal surface at subsequent depths of focus.<sup>74</sup> The confocality of the imaging system ensures that reflected light is detected only if it originates from a very small region around the focal plane.<sup>74</sup> The weighted peak reflectance is thought to represent the interface between the retinal surface and the vitreous. The measured depths of peak reflectance at various points in the optic disc are used to construct a topography map of the optic disc (e.g., see Fig. 1.9).

The measured subject rests his head on a head-and-chin rest and looks at a distant fixation target. Pupils are preferably not dilated and the room lights are left on. Image acquisition takes approxi-

mately 1.6 seconds per trial.<sup>75</sup> Because the wavelength of the HRT (670 nm) is shorter than that of the GDx NFA and GDx VCC (785 nm), image quality is more negatively affected by mild to moderate cataract. In general, three topography images are averaged on which analyses are performed. Magnification error is automatically corrected by using a patient's keratometry readings and the power of the correction lens used to acquire the images. The margin of the ONH is defined by manually drawing a contour line around the inner margin of the peripapillary scleral (Elschnig's) ring. A (standard) reference plane is determined at 50  $\mu\text{m}$  posterior to the mean peripapillary retinal height along the contour line at the temporal sector between 350 and 356 degrees. Structures within the outlined ONH above this reference plane are defined as neuroretinal rim, structures below this plane are deemed to be cup.

The first commercially available CSLO instrument was the HRT I (Fig. 1.8). Recently, various hardware changes have led to the development of the HRT II. Differences between these techniques (HRT I vs. II, respectively) are resolution of the image (256 x 256 pixels vs. 348 x 348 pixels), scanning angle (10°, 15°, or 20° vs. 15°), and scanning range along the z-axis (0.5 to 4.0 mm in 32 steps vs. 1.0 to 4.0 mm with 16 steps per mm). Whereas the HRT II has been marketed as a clinical routine instrument, the HRT I is more research oriented.

Measurements of the HRT are presented on a printout (Fig. 1.9). The printout includes a reflectance image of the disc and peripapillary area, a color-coded topography map, graphs of retinal surface height and various parameters (Fig. 1.9). In the lower right panel, a statistical analysis called the Moorfields Regression Analysis (MRA)<sup>76</sup> is displayed.

In the MRA, a subject's neuroretinal rim area, corrected for ONH size and age, is compared with data from 112 normal eyes of white subjects.<sup>76</sup> The measured rim area is classified as 1) normal (flagged with a green check mark) if it sits within the 95% prediction interval (PI), 2) borderline (yellow exclamation mark) if it sits between the 95% and 99% PI, and 3) outside normal limits (red cross) if the measurement sits below the 99% PI. The measured rim area is compared to normative data for 6 sectors and for the global rim. A final classification based on all 6 sectors and the global rim is printed in the lower left corner. A normal classification requires the MRA of all sectors and the global rim to be within normal limits, a borderline classification occurs when one or more of the sectors or the global rim is borderline, and an outside normal limits occurs when at least 1 sector or the global rim is outside normal limits.

In addition to the MRA, various other statistical analyses (e.g., linear discriminant functions [LDFs] by Bathija and by Mikelberg)<sup>77,78</sup> have been developed to discriminate between healthy and glaucomatous eyes.

The HRT has been shown to provide reasonably reproducible measurements of ONH topography.<sup>47</sup> Furthermore, the ability to discriminate between healthy and glaucomatous eyes has been shown to be fairly good with sensitivities and specificities ranging between 74% and 78% and between 81% and 94%, respectively.<sup>79</sup>

### **Short-wavelength automated perimetry**

In general, there are at least three subtypes of RGCs in the human retina: the magnocellular cells, the parvocellular cells, and the small bistratified cells.<sup>48</sup> SAP is non-specific in that it assesses the function of all retinal RGC subtypes at the same time. In humans, various visual function specific perimetry tests have been developed to target primarily one of the three mentioned RGC subtypes. Presumably, FDT assesses the magnocellular pathway and HRP assesses the parvocellular pathway.<sup>48</sup> SWAP allows preferential assessment of the function of the small bistratified (or blue-yellow) cells.<sup>48</sup>

The small bistratified ganglion cells are part of the short-wavelength sensitive (SWS) pathway, which consists of the s-cones, the s-cone bipolar cells, the small bistratified ganglion cells, and the downstream cortical processing.<sup>80</sup> In SWAP, a blue stimulus with a peak wavelength that approximates that of the peak response of the s-cones (440 nm) is presented on a high luminance yellow background (wavelength >530 nm).<sup>80</sup> The high luminance background helps to saturate the medium-wavelength, or green, sensitive cones (m-cones) and the long-wavelength, or red, sensitive cones (l-cones) and to suppress simultaneously rod activity while leaving the s-cones largely unaffected.<sup>81</sup> As a result, a degree of 'pure' SWS pathway response can be isolated which is not mediated by either the medium-wavelength sensitive (MWS) or long-wavelength sensitive (LWS) pathways.<sup>81</sup>

SWAP has been developed to allow earlier detection of glaucomatous functional loss than with SAP.<sup>80</sup> It is still not known why the SWS pathway may allow earlier detection of glaucomatous functional damage.<sup>82</sup> One theory, called the reduced redundancy theory,<sup>83</sup> that has been proposed is based on the assumption that sparsely represented ganglion cell subpopulations, with lower degrees of overlap between adjacent receptive fields than more abundant sub-populations, may demonstrate identifiable functional deficits earlier in the disease process.<sup>84</sup> This is because only a small number of cells must be lost prior to loss of adequate retinal receptive field coverage. Various studies have reported that SWAP may indeed show glaucomatous loss of visual function several years earlier than SAP.<sup>85-87</sup> However, these studies used their own normative database. In addition, they used different classifications for an abnormal visual field. Furthermore, the short- and long-term variability of measurements appear to be greater for SWAP than for SAP.<sup>82</sup> In addition, these studies have not addressed the specificity or the predictive value of abnormal SWAP

fields. Another factor that might limit the routine use of SWAP in clinical practice is that SWAP is more sensitive to mild and moderate cataract as yellowing of the lens and increased light scatter decrease the sensitivity of the eye to the blue stimulus.<sup>82</sup>



Figure 1.8. The Heidelberg Retina Tomograph I.

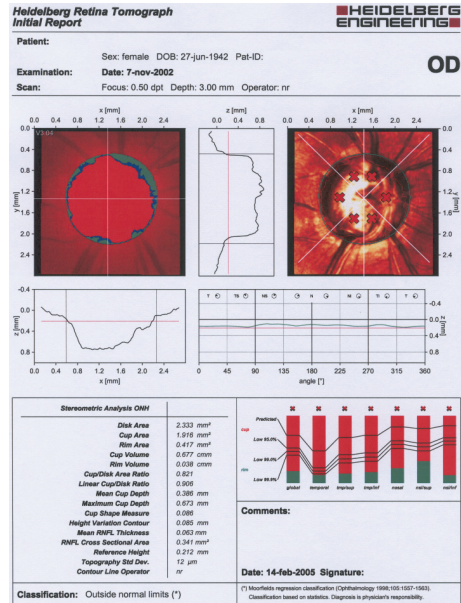
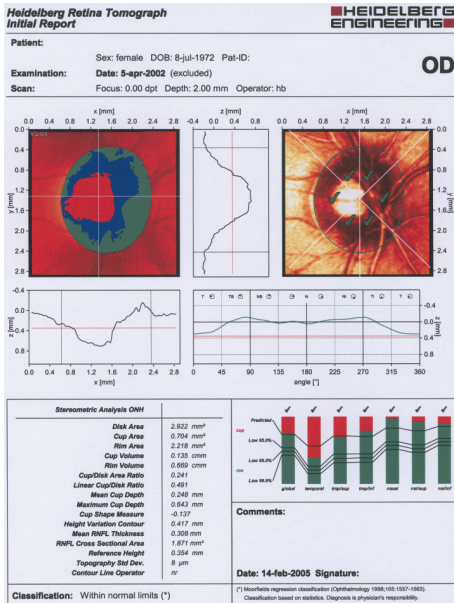


Figure 1.9. HRT printout of a healthy (left) and a glaucomatous (right) eye.

## Outline of this thesis

The objective of the research presented in this thesis was to evaluate various techniques that may be used in clinical practice for assessing function and structure in glaucoma.

In **chapter 2**, new developments in SLP were investigated. More specifically, in **chapter 2.1**, the ability of SLP with VCC to assess the morphology of the RNFL was evaluated and compared to that of SLP with FCC. To this end, the visualization of localized RNFL defects in SLP images with FCC and with VCC was compared with their visualization in red-free fundus photographs. At the time of the paper's publication, fixed and variable corneal compensation were referred to as fixed compensation (FC) and individualized compensation (IC), respectively. In **chapter 2.2**, the extent to which various amounts of incomplete anterior segment birefringence could distort RNFL measurements by SLP was evaluated. In **chapter 2.3**, a new method for compensating anterior segment birefringence, i.e., enhanced (variable) corneal compensation (ECC or  $v$ VCC), was described and evaluated.

In **chapter 3**, the accuracy of various techniques for detecting glaucoma was determined. In **chapter 3.1**, the diagnostic accuracy of the latest commercial SLP device, i.e., the GDx VCC, was investigated. Subsequently, in **chapter 3.2**, the diagnostic accuracy of CSLO by means of the HRT I and clinical assessment of stereoscopic ONH photographs was compared with that of the GDx VCC in a single population.

In **chapter 4**, the relationship between function and structure was evaluated. In **chapter 4.1**, the relationship between SAP and SLP-VCC by means of the GDx VCC was investigated. In **chapter 4.2**, the relationship between SAP and CSLO by means of the HRT I was evaluated and compared with the relationship between SAP and SLP-VCC in a single population.

Because glaucoma is often asymmetric in patients, some patients only have detectable visual field loss in one eye. The fellow eye then is unaffected when tested with standard automated perimetry. However, these so-called perimetrically unaffected eyes of glaucoma patients are at high risk of losing their visual function.<sup>16-18</sup> In **chapter 5**, we evaluated the RNFL with SLP-VCC in perimetrically unaffected fellow eyes of glaucoma patients. In addition, we compared the results to RNFL measurements in their fellow eyes with field loss and eyes of healthy subjects.

In **chapter 6**, the prevalence of glaucomatous defects with SWAP in subjects with an elevated intraocular pressure was determined for various published definitions of glaucomatous loss. Finally, **chapter 7** presents a general discussion of the research on the assessment of structure and function in glaucoma.

## References

1. Quigley HA. Neuronal death in glaucoma. *Prog Retin Eye Res* 1999;18:39-57.
2. American Academy of Ophthalmology. Preferred practice pattern. Primary open angle glaucoma. San Francisco, CA: American Academy of Ophthalmology, 2000.
3. Weinreb RN, Khaw PT. Primary open-angle glaucoma. *Lancet* 2004;363:1711-20.
4. European Glaucoma Society. Terminology and Guidelines for Glaucoma, 2nd ed. Savona, Italy: Dogma S.r.l., 2003.
5. Resnikoff S, Pascolini D, Etya'ale D, et al. Global data on visual impairment in the year 2002. *Bull World Health Organ* 2004;82:844-51.
6. Rahmani B, Tielsch JM, Katz J, et al. The cause-specific prevalence of visual impairment in an urban population. The Baltimore Eye Survey. *Ophthalmology* 1996;103:1721-6.
7. Coffey M, Reidy A, Wormald R, et al. Prevalence of glaucoma in the west of Ireland. *Br J Ophthalmol* 1993;77:17-21.
8. Quigley HA, Vitale S. Models of open-angle glaucoma prevalence and incidence in the United States. *Invest Ophthalmol Vis Sci* 1997;38:83-91.
9. Leydhecker W, Akiyama K, Neumann HG. Der intraokulare Druck gesunder menschlicher Augen. *Klin Monatsbl Augenheilkd* 1958;133:662-70.
10. Sommer A, Tielsch JM, Katz J, et al. Relationship between intraocular pressure and primary open angle glaucoma among white and black Americans. The Baltimore Eye Survey. *Arch Ophthalmol* 1991;109:1090-5.
11. Wolfs RC, Borger PH, Ramrattan RS, et al. Changing views on open-angle glaucoma: definitions and prevalences--The Rotterdam Study. *Invest Ophthalmol Vis Sci* 2000;41:3309-21.
12. Anton A, Andrada MT, Mujica V, et al. Prevalence of primary open-angle glaucoma in a Spanish population: the Segovia study. *J Glaucoma* 2004;13:371-6.
13. Quigley HA. Number of people with glaucoma worldwide. *Br J Ophthalmol* 1996;80:389-93.
14. Wong EY, Keeffe JE, Rait JL, et al. Detection of undiagnosed glaucoma by eye health professionals. *Ophthalmology* 2004;111:1508-14.
15. Coleman AL. Glaucoma. *Lancet* 1999;354:1803-10.
16. Chen PB, Park RJ. Visual field progression in patients with initially unilateral visual field loss from chronic open-angle glaucoma. *Ophthalmology* 2000;107:1688-92.
17. Susanna R, Drance SM, Douglas GR. The visual prognosis of the fellow eye in unocular chronic open-angle glaucoma. *Br J Ophthalmol* 1978;62:327-9.
18. Fontana L, Armas R, Garway-Heath DF, et al. Clinical factors influencing the visual prognosis of the fellow eyes of normal tension glaucoma patients with unilateral field loss. *Br J Ophthalmol* 1999;83:1002-5.
19. Dreyer EB, Lipton SA. New perspectives on glaucoma. *JAMA* 1999;281:306-8.
20. Kass MA, Heuer DK, Higginbotham EJ, et al. The Ocular Hypertension Treatment Study: a rand-



- omized trial determines that topical ocular hypotensive medication delays or prevents the onset of primary open-angle glaucoma. *Arch Ophthalmol* 2002;120:701-13.
21. Heijl A, Leske MC, Bengtsson B, et al. Reduction of intraocular pressure and glaucoma progression: results from the Early Manifest Glaucoma Trial. *Arch Ophthalmol* 2002;120:1268-79.
  22. Cioffi GA, Liebmann JM. Translating the OHTS results into clinical practice. *J Glaucoma* 2002;11:375-7.
  23. Weinreb RN, Friedman DS, Fechtner RD, et al. Risk assessment in the management of patients with ocular hypertension. *Am J Ophthalmol* 2004;138:458-67.
  24. Jonas JB, Budde WM, Panda-Jonas S. Ophthalmoscopic evaluation of the optic nerve head. *Surv Ophthalmol* 1999;43:293-320.
  25. Varma R, Steinmann WC, Scott IU. Expert agreement in evaluating the optic disc for glaucoma. *Ophthalmology* 1992;99:215-21.
  26. Abrams LS, Scott IU, Spaeth GL, et al. Agreement among optometrists, ophthalmologists, and residents in evaluating the optic disc for glaucoma. *Ophthalmology* 1994;101:1662-7.
  27. Greaney MJ, Hoffman DC, Garway-Heath DF, et al. Comparison of optic nerve imaging methods to distinguish normal eyes from those with glaucoma. *Invest Ophthalmol Vis Sci* 2002;43:140-5.
  28. Wollstein G, Garway-Heath DF, Fontana L, Hitchings RA. Identifying early glaucomatous changes. Comparison between expert clinical assessment of optic disc photographs and confocal scanning ophthalmoscopy. *Ophthalmology* 2000;107:2272-7.
  29. Girkin CA, McGwin G, Jr., Long C, et al. Subjective and objective optic nerve assessment in African Americans and whites. *Invest Ophthalmol Vis Sci* 2004;45:2272-8.
  30. Jonas JB, Nguyen NX, Naumann GO. The retinal nerve fiber layer in normal eyes. *Ophthalmology* 1989;96:627-32.
  31. Airaksinen PJ, Drance SM, Douglas GR, et al. Diffuse and localized nerve fiber loss in glaucoma. *Am J Ophthalmol* 1984;98:566-71.
  32. Sommer A, Katz J, Quigley HA, et al. Clinically detectable nerve fiber atrophy precedes the onset of glaucomatous field loss. *Arch Ophthalmol* 1991;109:77-83.
  33. Tuulonen A, Airaksinen PJ. Initial glaucomatous optic disk and retinal nerve fiber layer abnormalities and their progression. *Am J Ophthalmol* 1991;111:485-90.
  34. Jonas JB, Schiro D. Localised wedge shaped defects of the retinal nerve fibre layer in glaucoma. *Br J Ophthalmol* 1994;78:285-90.
  35. Quigley HA, Reacher M, Katz J, et al. Quantitative grading of nerve fiber layer photographs. *Ophthalmology* 1993;100:1800-7.
  36. Niessen AG, Van Den Berg TJ, Langerhorst CT, Bossuyt PM. Grading of retinal nerve fiber layer with a photographic reference set. *Am J Ophthalmol* 1995;120:577-86.
  37. Heijl A, Patella VM. Glaucomatous Visual Field Loss. Essential Perimetry. The Field Analyzer Primer, 3rd ed. Jena, Germany: Carl Zeiss Meditec, Inc., 2002; chap. 5.

38. Section 10: Glaucoma. Vol. 2003-2004. San Francisco, CA: American Academy of Ophthalmology, 2003.
39. Tuulonen A, Airaksinen PJ, Erola E, et al. The Finnish evidence-based guideline for open-angle glaucoma. *Acta Ophthalmol Scand* 2003;81:3-18.
40. Heijl A, Lindgren G, Olsson J. Normal variability of static perimetric threshold values across the central visual field. *Arch Ophthalmol* 1987;105:1544-9.
41. Heijl A, Lindgren A, Lindgren G. Test-retest variability in glaucomatous visual fields. *Am J Ophthalmol* 1989;108:130-5.
42. Keltner JL, Johnson CA, Quigg JM, et al. Confirmation of visual field abnormalities in the Ocular Hypertension Treatment Study. Ocular Hypertension Treatment Study Group. *Arch Ophthalmol* 2000;118:1187-94.
43. Airaksinen PJ, Drance SM, Douglas GR, et al. Visual field and retinal nerve fiber layer comparisons in glaucoma. *Arch Ophthalmol* 1985;103:205-7.
44. Johnson CA, Sample PhD PA, Zangwill LM, et al. Structure and function evaluation (SAFE): II. Comparison of optic disk and visual field characteristics. *Am J Ophthalmol* 2003;135:148-54.
45. Friedman DS, Wilson MR, Liebmann JM, et al. An evidence-based assessment of risk factors for the progression of ocular hypertension and glaucoma. *Am J Ophthalmol* 2004;138:S19-S31.
46. Bathija R, Gupta N, Zangwill L, Weinreb RN. Changing definition of glaucoma. *J Glaucoma* 1998;7:165-9.
47. Greenfield DS. Optic nerve and retinal nerve fiber layer analyzers in glaucoma. *Curr Opin Ophthalmol* 2002;13:68-76.
48. Sample PA. Glaucoma is present prior to its detection with standard automated perimetry: is it time to change our concepts? *Graefes Arch Clin Exp Ophthalmol* 2003;241:168-9.
49. Dreher AW, Reiter K. Retinal laser ellipsometry: A new method for measuring the retinal nerve fiber layer thickness distribution? *Clin Vision Sci* 1992;7:481-8.
50. Dreher AW, Reiter K. Scanning laser polarimetry of the retinal nerve fiber layer. *SPIE* 1992;1746:34-41.
51. Dreher AW, Bailey ED. Assessment of the retinal nerve fiber layer by scanning-laser polarimetry. *SPIE* 1993;1877:266-71.
52. Knighton RW, Huang X, Zhou Q. Microtubule contribution to the reflectance of the retinal nerve fiber layer. *Invest Ophthalmol Vis Sci* 1998;39:189-93.
53. Alberts B, Bray D, Lewis J, et al. The cytoskeleton. Molecular biology of the cell, Second edition ed. New York, United States of America: Garland Publishing, Inc., 1989; chap. 11.
54. Knighton RW, Huang XR. Analytical methods for scanning laser polarimetry. *Opt Exp* 2002;10:1179-89.
55. Weinreb RN, Dreher AW, Coleman A, et al. Histopathologic validation of Fourier-ellipsometry measurements of retinal nerve fiber layer thickness. *Arch Ophthalmol* 1990;108:557-60.



56. Zhou Q, Reed J, Betts RW, et al. Detection of glaucomatous retinal nerve fiber layer damage by scanning laser polarimetry with custom corneal compensation. *Proc SPIE Int Soc Opt Eng* 2003;4951:32-41.
57. Colen TP, Lemij HG. Sensitivity and specificity of the GDx: clinical judgment of standard printouts versus the number. *J Glaucoma* 2003;12:129-33.
58. Brink HB, van Blokland GJ. Birefringence of the human foveal area assessed in vivo with Mueller-matrix ellipsometry. *J Opt Soc Am A* 1988;5:49-57.
59. van Blokland GJ, Verhelst SC. Corneal polarization in the living human eye explained with a biaxial model. *J Opt Soc Am A* 1987;4:82-90.
60. Brink HB. Birefringence of the human crystalline lens in vivo. *J Opt Soc Am A* 1991;8:1788-93.
61. Greenfield DS, Knighton RW, Huang XR. Effect of corneal polarization axis on assessment of retinal nerve fiber layer thickness by scanning laser polarimetry. *Am J Ophthalmol* 2000;129:715-22.
62. Weinreb RN, Bowd C, Greenfield DS, Zangwill LM. Measurement of the magnitude and axis of corneal polarization with scanning laser polarimetry. *Arch Ophthalmol* 2002;120:901-6.
63. Knighton RW, Huang XR. Linear birefringence of the central human cornea. *Invest Ophthalmol Vis Sci* 2002;43:82-6.
64. Knighton RW, Huang XR, Greenfield DS. Analytical model of scanning laser polarimetry for retinal nerve fiber layer assessment. *Invest Ophthalmol Vis Sci* 2002;43:383-92.
65. Greenfield DS, Knighton RW, Feuer WJ, et al. Correction for corneal polarization axis improves the discriminating power of scanning laser polarimetry. *Am J Ophthalmol* 2002;134:27-33.
66. Garway-Heath DF, Greaney MJ, Caprioli J. Correction for the erroneous compensation of anterior segment birefringence with the scanning laser polarimeter for glaucoma diagnosis. *Invest Ophthalmol Vis Sci* 2002;43:1465-74.
67. Tjon-Fo-Sang MJ, Lemij HG. The sensitivity and specificity of nerve fiber layer measurements in glaucoma as determined with scanning laser polarimetry. *Am J Ophthalmol* 1997;123:62-9.
68. Zhou Q, Weinreb RN. Individualized compensation of anterior segment birefringence during scanning laser polarimetry. *Invest Ophthalmol Vis Sci* 2002;43:2221-8.
69. Weinreb RN, Bowd C, Zangwill LM. Scanning Laser Polarimetry in Monkey Eyes using Variable Corneal Polarization Compensation. *J Glaucoma* 2002;11:378-84.
70. Weinreb RN, Bowd C, Zangwill LM. Glaucoma detection using scanning laser polarimetry with variable corneal polarization compensation. *Arch Ophthalmol* 2003;121:218-24.
71. Tannenbaum DP, Hoffman D, Lemij HG, et al. Variable corneal compensation improves discrimination between normal and glaucomatous eyes with the scanning laser polarimeter. *Ophthalmology* 2004;111:259-64.
72. Lemij HG, Blumenthal EZ, Fechtner RD, et al. Scanning Laser Polarimetry (SLP). In: Weinreb RN, Greve EL, eds. *Glaucoma diagnosis. Structure and function*. The Hague, The Netherlands: Kugler Publications, 2004.

73. Laser Diagnostic Technologies I. RNFL analysis with GDx VCC: a primer and clinical guide, 251-0083B ed. San Diego, CA, United States of America: Laser Diagnostic Technologies, Inc., 2004.
74. Weinreb RN, Dreher AW, Bille JF. Quantitative assessment of the optic nerve head with the laser tomographic scanner. *Int Ophthalmol* 1989;13:25-9.
75. Heidelberg Retina Tomograph operating instructions, revision 3.0-4E ed. Dossenheim, Germany: Heidelberg Engineering GmbH, 2003.
76. Wollstein G, Garway-Heath DF, Hitchings RA. Identification of early glaucoma cases with the scanning laser ophthalmoscope. *Ophthalmology* 1998;105:1557-63.
77. Bathija R, Zangwill L, Berry CC, et al. Detection of early glaucomatous structural damage with confocal scanning laser tomography. *J Glaucoma* 1998;7:121-7.
78. Mikelberg FS, Parfitt C, Swindale N. Ability of the Heidelberg Retina Tomograph to detect early glaucomatous visual field loss. *J Glaucoma* 1995;4:242-7.
79. Ford BA, Artes PH, McCormick TA, et al. Comparison of data analysis tools for detection of glaucoma with the Heidelberg Retina Tomograph. *Ophthalmology* 2003;110:1145-50.
80. Sample PA. Short-wavelength automated perimetry: its role in the clinic and for understanding ganglion cell function. *Prog Retin Eye Res* 2000;19:369-83.
81. Wild JM. Short wavelength automated perimetry. *Acta Ophthalmol Scand* 2001;79:546-59.
82. Demirel S, Flanagan J, Sample PA. Short wavelength automated perimetry (SWAP). In: Weinreb RN, Greve EL, eds. Glaucoma diagnosis. Structure and function. The Hague, The Netherlands: Kugler Publications, 2004.
83. Johnson CA. Selective versus nonselective losses in glaucoma. *J Glaucoma* 1994;3:S32-S44.
84. Spry PG, Johnson CA, Mansberger SL, Cioffi GA. Psychophysical Investigation of Ganglion Cell Loss in Early Glaucoma. *J Glaucoma* 2005;14:11-9.
85. Johnson CA, Adams AJ, Casson EJ, Brandt JD. Blue-on-yellow perimetry can predict the development of glaucomatous visual field loss. *Arch Ophthalmol* 1993;111:645-50.
86. Sample PA, Taylor JD, Martinez GA, et al. Short-wavelength color visual fields in glaucoma suspects at risk. *Am J Ophthalmol* 1993;115:225-33.
87. Polo V, Larrosa JM, Pinilla I, et al. Predictive value of short-wavelength automated perimetry: a 3-year follow-up study. *Ophthalmology* 2002;109:761-5.





# 2

## **Developments in scanning laser polarimetry**



## 2.1 Visualization of localized retinal nerve fiber layer defects with the GDx with individualized and with fixed compensation of anterior segment birefringence

---

**Purpose:** To compare the visualization of localized retinal nerve fiber layer (RNFL) defects in GDx images with fixed and with individualized compensation of anterior segment birefringence (FC and IC, respectively) with their visualization in red-free fundus photographs.

**Design:** Observational case series.

**Participants:** Eight eyes of six glaucoma patients with localized, wedge-shaped RNFL defects in red-free fundus photographs with matching visual field defects.

**Methods:** We imaged all eyes with a GDx equipped with a variable corneal compensator (VCC). The VCC replaced the standard fixed compensator and could be set to compensate birefringence of up to 120 nm at any axis. Individual anterior segment birefringence was estimated from a macular retardation profile that resulted from the interaction between birefringence of the anterior segment and that of Henle's fiber layer. Measurements of RNFL retardation were made with the GDx with FC (60 nm of retardation with a slow axis of 15 degrees nasally downward) and with IC. Maps of retardation measurements with FC and IC were superimposed on red-free fundus photographs.

**Main Outcome Measures:** Visualization of localized RNFL defects.

**Results:** Localized RNFL defects were visible in GDx retardation maps obtained with IC. The defects closely matched those observed in red-free fundus photographs. With FC, however, the GDx retardation images did not correlate well with red-free fundus photography.

**Conclusions:** An individualized anterior segment compensation in the GDx improves the visualization of localized glaucomatous loss. *Ophthalmology* 2003;110:1512-1516.

---

**G**laucomatous atrophy of retinal ganglion cells and their axons may be localized, diffuse, or both.<sup>1-3</sup> With red-free fundus photography, localized defects may be visible as wedge-shaped, well demarcated, defects of the retinal nerve fiber layer (RNFL)<sup>4</sup> and they are more easily detected than diffuse loss.<sup>3,4</sup>

The RNFL can also be evaluated with the GDx (Laser Diagnostic Technologies, Inc., San Diego, CA, USA), a scanning laser polarimeter that constructs a pseudo-thickness map of the peripapillary RNFL by assessing its amount of birefringence.<sup>5,6</sup> Although glaucomatous loss is identified by the GDx, visualization of localized RNFL defects with this technique has been

disappointing,<sup>7</sup> which may be due to anterior segment birefringence.<sup>8-10</sup>

The standard GDx features a built-in fixed retarder to compensate for the birefringence of the anterior segment, which is exhibited by the cornea and, to a lesser extent, the crystalline lens. Fixed compensation (FC), however, may be significantly inadequate in many eyes due to large inter- and intraindividual variability in corneal birefringence.<sup>8,9</sup> As inadequate anterior segment compensation may lead to spurious measurements,<sup>10</sup> we speculated that the GDx' inability to detect localized RNFL defects is possibly due to such an inadequate compensation. Therefore, we measured glaucoma patients with a prototype of a GDx equipped with a so-called variable corneal compensator (VCC), that allows one to compensate an individual eye's anterior segment birefringence (individualized compensation; IC).<sup>11</sup> We compared the visualization of localized RNFL defects in GDx images with FC and with IC with their visualization in red-free fundus photographs.

## Methods

We used a GDx with VCC to image 8 eyes of 6 glaucoma patients. All eyes had been shown to have at least 1 localized, wedge-shaped, RNFL defect<sup>4</sup> visible with digital red-free fundus photography (TRC-50IA retinal camera, Topcon Medical Systems, Inc., Paramus, NJ, USA with a MegaPlus 1.4 CCD camera, Redlake MASD, Inc., San Diego, CA, USA). Red-free fundus photography was performed in these subjects because a glaucomatous defect was suspected by a glaucoma specialist on routine clinical ophthalmoscopy. For fundus photography, pupils were dilated with 0.5% Tropicamide and 5% Phenylephrine eye drops. The age of the patients varied between 49 and 73 years. Four patients were men. None of the subjects had any significant history of ocular diseases other than glaucoma, except for 1 patient who had undergone laser treatment 9 years ago for a small peripheral retinal defect. The Snellen visual acuity varied across eyes between 20/30 and 20/15. The IOP varied between 11 mmHg and 21 mmHg with medication. Slit-lamp examination of the eyes was unremarkable in all, except for 2 eyes that showed a slight nuclear sclerosis. Fundoscopy showed no macular disease in any of the eyes. All had parapapillary chorioretinal alpha zone atrophy.<sup>12</sup> Only one showed beta zone atrophy.<sup>12</sup> The RNFL defects all matched reproducible sensitivity losses in visual field testing (Achromatic Automated Perimetry, 24-2 Full Threshold or 24-2 SITA-Standard Test Paradigm, Humphrey Field Analyzer, Zeiss Humphrey Systems, Dublin, CA, USA). The GDx with VCC was kindly provided by its manufacturer. The VCC could be set manually to compensate anterior segment birefringence of up to 120 nm at any axis. Our institutional Ethics Committee approved this study and all subjects gave their informed consent.

For each eye, 3 high quality scans of the peripapillary region were obtained with the VCC set to compensate 60 nm of retardation with a slow axis of 15 degrees nasally downward (ND), which equals FC in the standard GDx.<sup>11</sup> Scans were deemed to be of high quality if they met



the following criteria: centered optic disk, image in focus, even and just illumination throughout the image, and absence of motion artifacts. The resolution of the images was 256 x 256 pixels, covering an area of 15° x 15° in scanning angle, as in the standard GDx. Then, to estimate an eye's anterior segment birefringence, 3 high quality scans of the macular region were made with the VCC set to compensate 0 nm of retardation. The interaction between the birefringence of the radially oriented axons of the photoreceptors that constitute Henle's fiber layer in the macula, and the anterior segment birefringence, resulted in a bow-tie shaped pattern in the retardation image.<sup>13</sup> A 10-pixel-wide circular band with a diameter of 80 pixels was placed on the macular retardation map and manually centered on the middle of the bow-tie. A dedicated algorithm, incorporated into the GDx software, determined the anterior segment birefringence from retardation measurements over this circle. The working principle of this algorithm was as follows:<sup>11,13</sup> the anterior segment slow axis coincides with the orientation of the bright axis of the bow-tie, as the alignment of the slow axes of the anterior segment and the photoreceptor axons result in a summation of retardation. The trough in the bow-tie pattern occurs where both slow axes are perpendicular to one another and retardation is subtracted. According to Zhou and Weinreb,<sup>11</sup> the magnitude of anterior segment birefringence can then be approximated by the average of the retardation profile if the retardation of the anterior segment is higher than that of Henle's fiber layer and by half of the modulation of the retardation profile if the retardation of the anterior segment is lower than that of Henle's fiber layer.

The average of the 3 measurements of anterior segment birefringence was used to set the VCC accordingly. Adequate IC of the anterior segment was verified by making 3 macula scans that had to show donut- or cross-shaped retardation patterns.<sup>13</sup> Then, 3 high quality scans with IC were obtained of the peripapillary region.

To ensure the same orientation of the slow axes of the birefringent structures in the eye to that of the VCC, we saw to it that patients had their heads as upright as possible during all measurements. The pupils of the patients were undilated and the room lights were left on.

The highest quality retardation image with FC and the highest quality retardation image with IC were displayed in a gray scale instead of the standard color palette to optimize contrast, as is illustrated in Figure 2.1.1. They were then cropped from the GDx computer screen and subsequently processed with computer software (PHOTO-PAINT, version 8, Corel Corporation, Ottawa, Ontario, Canada): the gray scale of the retardation image was rescaled by ignoring 2% of the darkest and 2% of the lightest pixel values. The red-free RNFL photographs were optimized to show the localized defects and the striation of the RNFL with standard image enhancement techniques. The GDx images were placed over the RNFL photograph and manually resized and rotated to align the blood vessels. Visualization of localized RNFL defects was then compared between red-free photos and retardation images with FC and IC.

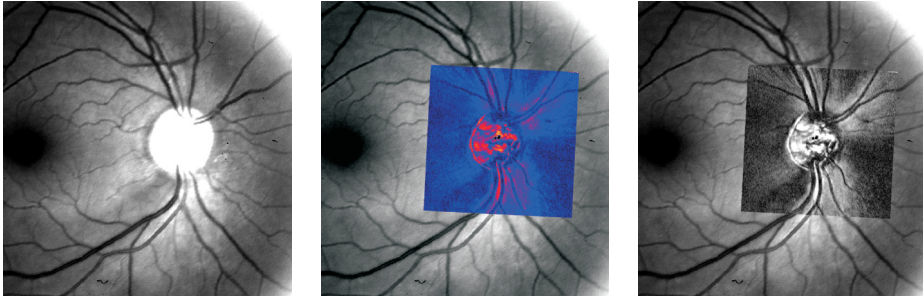


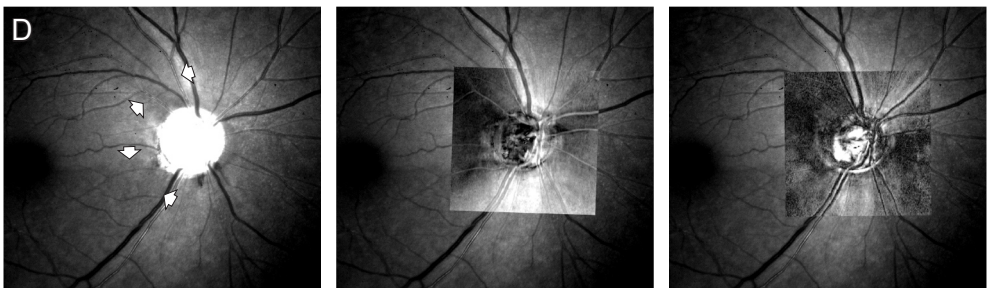
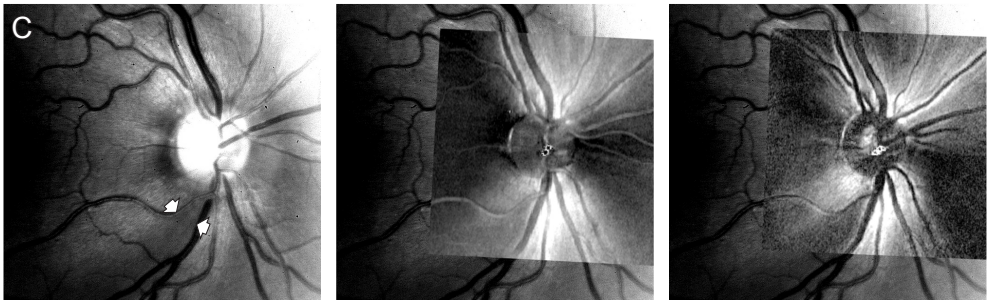
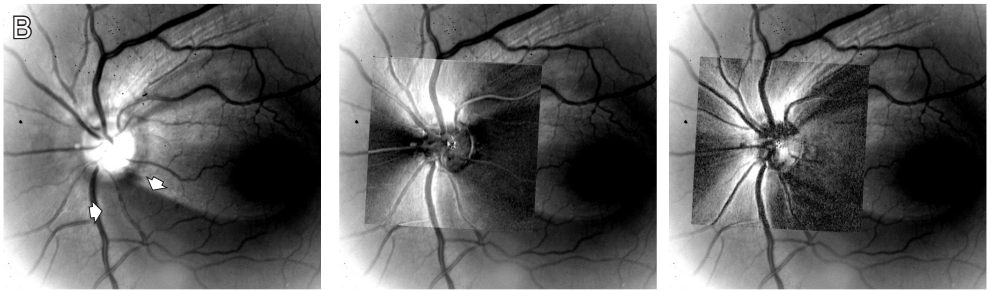
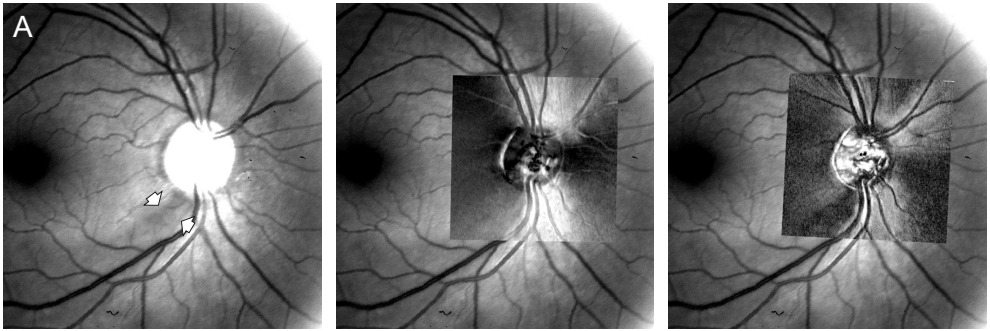
**Figure 2.1.1.** Red-free fundus photograph of the right eye of a glaucoma patient with a localized defect of the retinal nerve fiber layer (RNFL) inferotemporally (*left*). In the middle, a GDx retardation map with standard color palette placed over the fundus photograph. When displayed in a gray scale, with lighter shades representing high amounts of retardation and darker shades representing low amounts, the visualization of the RNFL defect and of the striations improves (*right*).

## Results

The retinal retardation maps obtained with the GDx with IC clearly showed all localized RNFL defects, and matched the red-free fundus photographs. Figure 2.1.2A shows the right eye of a glaucoma patient with an inferotemporal wedge-shaped RNFL defect. The defect was clearly visible on the IC retardation image (Fig. 2.1.2A, *right*). Its demarcations corresponded well with those identified in the red-free fundus photograph and could even be followed onto the photo. In this eye, the measured anterior segment birefringence was 19 nm with a slow axis of 64.3 degrees ND. The RNFL defect did not show in the GDx retardation image made with FC (Fig. 2.1.2A, *middle*).

In 6 glaucomatous eyes, the localized defects were visible both in the FC and IC retardation images, as illustrated in Figures 2.1.2B and 2.1.2C. In all these cases, the RNFL defects were most marked in the IC retardation images. The more the anterior segment birefringence deviated both in magnitude and in axis from the anterior segment birefringence compensated by FC, the worse the retardation images correlated with the red-free fundus photographs. Also note that with FC, the retardation images sometimes suggested thick RNFL bundles that were ill positioned when compared to red-free photographs (cf. Fig. 2.1.2B, *left* and *middle*; superiorly to the optic disk).

**Figure 2.1.2** (→). Examples of localized retinal nerve fiber layer (RNFL) defects, as visualized with red-free fundus photography (*left*), with a GDx with fixed compensation (FC; *middle*) and with individualized compensation (IC; *right*) of anterior segment birefringence. White arrows indicate the wedge-shaped defects. The GDx retardation images have been superimposed on the corresponding red-free fundus photograph. The magnitudes and corneal axes of these eyes were 19 nm and 64.3° (A), 26.7 nm and 32.7° (B), 30 nm and 30.3° (C), and 39 nm and 51.3° (D), respectively. The localized RNFL defects are clearly visible in retardation maps taken with IC, whereas they are poorly visualized in GDx images taken with FC. In one eye (D), the edges of the defects with the papillomacular bundle, as seen on the red-free fundus photograph, are not visualized by the GDx measurement with IC. Physiological striation of the RNFL is readily visible on the IC retardation maps (e.g. B, superiorly to the optic disk, *right*).



In one severely glaucomatous eye (Fig. 2.1.2D) with wedge-shaped defects both supero- and inferotemporally, the diffuse RNFL loss was apparent in the IC retardation image but the sharp, albeit faint, demarcation with the papillomacular bundle that was seen in the red-free fundus photograph could not be identified. The FC retardation image showed RNFL loss only superotemporally, also failing to clarify the faint demarcation with the papillomacular bundle. Apart from the glaucomatous defects, physiological striations of the RNFL were visible in the IC retardation maps, and corresponded well with the red-free photographs, as can be seen in Figure 2.1.2 (e.g. Fig. 2.1.2B, *left* and *right*; superiorly to the optic disk).

## Discussion

We have currently shown that the structure of the RNFL as seen in red-free fundus photographs is clearly visualized in GDx retardation maps made with individualized compensation of anterior segment birefringence. Both localized glaucomatous RNFL defects and physiological striations appeared remarkably similar for the two imaging technologies. To our knowledge, this is the best agreement ever reported between two essentially different technologies that image the RNFL in vivo.

With standard GDx compensation, localized RNFL loss was often difficult and sometimes even impossible to detect, depending on the deviation of an eye's anterior segment birefringence from the one compensated by standard FC. In addition, arcuate bundles sometimes showed up in apparently ill positions in FC images when compared to red-free photographs. Niessen et al<sup>14</sup> also found a weak correlation between red-free fundus photography and images taken with a predecessor of the standard GDx that also was provided with FC. Greenfield et al<sup>8</sup> have shown that misalignment of the slow axes of the anterior segment and of the compensator distorts GDx measurements. Recently, Knighton and Huang<sup>10</sup> have reasoned that, in many eyes, the peripapillary retardation image can not correspond to the spatial distribution of RNFL thickness because of incomplete cancellation of anterior segment birefringence. Only when this birefringence is completely neutralized will it reflect RNFL thickness, which is supported by our results.

In some areas of the well-compensated GDx images, however, there was poor agreement in the appearance of the RNFL with the red-free photographs, especially in the temporal region (e.g. cf. Fig. 2.1.2C, *left* and *right*). The observed brightness of the RNFL in red-free fundus photographs depends on the angle of the incident illuminating beam.<sup>15</sup> As a result, equally thick areas in different parts of the fundus do not necessarily appear equally bright.<sup>15</sup> The poor agreement between red-free photographs and GDx images in some areas may also have been caused by a suboptimal quality of the red-free photographs, with an attenuated specular reflectivity in the

temporal area, e.g. because of insufficiently dilated pupils or media opacities. On the other hand, the rescaling of the color palette of the GDx images may have exaggerated the magnitude of retardation in this area. Any mismatch between the GDx images and the red-free photographs may perhaps also underline that the two techniques examine different aspects of the RNFL, i.e., birefringence and specular reflectivity.

This may also hold true for the advanced glaucomatous case (Fig. 2.1.2D) in which the faint, but distinct border of an RNFL wedge defect with the papillomacular bundle, as seen in the red-free photograph, could not be identified with SLP. On the other hand, the GDx may also have been too insensitive to detect such a faint transition in thickness in a generally thinned RNFL.

We estimated anterior segment birefringence from the macular retardation profile that resulted from the interaction in birefringence between the anterior segment and Henle's fiber layer. We achieved good compensation in the macular measurements of retardation with IC, as these images all showed donut- or cross-shaped retardation patterns. However, it is unclear how well retardation measurements with IC of the peripapillary region were compensated, because corneal birefringence varies with the location of entry of the illuminating beam,<sup>16</sup> and the beam's optical path to the macula and to the optic nerve head do not necessarily coincide. The effect of this disturbance on the retardation measurements, as well as its clinical significance, needs to be determined. In addition, the reproducibility and clinical applicability of this technique for assessing anterior segment birefringence still has to be assessed.<sup>11</sup> Especially subjects with macular disease might not be suitable for this technique (Bagga H, Greenfield DS, Knighton RW. SLP with variable corneal compensation in eyes with macular pathology [abstract]. 2002 Annual Meeting Abstract and Program Planner accessed at [www.arvo.org](http://www.arvo.org). Association for Research in Vision and Ophthalmology. Abstract 250).

Our comparisons between scanning laser polarimetry (SLP) and red-free fundus photography were only qualitative. As SLP is a quantitative technique, it would be of interest to directly compare the magnitude of retardation with histological measurements of RNFL thickness.

Red-free fundus photography is not routinely used in clinical care, as even well trained photographers can obtain high quality photographs in only a limited number of patients because of, among other things, media opacities and insufficient pupil dilation.<sup>2,17-19</sup> In addition, interpretation of red-free photography is subjective, although some attempts have been made to quantify the analysis.<sup>20,21</sup> The GDx, however, has the potential to be widely used in clinical practice because of its short acquisition time and its ability to obtain high quality measurements in almost any subject, even with cataract.<sup>14,19</sup> Moreover, GDx measurements can be interpreted both qualitatively, as we have currently done, and quantitatively, by comparing the data to retardation measurements in healthy individuals. Also, quantitative analysis will enable the clinician to use

the GDx objectively for follow-up of both glaucoma patients and glaucoma suspects, by looking for statistically significant local and/or diffuse changes in RNFL retardation.

In summary, individualized compensation of anterior segment birefringence in the GDx enhances the visualization of localized glaucomatous loss, and may improve detection, as well as follow-up, of glaucoma patients.

## References

1. Airaksinen PJ, Drance SM, Douglas GR, et al. Diffuse and localized nerve fiber loss in glaucoma. *Am J Ophthalmol* 1984;98:566-71.
2. Sommer A, Katz J, Quigley HA, et al. Clinically detectable nerve fiber atrophy precedes the onset of glaucomatous field loss. *Arch Ophthalmol* 1991;109:77-83.
3. Tuulonen A, Airaksinen PJ. Initial glaucomatous optic disk and retinal nerve fiber layer abnormalities and their progression. *Am J Ophthalmol* 1991;111:485-90.
4. Jonas JB, Schiro D. Localised wedge shaped defects of the retinal nerve fibre layer in glaucoma. *Br J Ophthalmol* 1994;78:285-90.
5. Dreher AW, Reiter K. Scanning laser polarimetry of the retinal nerve fiber layer. *SPIE* 1992;1746:34-41.
6. Lemij HG. The value of polarimetry in the evaluation of the optic nerve in glaucoma. *Curr Opin Ophthalmol* 2001;12:138-42.
7. Nicolela MT, Martinez-Bello C, Morrison CA, et al. Scanning laser polarimetry in a selected group of patients with glaucoma and normal controls. *Am J Ophthalmol* 2001;132:845-54.
8. Greenfield DS, Knighton RW, Huang XR. Effect of corneal polarization axis on assessment of retinal nerve fiber layer thickness by scanning laser polarimetry. *Am J Ophthalmol* 2000;129:715-22.
9. Knighton RW, Huang XR. Linear birefringence of the central human cornea. *Invest Ophthalmol Vis Sci* 2002;43:82-6.
10. Knighton RW, Huang XR, Greenfield DS. Analytical model of scanning laser polarimetry for retinal nerve fiber layer assessment. *Invest Ophthalmol Vis Sci* 2002;43:383-92.
11. Zhou Q, Weinreb RN. Individualized compensation of anterior segment birefringence during scanning laser polarimetry. *Invest Ophthalmol Vis Sci* 2002;43:2221-8.
12. Jonas JB, Budde WM, Panda-Jonas S. Ophthalmoscopic evaluation of the optic nerve head. *Surv Ophthalmol* 1999;43:293-320.
13. Brink HB, van Blokland GJ. Birefringence of the human foveal area assessed in vivo with Mueller-matrix ellipsometry. *J Opt Soc Am A* 1988;5:49-57.
14. Niessen AG, Van Den Berg TJ, Langerhorst CT, Greve EL. Retinal nerve fiber layer assessment by scanning laser polarimetry and standardized photography. *Am J Ophthalmol* 1996;121:484-93.
15. Knighton RW, Zhou Q. The relation between the reflectance and thickness of the retinal nerve fiber layer. *J Glaucoma* 1995;4:117-23.

16. Van Blokland GJ, Verhelst SC. Corneal polarization in the living human eye explained with a biaxial model. *J Opt Soc Am A* 1987;4:82-90.
17. Sommer A, Quigley HA, Robin AL, et al. Evaluation of nerve fiber layer assessment. *Arch Ophthalmol* 1984;102:1766-71.
18. Wang F, Quigley HA, Tielsch JM. Screening for glaucoma in a medical clinic with photographs of the nerve fiber layer. *Arch Ophthalmol* 1994;112:796-800.
19. Kremmer S, Ayerterey HD, Selbach JM, Steuhl KP. Scanning laser polarimetry, retinal nerve fiber layer photography, and perimetry in the diagnosis of glaucomatous nerve fiber defects. *Graefes Arch Clin Exp Ophthalmol* 2000;238:922-6.
20. Quigley HA, Reacher M, Katz J, et al. Quantitative grading of nerve fiber layer photographs. *Ophthalmology* 1993;100:1800-7.
21. Niessen AG, Van Den Berg TJ, Langerhorst CT, Bossuyt PM. Grading of retinal nerve fiber layer with a photographic reference set. *Am J Ophthalmol* 1995;120:577-86.





## 2.2 Effects of inadequate anterior segment compensation on measurements with scanning laser polarimetry

---

We systematically explored the effects of poor anterior segment compensation on scanning laser polarimetry (SLP) measurements of the retinal nerve fiber layer (RNFL). We used a prototype scanning laser polarimeter GDx with an adjustable compensator to neutralize anterior segment birefringence. By systematically varying the magnitude and axis of anterior segment compensation in a healthy and a glaucomatous eye, we observed marked changes in RNFL appearance: the healthy eye could appear to have glaucomatous damage, whereas the glaucomatous eye could appear to have a thicker and healthier RNFL. Even small amounts of uncompensated corneal birefringence, which may occur in routine clinical use, resulted in apparent changes in RNFL morphology. We think that knowledge of this effect is important when using SLP in clinical practice. *Ophthalmic Surgery Laser & Imaging, in press.*

---

Scanning laser polarimetry (SLP), featured in the GDx NFA and the GDx VCC (Carl Zeiss Meditec, Dublin, CA, USA), estimates retinal nerve fiber layer (RNFL) thickness by measuring the retardation of polarized light by the birefringent RNFL.<sup>1</sup> To cancel retardation by the cornea and lens, the GDx NFA is equipped with a so-called fixed corneal compensator (FCC) that cancels a fixed amount of birefringence reflecting the median values in the general population (i.e., a corneal polarization magnitude [CPM] of 60 nm and a corneal polarization axis [CPA] of 15° nasally downward [ND]). FCC, however, incompletely neutralizes anterior segment retardation in many eyes due to large inter-eye variability of corneal birefringence,<sup>2</sup> which may lead to spurious measurements.<sup>3</sup> SLP with a variable corneal compensator (VCC), featured in the GDx VCC, allows eye-specific compensation, resulting in more accurate assessment of the RNFL<sup>3</sup> and an increased diagnostic accuracy.<sup>4</sup>

In the current report, we systematically varied the anterior segment compensation in a healthy and a glaucomatous eye in order to clarify the effect of residual anterior segment birefringence on measurements of RNFL retardation with SLP.

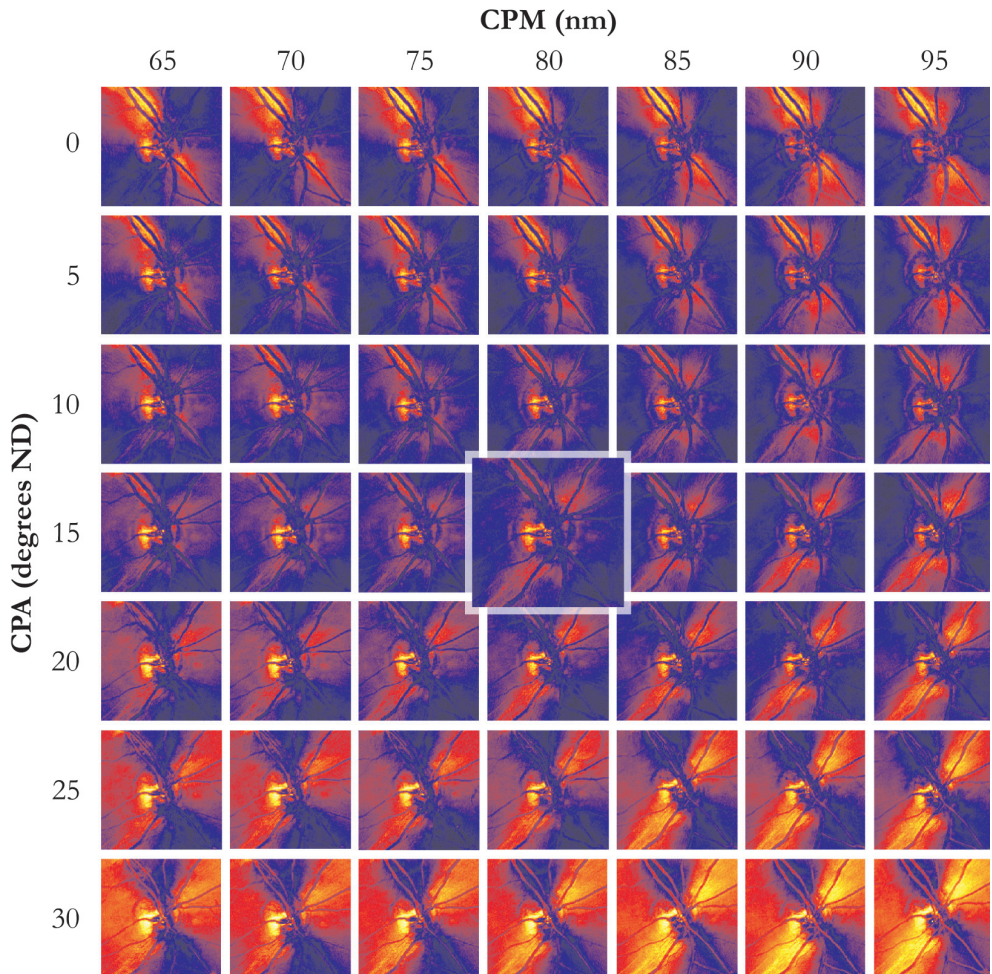


**Figure 2.2.1.** SLP measurements of a healthy right eye with various amounts of compensation for corneal polarization magnitude (CPM) and corneal polarization axis (CPA), relative to the eye's corneal birefringence (CPM=80nm; CPA=15° nasally downward [ND]). In the central image, corneal birefringence is completely neutralized. Bright colors represent higher retardation values; dim colors represent lower retardation values.

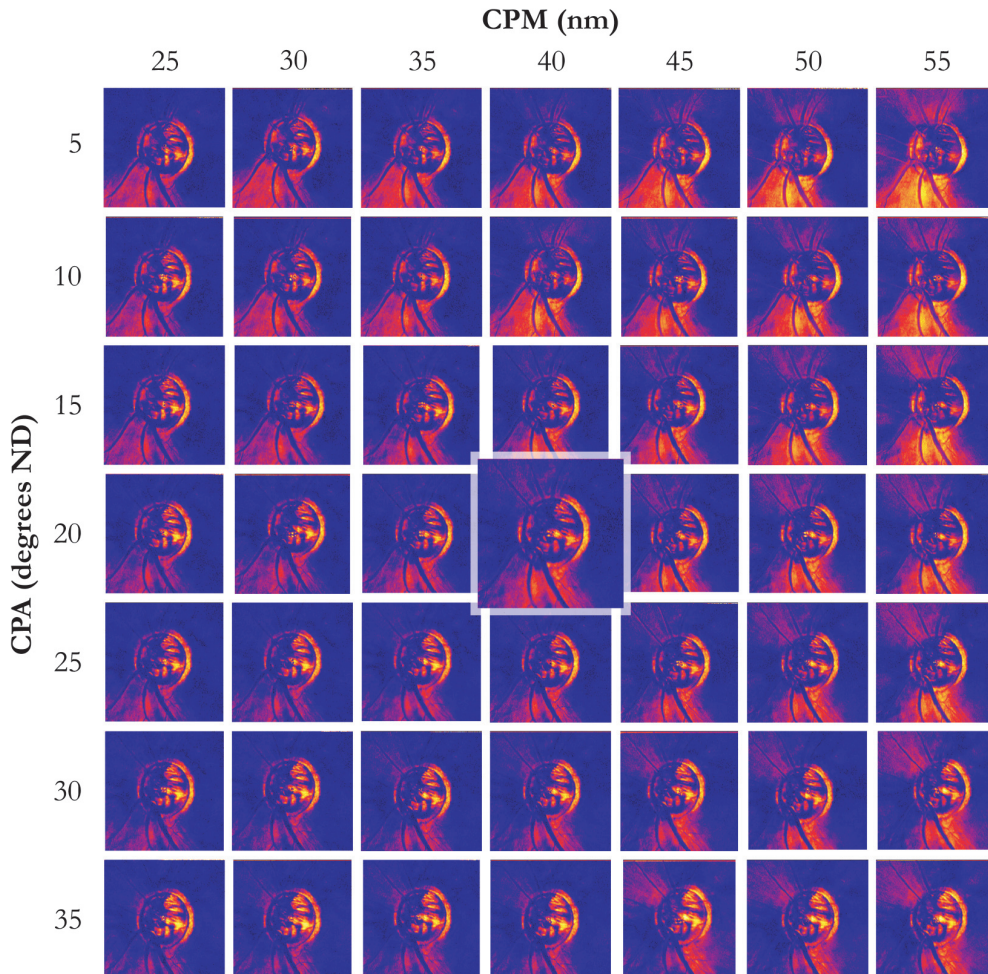


**Figure 2.2.2.** Measurements with SLP of a left eye of a glaucoma patient with various amounts of compensation for CPM and CPA, relative to the eye's corneal birefringence (CPM=40nm; CPA=20° ND). In the central image, corneal birefringence is completely neutralized. Color coding as in figure 2.2.1.

## Case Report

We measured the right eye of a healthy subject, with healthy looking optic discs, normal visual fields, and intraocular pressures of <21mmHg, with a modified GDx NFA in which the FCC had been replaced by a VCC that could be adjusted manually.<sup>5</sup> In addition, we measured the left eye of a glaucoma patient, with a glaucomatous looking optic nerve head and corresponding visual field loss. The axis and magnitude of anterior segment birefringence were determined by macular polarimetry images with the variable compensator set to 0 nm, as described by Zhou and Weinreb.<sup>5</sup> For each eye, 49 measurements were obtained with systematically stepwise varying degrees of compensation for CPM and CPA, relative to each eye's anterior segment birefringence. Retardation images have been shown in figures 1 and 2. With complete compensation for CPM and CPA (central images), the retardation image in the healthy subject showed a retardation pattern typical for healthy subjects, with high values (bright colors) superiorly and inferiorly around the vessels, and low values (dim colors) temporally and nasally. In the glaucoma patient, especially retardation values in the superior region were low.

By varying the degree of compensation for CPM and CPA, the pattern of retardation changed markedly in both subjects. Notably in the healthy subject, the apparent positions of the arcuate bundles could be altered (cf. two uppermost rows of frames to two lowest in Fig. 1). In addition, the healthy eye could appear to have glaucomatous damage inferiorly, for example when compensated for a CPM of 70nm and a CPA of 10° ND (Fig. 1). In the glaucoma patient, compensation for a CPM of 55nm and a CPA of 10° ND resulted in an apparent increase in RNFL thickness (Fig. 2).

## Discussion

The two series of retardation images in this case report illustrate to what extent the apparent RNFL thickness in SLP can be artificially increased or decreased as a result of incomplete compensation of anterior segment birefringence. For SLP with FCC, with its fixed compensation of anterior segment birefringence, such artefacts may occur in many subjects due to the large variability in corneal birefringence.<sup>6,7</sup> When switching from SLP with FCC to VCC, with eye-specific compensation of anterior segment birefringence, changes in the pattern of RNFL as illustrated in the present report will have to be expected. We think this requires setting a new baseline when monitoring glaucomatous changes of the RNFL over time.

By stepwise varying the compensation for corneal polarization axis and corneal polarization magnitude, we showed that even small changes of  $\pm 5^\circ$  in compensation for CPA resulted in distinct changes in the retardation images. Such small amounts of uncompensated corneal birefringence may occur in GDx VCC measurements with automated compensation with routine clinical use, either mimicking or masking glaucomatous progression. In fact, CPA may vary up

to 13° between measurements in individual eyes.<sup>8</sup> Therefore, we suggest determining an eye's anterior segment birefringence at every visit and asking patients to keep their heads in the same position on the GDx VCC face mask between measurements of anterior segment birefringence and subsequent assessment of RNFL birefringence.

We currently evaluated the effect of residual anterior segment birefringence on SLP measurements only qualitatively. Future studies may also quantitatively assess the effect of residual anterior segment birefringence in the individual eye.

Knowledge of the extent of these effects may improve clinical use of SLP in the diagnosis and monitoring of glaucoma.

## References

1. Weinreb RN, Dreher AW, Coleman A, Quigley H, Shaw B, Reiter K. Histopathologic validation of Fourier-ellipsometry measurements of retinal nerve fiber layer thickness. *Arch Ophthalmol* 1990;108:557-60.
2. Weinreb RN, Bowd C, Greenfield DS, Zangwill LM. Measurement of the magnitude and axis of corneal polarization with scanning laser polarimetry. *Arch Ophthalmol* 2002;120:901-6.
3. Reus NJ, Colen TP, Lemij HG. Visualization of localized retinal nerve fiber layer defects with the GDx with individualized and with fixed compensation of anterior segment birefringence. *Ophthalmology* 2003;110:1512-6.
4. Weinreb RN, Bowd C, Zangwill LM. Glaucoma detection using scanning laser polarimetry with variable corneal polarization compensation. *Arch Ophthalmol* 2003;121:218-24.
5. Zhou Q, Weinreb RN. Individualized compensation of anterior segment birefringence during scanning laser polarimetry. *Invest Ophthalmol Vis Sci* 2002;43:2221-8.
6. Greenfield DS, Knighton RW, Huang XR. Effect of corneal polarization axis on assessment of retinal nerve fiber layer thickness by scanning laser polarimetry. *Am J Ophthalmol* 2000;129:715-22.
7. Knighton RW, Huang XR. Linear birefringence of the central human cornea. *Invest Ophthalmol Vis Sci* 2002;43:82-6.
8. Greenfield DS, Knighton RW. Stability of corneal polarization axis measurements for scanning laser polarimetry. *Ophthalmology* 2001;108:1065-9.





## 2.3 Enhanced imaging algorithm for scanning laser polarimetry with variable corneal compensation

---

**Purpose:** To describe and investigate a method for improving assessment of retinal nerve fiber layer (RNFL) morphology with scanning laser polarimetry (SLP) with variable corneal compensation (VCC).

**Methods:** By neutralizing anterior segment birefringence with a variable compensator, the current VCC method allows direct measurement of RNFL retardation. In the new method, named ECC, instead of ‘nulling’ the anterior segment birefringence, the variable compensator was set to introduce a ‘bias’ birefringence of approximately 55 nm with its slow axis close to vertical in the measurement beam. This bias was removed mathematically for each individual pixel to produce the RNFL image. In 177 eyes of healthy subjects, glaucoma patients, and subjects with ocular hypertension, retardation images were obtained with both VCC and ECC methods.

**Results:** In the tested eyes, images obtained with ECC showed the expected RNFL appearance better than with VCC. In addition, atypical retardation patterns were less frequent with ECC. The amount of residual anterior segment birefringence dropped statistically significantly with ECC in the various groups. Measurements of peripapillary RNFL retardation showed reduced temporal and nasal values with ECC, whereas superior and inferior values were not statistically significantly different between VCC and ECC. The dynamic range appeared to have increased with ECC. The accuracy of TSNIT Average and Inferior Average for detecting glaucoma was higher with ECC than with VCC.

**Conclusions:** RNFL morphology may be better assessed with the presented ECC method than with standard VCC. ECC may be implemented in the current GDx VCC systems by means of a software upgrade. We suspect that it may enhance the clinical utility of the GDx VCC in glaucoma management. *Invest Ophthalmol Vis Sci, submitted.*

---

Scanning laser polarimetry (SLP) has been developed for detecting and monitoring glaucoma, an acquired progressive optic neuropathy with atrophy of retinal ganglion cells and their axons.<sup>1</sup> SLP is based on the presumed form birefringence of the microtubules in the retinal nerve fiber layer (RNFL).<sup>2</sup> Their parallel arrangement results in a change in the retardation of passing polarized light. In SLP, the back of the eye is scanned with a polarized laser beam and the retardation of the backscattered light that has double passed the RNFL is

determined. The amount of retardance exhibited by the RNFL is proportional to its thickness,<sup>3</sup> although the slope of the linear relationship may vary around the optic nerve head.<sup>4,5</sup>

Two structures in the anterior segment, i.e. the cornea and, to a lesser extent, the lens, are also birefringent. In order to assess RNFL retardation, anterior segment retardation needs to be neutralized.<sup>6,7</sup> Earlier commercial SLPs were equipped with a fixed corneal compensator (FCC) that cancelled a fixed amount of birefringence reflecting the median magnitude and axis of anterior segment birefringence in the general population.<sup>6</sup> Recently, SLP with variable corneal compensation (VCC) was introduced, which allows eye-specific compensation of anterior segment birefringence.<sup>8</sup> This technique is implemented in the commercially available GDx VCC (Carl Zeiss Meditec, Inc., Dublin, CA, USA). SLP-VCC has been shown to allow a more accurate assessment of RNFL morphology<sup>9</sup> with a higher diagnostic accuracy for detecting glaucoma<sup>10,11</sup> than SLP-FCC.<sup>12</sup> Further, measurements with SLP-VCC have been shown to correlate well with functional measurements by standard automated perimetry.<sup>13,14</sup>

Typically, in healthy subjects, larger amounts of retardation are apparent next to the blood vessels superior and inferior to the optic nerve head (ONH) (e.g. Fig. 2.3.1A). The amount of retardation decreases with increasing distance from the ONH. In glaucomatous eyes, the loss of nerve fibers is visible as a localized and/or diffuse decrease in the amount of retardation (e.g. Fig. 2.3.1B). In approximately 7% of subjects, atypical patterns of increased retardation may be apparent in images obtained with SLP-VCC (e.g. Fig. 2.3.1C and D, *left*).<sup>10</sup> The RNFL in these so-called atypical scans may be difficult to interpret. The source of this aberrant retardation is unknown, although it appears to occur more frequently in eyes with lightly pigmented fundi, in myopes, and in eyes of elderly subjects in which the signal-to-noise ratio of the SLP images is relatively poor.<sup>10</sup>

Although compensation of anterior segment birefringence in the individual eye seems to be adequate with SLP-VCC in general, a small amount of residual anterior segment birefringence can be observed in some eyes (e.g. Fig. 2.3.1E, *left*), which may lead to erroneous measurements of the RNFL.<sup>9</sup>

Both atypical retardation patterns and residual anterior segment birefringence adversely affect the accuracy of RNFL assessment with SLP. In this paper, we present a method that minimizes atypical retardation patterns and residual anterior segment birefringence, which may improve the accuracy of RNFL assessment in affected eyes. We investigated this new method in healthy eyes, glaucomatous eyes, and eyes of subjects with ocular hypertension.



## Methods

### Subjects

One hundred and sixty-five subjects (29 healthy subjects, 70 glaucoma patients, and 78 subjects with ocular hypertension) were recruited consecutively for the present study between February and July 2004 at The Rotterdam Eye Hospital. The research adhered to the tenets of the Declaration of Helsinki. The institutional human experimentation committee had approved the research. Informed consent was obtained from the subjects after explanation of the nature and possible consequences of the study.

All subjects were measured with standard automated perimetry (SAP) by means of the Humphrey Field Analyzer II (Carl Zeiss Meditec, Inc., Dublin, CA, USA) 24-2 Full Threshold (FT) or Swedish interactive threshold algorithm (SITA) Standard test program. All visual fields were reliable. Reliability criteria applied were: 1) fixation losses <25% and 2) false-positive and false-negative response rates  $\leq 20\%$  for the FT test paradigm and  $\leq 7\%$  for the SITA-Standard test program. In glaucomatous eyes with advanced field loss, higher false-negative response rates were accepted: up to 33% for the FT paradigm and up to 12% for the SITA-Standard paradigm.

All healthy subjects had normal visual fields with SAP, i.e., a glaucoma hemifield test (GHT) within normal limits and no nerve fiber bundle visual field defects in the total and/or pattern deviation probability plots. In addition, they were of white ethnic origin and had a visual acuity of 20/40 or better. None had a significant history of ocular disease, a history of intra-ocular surgery (except for any uncomplicated cataract surgery), relatives in the first and/or second degree with glaucoma, any significant coexisting diseases, or systemic diseases with possible ocular involvement, such as diabetes mellitus. Furthermore, slit-lamp examination was unremarkable; they had healthy-looking optic discs (no diffuse or local rim thinning and no optic disc hemorrhages), an IOP of 21 mmHg or less in both eyes, and open angles upon gonioscopy. Their mean  $\pm$  SD 'mean deviation' (MD) and mean  $\pm$  SD pattern standard deviation (PSD) were  $0.27 \pm 1.02$  dB and  $1.69 \pm 0.51$  dB, respectively.

Glaucoma patients had a glaucomatous appearance of at least one of their optic discs (with notching or thinning of the neuroretinal rim), a corresponding nerve fiber bundle visual field defect with SAP, and open angles by gonioscopy. Visual field defects had to be confirmed on at least one separate examination. All patients with glaucoma were of white ethnic origin and had a visual acuity of 20/40 or better. Patients with any significant coexisting diseases other than glaucoma, systemic diseases with possible ocular involvement, such as diabetes mellitus, or a history of intra-ocular surgery (except for any uncomplicated cataract or glaucoma surgery) were excluded. Their mean  $\pm$  SD MD and mean  $\pm$  SD PSD were  $-12.15 \pm 8.07$  dB (range, -30.40 to 0.61) and  $9.25 \pm 3.66$  dB, respectively.

All subjects with ocular hypertension had an IOP of  $\geq 22$  mmHg and  $\leq 32$  mmHg and normal

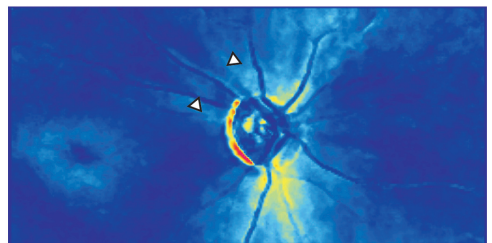
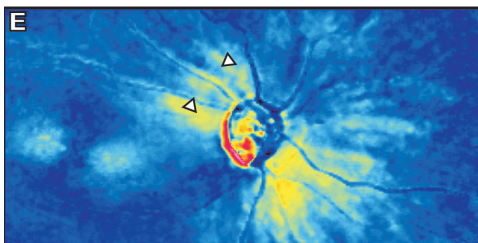
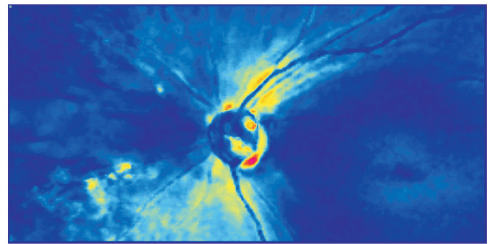
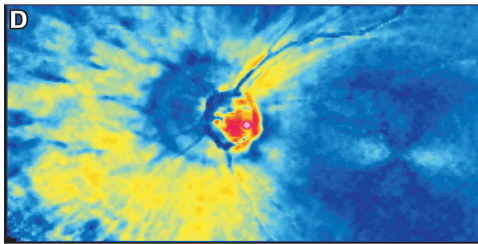
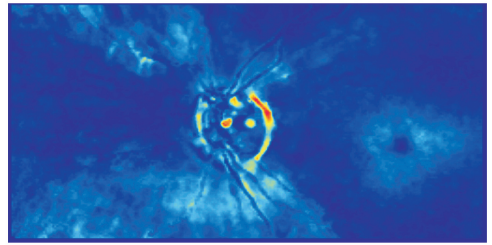
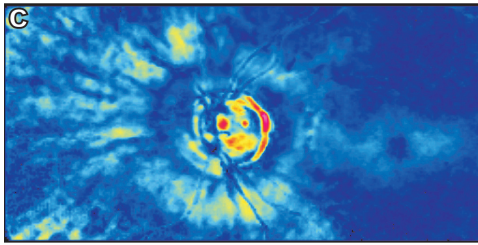
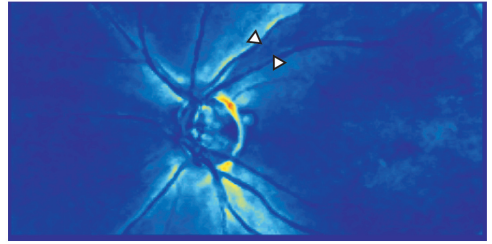
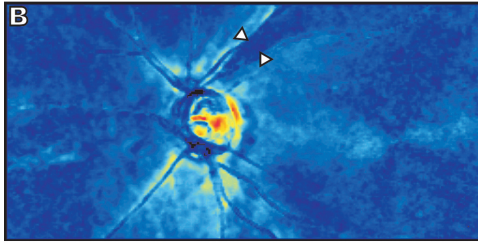
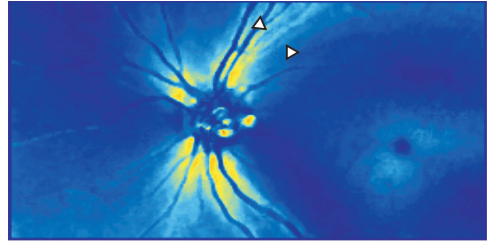
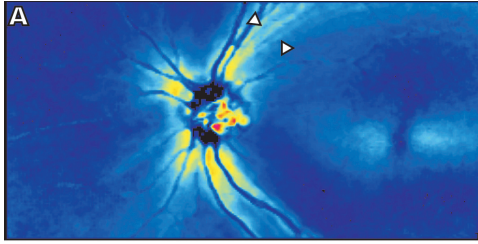


**Figure 2.3.1** (←). Retardation images of four left eyes and one right eye with standard VCC (*left*) and currently presented ECC (*right*). Brighter colors represent a thicker RNFL; darker colors represent a thinner RNFL. (A): A healthy subject's eye (MD, 0.45 dB; PSD, 1.19 dB); residual retardation is 8 nm for VCC and 2 nm for ECC. The typical scan score was 99 and 100 for VCC and ECC, respectively. (B): A glaucoma patient's eye (MD, -6.19 dB; PSD, 8.8 dB); residual retardation was 5 nm for VCC and 1 nm for ECC. The typical scan score was 89 and 100 for VCC and ECC, respectively. (C): A glaucoma patient's eye (MD, -20.55 dB; PSD, 10.18 dB); residual retardation was 5 nm for VCC and 1 nm for ECC. The typical scan score was 45 and 100 for VCC and ECC, respectively. (D): A glaucoma patient's eye (MD, -3.04 dB; PSD, 6.14 dB); residual retardation was 6 nm for VCC and 0 nm for ECC. The typical scan score was 37 and 100 for VCC and ECC, respectively. (E): A glaucoma patient's right eye (MD, -11.69 dB; PSD, 13.66 dB); residual retardation was 12 nm for VCC and 0 nm for ECC. The typical scan score was 59 and 100 for VCC and ECC, respectively. With VCC, the large amount of residual anterior segment birefringence in the macular region had an axis of 23 degrees nasally downward. The RNFL appeared to be rotated in the same direction. With ECC, the apparent distortion of the RNFL measurement had disappeared.

visual fields on at least two separate occasions. The appearance of the optic disc was not a selection criterion. All subjects with ocular hypertension were of white ethnic origin and had a visual acuity of 20/40 or better. Patients with a history of intra-ocular surgery (except for any uncomplicated cataract surgery), any significant coexisting diseases, or systemic diseases with possible ocular involvement, such as diabetes mellitus, were excluded. Their mean  $\pm$  SD MD and mean  $\pm$  SD PSD were  $0.44 \pm 1.28$  dB and  $1.68 \pm 0.57$  dB, respectively.

Only one eye was randomly selected for analysis in the present study if both were eligible.

The mean  $\pm$  SD age of the healthy subjects, glaucoma patients, and subjects with ocular hypertension was  $60 \pm 13$ ,  $68 \pm 9$ , and  $63 \pm 10$  years, respectively. The difference in age between the various groups was statistically significant (one way ANOVA,  $P=0.002$ ). In 13/29 (45%) healthy subjects, 33/70 (47%) glaucomatous subjects, and 39/78 (50%) ocular hypertensive subjects, the right eye was used for analysis. Twelve of the 17 (41%) healthy subjects, 37 of the 70 (53%) glaucoma patients, and 43 of the 78 (55%) ocular hypertensive subjects were men.

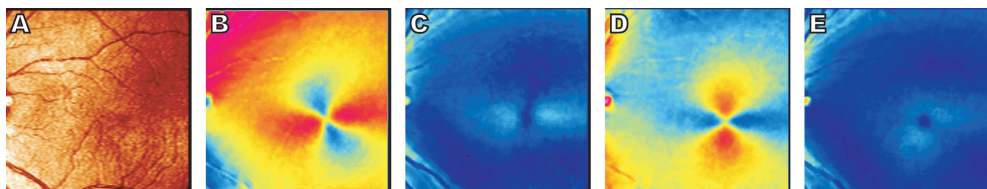


**Figure 2.3.2.** Macular images of a healthy subject's left eye. (A): Reflection image. (B): retardation image without any compensation of anterior segment birefringence (50 nm and  $19.6^\circ$  nasally downward [ND]). (C): retardation image with standard VCC compensation (13 nm and  $-78.3^\circ$  ND). (D): retardation image with artificially induced bias (27 nm and  $82.2^\circ$  ND). (E): retardation image with anterior segment compensation by the currently presented ECC method (2 nm and  $50.5^\circ$  ND). Note that residual birefringence is less with ECC than with VCC.

### SLP Measurements

SLP measurements were performed with the commercially available GDx VCC (software version 5.4.0; Carl Zeiss Meditec, Inc., Dublin, CA, USA). The GDx VCC used a near infrared laser beam with a wavelength of 785 nm to scan the ocular fundus. The field of view was 40° horizontally x 20° vertically at a density of 256 x 128 pixels, respectively. The scanned area included the papillary and the macular regions of the eye. The GDx VCC produced a reflection image that was generated from light reflected back from the fundus of the eye. In addition, it produced a retardation image that had been constructed from the 32,768 (256 x 128) individual retardation values. The amount of retardation was displayed as apparent RNFL thickness ( $\mu\text{m}$ ) based on a conversion factor of 0.67 nm/ $\mu\text{m}$ .<sup>15</sup> The GDx VCC was equipped with a variable corneal compensator that consisted of two identical linear retarders in rotating mounts so that both the retardation and axis of the unit could be adjusted. To measure an individual's eye polarization axis and magnitude of the cornea (and the lens), an SLP image of the macula (Fig. 2.3.2A) was acquired with the retardation of the compensator set to zero. The combination of the birefringence of the radially oriented axons of the photoreceptors that constitute Henle's fiber layer in the macula and the birefringence of the anterior segment resulted in a bow-tie like retardation pattern in the macula (Fig. 2.3.2B). One of two dedicated algorithms incorporated into the GDx VCC, i.e., the 'bow-tie' method and the 'screen' method, determined the magnitude and axis of anterior segment birefringence from the macular retardation profile. These algorithms have been described in detail elsewhere.<sup>8,15,16</sup> In short, the 'bow-tie' method calculated the anterior segment birefringence from the macular retardation profile obtained at a locus of points along a circle centered on the fovea.<sup>8</sup> The 'screen' method averaged the signals from the parallel channel and the crossed channel over a large square area of the macula centered on the fixation target to extract the anterior segment birefringence.<sup>15</sup> While the 'bow-tie' method works well in eyes with normal macula, the 'screen' method is more robust in eyes with macular pathology and a damaged Henle's fiber layer.<sup>16</sup>

In the currently implemented VCC technique, the compensator was automatically adjusted to neutralize the eye's anterior segment birefringence based on the measured values with the 'bow-tie' method. The eye was then scanned with individualized compensation to measure the amount of retinal retardation. With anterior segment birefringence compensated, the retardation pattern in the macular region should exhibit a uniform and weak retardation pattern with a cross- or donut-shaped distribution (Fig. 2.3.2C). As an alternative to the existing VCC method, a new software method, named enhanced corneal compensation (ECC), was developed that requires no hardware modification to the GDx VCC system and provides individualized corneal compensation with enhanced SLP measurement sensitivity. The rationale of this technique was as follows: the sensitivity of SLP to measuring small differences in retardation ultimately depends on the ability to detect small differences in polarization signal amplitude. SLP sensitivity

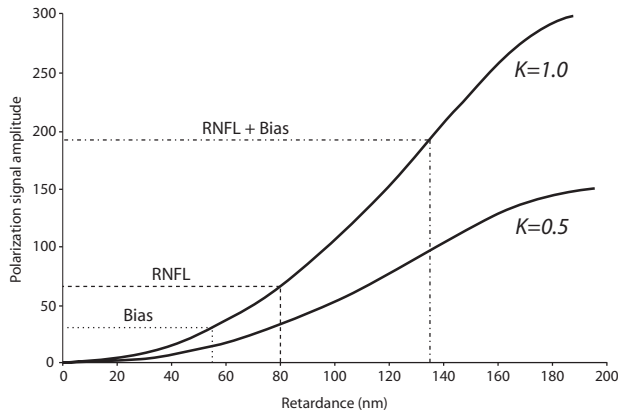


**Figure 2.3.3.** Plot of polarization signal amplitude versus retardation for different degrees of normalized polarization maintaining fundus reflectance ( $K$ ). See text for further details. RNFL, retinal nerve fiber layer.

(the slope of the curve) is inherently low at small retardation values, as shown in figure 2.3.3. Depolarization or reduction in reflected light intensity results in a lower intensity curve and proportionally decreased sensitivity, as illustrated with the curves for  $K=1.0$  and  $K=0.5$ , where  $K$  represents the normalized polarization maintaining fundus reflectance. Low sensitivity makes the retardation measurement susceptible to optical noise (e.g., stray light) and electronic noise (e.g., noise and digitization error). The principle of the new method, illustrated in figure 3, was to superimpose RNFL birefringence onto a large, known birefringence ('bias retarder'). The bias retarder was formed by the combination of the variable compensator and the anterior segment. Rather than adjusting VCC to neutralize the anterior segment birefringence, the compensator was adjusted so that the combination had a retardation of approximately 55 nm and a slow axis close to vertical. The bias retarder therefore shifted the retardation measurement into a more sensitive region (Fig. 2.3.3).

With ECC, SLP measured an amount of retardation that was higher than retinal retardation alone (Fig. 2.3.2D). The birefringence, induced by the bias retarder, was determined from the macular region with the 'screen' method described earlier. Based on Mueller calculus for a double-pass SLP system, the retinal retardation was mathematically extracted from the total retardation image based on knowledge of the bias retarder retardation and axis, as well as knowledge of the point-by-point total retardation and axis.<sup>17</sup> Successful removal of bias retardation from the final retinal retardation image was evident from the uniform retardation pattern in the macula (Fig. 2.3.2E).

Three trained and experienced technicians performed the GDx VCC measurements in both eyes of all subjects. Pupils of subjects were undilated and the room lights were left on. The spherical



	Typical scan parameter value		<i>P</i>
	<i>VCC</i>	<i>ECC</i>	
Normal	89.0 ± 14.8 (50-100)	99.3 ± 1.8 (92-100)	0.001
Glaucoma	71.2 ± 28.6 (0-100)	97.8 ± 6.1 (69-100)	< 0.001
Ocular hypertension	85.9 ± 19.1 (19-100)	99.9 ± 0.6 (95-100)	< 0.001

**Table 2.3.1.** Values of the typical scan score (possible range, 0-100) in scanning laser polarimetry measurements with the VCC method and the ECC method in healthy eyes, glaucomatous eyes, and eyes with ocular hypertension. Data have been given as mean ± SD (range). Differences were tested for statistical significance with a paired *t* test.

equivalent refractive error of each eye was entered into the software to allow the GDx VCC to focus on the retina. If necessary, the focus was adjusted manually in 0.25 diopters steps. For each subject, anterior segment birefringence was assessed, after which images were obtained from both eyes with VCC first and with ECC second. Subjects were asked to keep their heads positioned on the GDx VCC system's face mask between acquisitions. To maintain the same orientation of the slow axes of the birefringent structures in the eye to that of the instrument's compensator, the operator saw to it that patients had their heads in the same position during all measurements.

All accepted scans were of high quality, i.e. with a centered optic disc, well-focused, evenly and justly illuminated throughout the image, and without any motion artifacts. No images were excluded from analysis that were flagged by the GDx VCC software as 'results may not be compatible with normative database'. The software flags an image as such when the typical scan score is 25 or lower. The typical scan score (range, 0-100) is a proprietary measure provided by the GDx VCC software, which indicates whether the observed retardation pattern is typical for the human healthy or glaucomatous RNFL. This score has been described in detail elsewhere.<sup>18</sup> In short, similar to the NFI parameter, the typical scan score was the output of a machine learning classifier based on a support vector machine. In scans that display an atypical pattern of retardation (e.g. Fig. 2.3.1C and D, *right*), the typical scan score is lower.

Residual anterior segment birefringence was assessed in images obtained with VCC and ECC by determining the amount of retardation in the macula region with the 'bow-tie' method.

	CPM without compensation	CPM, residual		
		<i>VCC</i>	<i>ECC</i>	<i>P</i>
Normal	36.6 ± 13.0 (7-64)	6.5 ± 2.7 (1-11)	1.9 ± 1.9 (0-8)	< 0.001
Glaucoma	38.6 ± 14.1 (2-75)	6.4 ± 3.1 (0-18)	1.8 ± 1.4 (0-6)	< 0.001
Ocular hypertension	39.7 ± 15.2 (1-67)	6.1 ± 2.9 (1-21)	1.6 ± 1.3 (0-5)	< 0.001

**Table 2.3.2.** Corneal polarization magnitude (CPM, expressed in μm of retardation) of healthy eyes, glaucoma eyes, and eyes with ocular hypertension and residual CPM with correction by a variable corneal compensator with VCC and ECC method. Data have been given as mean ± SD (range). Differences in residual CPM with VCC and ECC were tested for statistical significance with a paired *t* test.

Parameter	Unit	Normal			Glaucoma			Ocular Hypertension		
		VCC	ECC	P	VCC	ECC	P	VCC	ECC	P
TSNIT Average	μm	52.7 ± 6.0	50.2 ± 5.2	<0.001	41.1 ± 8.2	36.9 ± 6.1	<0.001	52.3 ± 5.3	48.9 ± 4.6	<0.001
Temporal Average	μm	28.9 ± 7.9	16.7 ± 5.1	<0.001	36.4 ± 12.5	17.3 ± 5.1	<0.001	32.3 ± 9.8	16.4 ± 3.7	<0.001
Superior Average	μm	62.8 ± 8.0	62.9 ± 7.8	0.82	42.7 ± 9.2	42.9 ± 8.9	0.76	63.1 ± 7.8	62.6 ± 7.9	0.26
Nasal Average	μm	41.2 ± 7.0	32.8 ± 6.3	<0.001	32.6 ± 6.4	26.3 ± 6.5	<0.001	38.4 ± 8.9	29.9 ± 7.1	<0.001
Inferior Average	μm	59.6 ± 8.6	61.7 ± 8.3	0.012	46.5 ± 11.9	45.3 ± 9.4	0.18	58.0 ± 8.0	60.1 ± 6.7	<0.001
TSNIT Std. Dev.	μm	18.9 ± 3.7	24.5 ± 4.1	<0.001	11.9 ± 3.2	16.4 ± 3.9	<0.001	18.5 ± 4.2	23.9 ± 3.4	<0.001
Peak-to-trough	μm	66.3 ± 10.5	75.5 ± 10.0	<0.001	45.6 ± 11.7	56.9 ± 12.6	<0.001	66.0 ± 12.0	75.2 ± 9.7	<0.001
Temporal Minimum	μm	22.9 ± 6.8	12.5 ± 4.5	<0.001	31.0 ± 11.6	13.2 ± 4.0	<0.001	25.8 ± 9.6	12.4 ± 3.2	<0.001
Nasal Minimum	μm	29.9 ± 7.1	17.8 ± 7.1	<0.001	25.5 ± 5.9	17.2 ± 7.1	<0.001	28.3 ± 9.1	16.2 ± 6.5	<0.001

**Table 2.3.3.** Various parameters describing scanning laser polarimetry measurements with VCC and ECC method in healthy eyes, glaucoma eyes, and eyes with ocular hypertension. Data have been given as mean ± SD. Differences in measurements with VCC and ECC were tested for statistical significance with a paired *t* test.

	Superior region				Inferior region			
	VCC		ECC		VCC		ECC	
	Average	$\Delta$	Average	$\Delta$	Average	$\Delta$	Average	$\Delta$
Healthy eyes	75.5	} 47.3	77.3	} 51.5	73.8	} 42.6	75.7	} 46.4
Glaucoma eyes	28.5		25.8		31.2		29.3	

**Table 2.3.4.** Average amount of retardation ( $\mu\text{m}$ ) in the superior and inferior regions measured with VCC and with ECC in the 10% of healthy eyes with the largest amount of retardation and in the 10% of glaucoma eyes with the smallest amount of retardation. The difference in retardation between the healthy and glaucoma eyes have been presented as well.

### Data analysis

The margin of the optic disc was manually marked with an ellipse in the reflection image of the fundus. The GDx VCC software positioned a circular band, 8 pixels wide ( $-0.4$  mm in an emmetropic eye) and with an inner diameter of 54 pixels ( $-2.5$  mm in an emmetropic eye), centered on the center of the ellipse. The instrument processed the retardation values within this band to give 256 values evenly distributed along the circle. These values were subsequently grouped into 64 sectors and exported by the software. The measurement band was divided into 4 sectors: a temporal one (extending from  $335^\circ$  to  $24^\circ$ , relative to the temporal meridian), a superior one ( $25^\circ$  to  $144^\circ$ ), a nasal one ( $145^\circ$  to  $214^\circ$ ), and an inferior one ( $215^\circ$  to  $334^\circ$ ). Based on the retardation values within this band, we determined the average amount of retardation in all sectors and in the temporal, superior, nasal, and inferior regions: TSNIT Average, Temporal Average, Superior Average, Nasal Average, and Inferior Average, respectively. In addition, we calculated the SD of the mean amount of retardation beneath the entire measurement band (TSNIT Std. Dev.) and determined the peak-to-trough values in the TSNIT plot. Furthermore, we determined the minimum amount of retardation in the temporal and nasal regions: Temporal Minimum and Nasal Minimum, respectively.

	CPM, residual			
	VCC		ECC	
	$r_s$	$P$	$r_s$	$P$
Temporal Average	0.26	0.006	-0.02	0.83
Superior Average	-0.07	0.48	0.08	0.42
Nasal Average	0.23	0.016	-0.04	0.71
Inferior Average	-0.14	0.15	-0.17	0.077

**Table 2.3.5.** Association, expressed as Spearman's rank correlation coefficient ( $r_s$ ), between amount of retardation in 4 peripapillary regions and residual anterior segment birefringence measured with VCC and ECC in healthy and ocular hypertensive eyes.



To investigate whether the range in measurements had increased with ECC compared to VCC, we identified, for the superior and inferior regions separately, 10% of healthy eyes with the largest amount of retardation by ECC and 10% of glaucomatous eyes with the smallest amount of retardation by ECC. For both VCC and ECC, we averaged the amounts of retardation in each

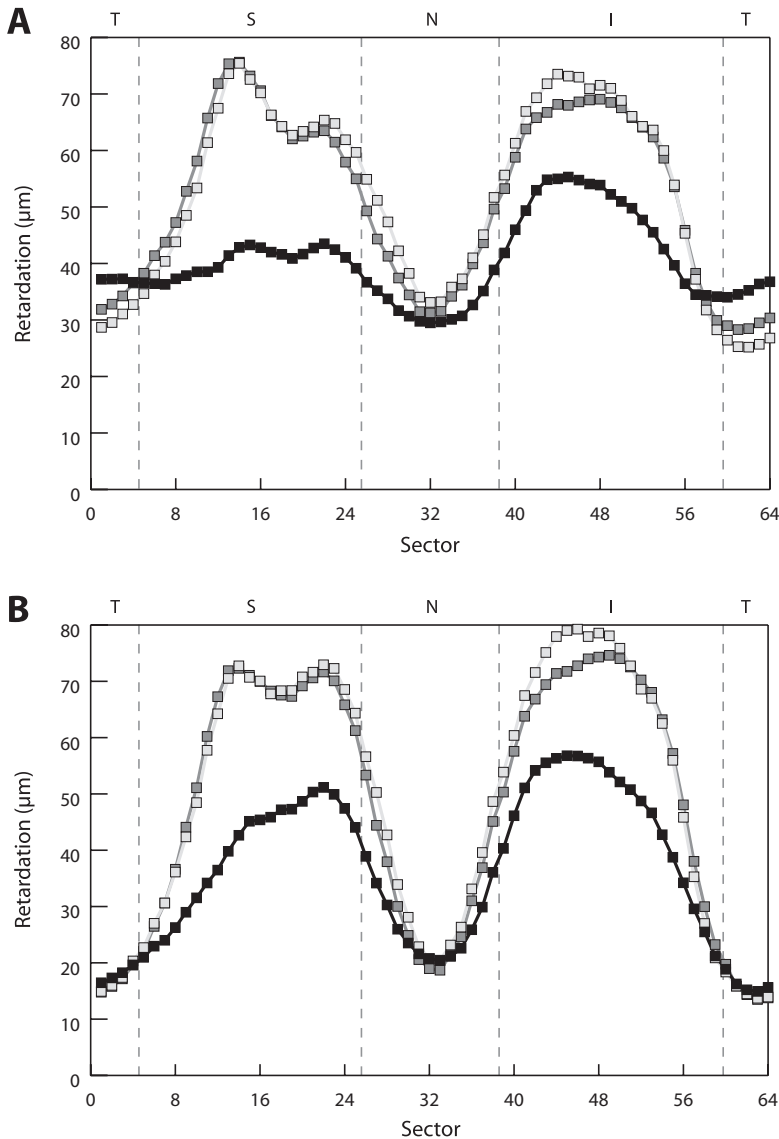


**Figure 2.3.4.** Peripapillary retinal nerve fiber layer retardation measured with scanning laser polarimetry with variable corneal compensation (VCC; A) and with ECC (B) in healthy eyes (■), eyes with ocular hypertension (■), and glaucoma eyes (■). T, temporal; S, superior; N, nasal; I, inferior.

	Unit	VCC	ECC	Difference	P
TSNIT Average	μm	0.87 (0.035; 0.80-0.94)	0.96 (0.017; 0.93-1.00)	-0.09	0.004
Superior Average	μm	0.95 (0.019; 0.92-0.99)	0.98 (0.011; 0.96-1.00)	-0.03	0.062
Inferior Average	μm	0.81 (0.045; 0.72-0.89)	0.90 (0.031; 0.84-0.96)	-0.09	0.002
TSNIT Std. Dev.	μm	0.93 (0.026; 0.88-0.98)	0.93 (0.030; 0.87-0.99)	0	0.87

**Table 2.3.6.** Diagnostic accuracy, expressed as area under the receiver operating characteristic (ROC) curve (standard error; 95% confidence interval), for various parameters for discriminating between healthy eyes and eyes with glaucoma.

group. We then calculated the differences in the amount of retardation between the healthy eyes and the glaucomatous eyes for VCC and ECC separately.

Furthermore, we determined the accuracy of SLP-VCC and SLP-ECC for discriminating between healthy and glaucomatous eyes by calculating the areas under the receiver operating characteristic (ROC) curves (AUCs) for 4 clinically used parameters (i.e., TSNIT Average, Superior Average, Inferior Average, and TSNIT Std. Dev.) obtained with VCC and with ECC. The 95% confidence intervals (CIs) for the AUCs were calculated as the point estimates of the  $AUC \pm 1.96 * \text{standard error}$ . Differences in AUCs of parameters obtained with VCC and ECC were tested for statistical significance with the paired samples test described by DeLong et al.<sup>19</sup>

We used paired and unpaired t-tests to evaluate differences in measurements within and between groups, respectively. In the present study, a  $P$  value of less than 0.05 was considered statistically significant. For paired comparisons, the  $\alpha$  was adjusted to the number of comparisons within each analysis with the Bonferroni correction to allow for multiple testing. Statistical analyses were performed with SPSS for Windows (release 12.0.1, 2003, SPSS Inc., Chicago, IL, USA).

## Results

Figure 1 shows five examples of retardation images acquired with standard VCC (*left*) and with ECC (*right*); the peripapillary and the macular regions have been displayed. These examples illustrate that the retardation images taken with ECC showed the expected RNFL appearance much better than images acquired with VCC (e.g., Fig. 2.3.1B, cf. *right* and *left*). Furthermore, atypical retardation patterns appeared less often and were less pronounced in ECC images than in VCC images (e.g. Fig. 2.3.1C and D, cf. *right* and *left*). This was reflected in the typical scan score that was statistically significantly higher ( $P \leq 0.001$ ;  $\alpha = 0.017$ , 3 comparisons) for images with the ECC method than with the VCC method in all subjects (Table 2.3.1). The morphology of the RNFL looked similar for images obtained with either VCC or ECC in almost every eye. For example, in Fig. 2.3.1A, several slit-like defects superotemporal to the optic disc were equally well visible with both methods. Similarly, the localized RNFL defects superotemporal to the optic disc in Figs 2.3.1B and 2.3.1E could be marked with either method.

Images obtained with ECC contained statistically significantly ( $P < 0.001$ ;  $\alpha = 0.017$ , 3 comparisons) less residual anterior segment birefringence than images obtained with VCC (Table 2.3.2 and Fig. 2.3.1, cf. macular regions in the *left* and *right* panels). Images taken with VCC often showed a horizontally placed bow-tie (Fig. 2.3.1, *left*). The mean  $\pm$  SD axis of this residual anterior segment birefringence in healthy, ocular hypertensive, and glaucoma eyes was  $8^\circ \pm 21^\circ$  nasally downward. In images with a large residual amount of birefringence, the morphology of the RNFL sometimes appeared to be rotated (e.g. Fig. 2.3.1E, *left*).

Peripapillary retardation values measured with VCC and ECC have been presented in Figs 2.3.4A and 2.3.4B, respectively. The shapes of these so-called TSNIT graphs were markedly different between the two methods. Statistically, TSNIT Average, Temporal Average, Nasal Average, Temporal Minimum, and Nasal Minimum were statistically significantly ( $P \leq 0.001$ ,  $\alpha = 0.006$ , 9 comparisons) lower with ECC than with VCC in all subjects (Table 2.3.3). TSNIT Std. Dev. and the peak-to-trough values were statistically significantly ( $P < 0.001$ ,  $\alpha = 0.006$ , 9 comparisons) higher with ECC than with VCC (Table 2.3.3), which was apparent as a larger modulation of the TSNIT graph with ECC (cf. Figs 2.3.4B and 2.3.4A, respectively). The parameters Superior Average and Inferior Average were not statistically significantly ( $P \geq 0.012$ ,  $\alpha = 0.006$ , 9 comparisons) different between ECC and VCC in any of the tested groups, except for the Inferior Average in the subjects with ocular hypertension ( $P < 0.001$ , Table 2.3.3). This difference, however, was small (on average  $2.1 \mu\text{m}$ ).

The difference in the amount of retardation between healthy eyes with the largest amount of retardation and the glaucoma eyes with the smallest amount of retardation have been presented in Table 2.3.4. In both the superior and inferior regions, the range of measurements appeared larger for measurements with ECC than with VCC.

Of note, in images obtained with VCC, the average values in the temporal quadrant (Temporal Average) were statistically significantly higher in glaucoma eyes ( $36.6 \mu\text{m}$ ) than in healthy eyes ( $28.6 \mu\text{m}$ ) ( $P < 0.001$ ) (Fig. 2.3.4, cf. A and B). In images obtained with ECC, this difference was not statistically significant (glaucoma eyes and healthy eyes:  $17.3 \mu\text{m}$  and  $16.0 \mu\text{m}$ , respectively;  $P = 0.22$ ). In addition, the amount of retardation in the temporal region in healthy and ocular hypertensive eyes measured with VCC was statistically significantly ( $P = 0.006$ ,  $\alpha = 0.013$ , 4 comparisons) correlated with the amount of residual anterior segment birefringence (Table 2.3.5). In the nasal region, this correlation was of borderline significance ( $P = 0.016$ ,  $\alpha = 0.013$ , 4 comparisons). With ECC, no relationship was apparent between measured peripapillary retardation and residual anterior segment birefringence (Table 2.3.5). These data suggest that

some of the differences between VCC and ECC were due to an artifactual increase in RNFL retardation in the temporal and nasal regions and decrease in certain sectors of the superior and inferior regions caused by the compensation residual with VCC.

The AUCs of the four clinically used parameters obtained with SLP-VCC and with SLP-ECC have been presented in Table 2.3.6. The AUCs of the parameters TSNIT Average and Inferior Average were statistically significantly larger ( $P = 0.004$  and  $P = 0.002$ , respectively;  $\alpha = 0.013$ , 4 comparisons) for measurements with ECC than with VCC. No statistically significant difference between measurements with VCC and ECC was found for the other two parameters.

## Discussion

We have currently presented a new method, called ECC, that improves the signal to noise ratio of RNFL retardation measurements with SLP by shifting the measurements to a more sensitive detection range of the instrument. The shift is made by introducing a preset measurement bias that is afterwards mathematically removed from the measurements. Measurements obtained with ECC appeared to represent the expected RNFL morphology better than or otherwise as well as those made with standard VCC. ECC may be implemented in the current GDx VCC simply by a software upgrade.

With ECC, atypical retardation patterns were less frequent. As VCC scans with an atypical retardation pattern may be difficult to interpret clinically, we suspect that more glaucoma patients and glaucoma suspects may be assessed reliably with ECC. The origin of atypical scans is not yet fully understood. However, it appears to be associated with a low signal-to-noise ratio. In areas of low retardation (i.e., where the RNFL is thin), the measurements are susceptible to both optical and electronic noise. By introducing and later removing a preset measurement bias, the instrument's measurement sensitivity is enhanced, thereby reducing its susceptibility to such errors. This may explain why atypical retardation is reduced with ECC.

By mathematically removing the induced bias in images obtained with this method, the residual of anterior segment birefringence compensation was also reduced with ECC compared to VCC. With VCC, the RNFL morphology appeared rotated in some eyes, probably due to the interaction between RNFL retardation and residual anterior segment retardation. In addition, the residual anterior segment birefringence in VCC images, with its mean axis close to the horizontal, artifactualy increased retardation in the temporal and nasal parapapillary regions and reduced retardation in the superior and inferior regions where the nerve fiber bundles are nearly perpendicular to the slow axis of the compensation residual. Because the images were better compensated with ECC than with VCC, ECC may improve computer-assisted analysis of RNFL

loss, such as the automated detection of localized RNFL defects,<sup>20</sup> which may aid clinicians in the interpretation of the polarimetry data.

With less residual anterior segment birefringence, ECC may also improve the instrument's accuracy for diagnosing and monitoring glaucoma. In fact, we showed that the diagnostic accuracy of the parameters TSNIT Average and Inferior Average for discriminating between healthy eyes and eyes with glaucoma was higher in measurements with ECC than with VCC. As we presently included mostly patients with glaucoma of moderate to severe severity, future studies may address whether the diagnostic accuracy of ECC has also improved over VCC in patients with mild glaucomatous damage. Of note, the AUCs that we presently found for VCC and ECC may both have been favorably biased by the statistically significant difference in age between healthy subjects and patients with glaucoma. Future studies need to determine the diagnostic accuracy in an age-matched population.

The SLP retardation measurement floor appeared to be lower with ECC than with VCC. Therefore, we think that the dynamic range of measurements may be larger with ECC. With a larger dynamic range, ECC SLP then might increase the ability to monitor glaucoma patients over a longer time period. The ability to monitor glaucomatous thinning of the RNFL over time also depends on the reproducibility of measurements and sensitivity of a device to measuring small changes. Therefore, follow-up studies in eyes with, especially, more advanced RNFL loss will have to show whether the detection of progressive damage has indeed improved with ECC.

With VCC, the Temporal Average was higher in glaucomatous eyes than in healthy ones, which was most likely due to measurement artifacts. In ECC, we found no difference in RNFL retardation between healthy and glaucomatous eyes in the nasal and temporal segments. One would have expected glaucomatous eyes to have a thinner RNFL in these regions as well, especially in advanced glaucomatous eyes. The source of this retardation, whether it is biological or artifactual, remains to be investigated. Alternative techniques, such as polarization sensitive optical coherence tomography (PS-OCT)<sup>4</sup> may be employed to provide additional insight. In addition, small atypical retardation patches still remained in some images obtained with ECC (e.g., Fig. 2.3.1D), which should also be investigated in the future.

The dynamic range of the SLP system in the GDx VCC is a quarter of its laser's wavelength, i.e., approximately 195 nm. However, the maximum amount of retardation measured by the GDx VCC is 130 nm, which is a software-set limit. If in a given eye, the total amount of retardation induced by the RNFL and the 55 nm retardation bias were to exceed 130 nm, the measured values would be cropped at 130 nm. In such a case, measurement with the standard

VCC method would be recommended. However, such cases are rarely observed. In addition, such an eye is unlikely to have a critically thinned RNFL.

In conclusion, ECC appears to yield improved SLP images of the RNFL, compared to VCC, which may allow clinicians a more accurate assessment of the retinal nerve fiber layer with the GDx VCC for diagnosing and monitoring glaucoma.

## References

1. Quigley HA. Neuronal death in glaucoma. *Prog Retin Eye Res.* 1999;18:39-57.
2. Knighton RW, Huang X, Zhou Q. Microtubule contribution to the reflectance of the retinal nerve fiber layer. *Invest Ophthalmol Vis Sci.* 1998;39:189-93.
3. Weinreb RN, Dreher AW, Coleman A, et al. Histopathologic validation of Fourier-ellipsometry measurements of retinal nerve fiber layer thickness. *Arch Ophthalmol.* 1990;108:557-60.
4. Cense B, Chen TC, Park BH, Pierce MC, De Boer JF. Thickness and birefringence of healthy retinal nerve fiber layer tissue measured with polarization-sensitive optical coherence tomography. *Invest Ophthalmol Vis Sci.* 2004;45:2606-12.
5. Huang XR, Bagga H, Greenfield DS, Knighton RW. Variation of peripapillary retinal nerve fiber layer birefringence in normal human subjects. *Invest Ophthalmol Vis Sci.* 2004;45:3073-80.
6. Greenfield DS, Knighton RW, Huang XR. Effect of corneal polarization axis on assessment of retinal nerve fiber layer thickness by scanning laser polarimetry. *Am J Ophthalmol.* 2000;129:715-22.
7. Weinreb RN, Bowd C, Greenfield DS, Zangwill LM. Measurement of the magnitude and axis of corneal polarization with scanning laser polarimetry. *Arch Ophthalmol.* 2002;120:901-6.
8. Zhou Q, Weinreb RN. Individualized compensation of anterior segment birefringence during scanning laser polarimetry. *Invest Ophthalmol Vis Sci.* 2002;43:2221-8.
9. Reus NJ, Colen TP, Lemij HG. Visualization of localized retinal nerve fiber layer defects with the GDx with individualized and with fixed compensation of anterior segment birefringence. *Ophthalmology.* 2003;110:1512-6.
10. Reus NJ, Lemij HG. Diagnostic accuracy of the GDx VCC for glaucoma. *Ophthalmology.* 2004;111:1860-5.
11. Medeiros FA, Zangwill LM, Bowd C, Weinreb RN. Comparison of the GDx VCC scanning laser polarimeter, HRT II confocal scanning laser ophthalmoscope, and Stratus OCT optical coherence tomograph for the detection of glaucoma. *Arch Ophthalmol.* 2004;122:827-37.
12. Tannenbaum DP, Hoffman D, Lemij HG, et al. Variable corneal compensation improves discrimination between normal and glaucomatous eyes with the scanning laser polarimeter. *Ophthalmology.* 2004;111:259-64.
13. Reus NJ, Lemij HG. The relationship between standard automated perimetry and GDx VCC measurements. *Invest Ophthalmol Vis Sci.* 2004;45:840-5.

14. Schlottmann PG, De Cilla S, Greenfield DS, Caprioli J, Garway-Heath DF. Relationship between visual field sensitivity and retinal nerve fiber layer thickness as measured by scanning laser polarimetry. *Invest Ophthalmol Vis Sci.* 2004;45:1823-9.
15. Zhou Q, Reed J, Betts RW, et al. Detection of glaucomatous retinal nerve fiber layer damage by scanning laser polarimetry with custom corneal compensation. *Proc SPIE Int Soc Opt Eng.* 2003;4951:32-41.
16. Knighton RW, Huang XR. Analytical methods for scanning laser polarimetry. *Opt Exp.* 2002;10:1179-89.
17. Zhou Q. Retinal scanning laser polarimetry and methods to compensate for corneal birefringence. 2004 report of the Belgium Ophthalmology Societies - New optics of the human eye (in press). 2004.
18. Bagga H, Greenfield DS, Feuer WJ. Quantitative assessment of atypical birefringence images using scanning laser polarimetry with variable corneal compensation. *Am J Ophthalmol.* 2005;139:437-46.
19. DeLong ER, DeLong DM, Clarke-Pearson DL. Comparing the areas under two or more correlated receiver operating characteristic curves: a nonparametric approach. *Biometrics.* 1988;44:837-45.
20. Vermeer KA, Vos FM, Lemij HG, Vossepoel AM. Detecting glaucomatous wedge shaped defects in polarimetric images. *Med Image Anal.* 2003;7:503-11.





# 3

## Diagnostic accuracies for glaucoma



## 3.1 Diagnostic accuracy of the GDx VCC for glaucoma

---

**Purpose:** To determine the diagnostic accuracy of the GDx VCC in the diagnosis of glaucoma.

**Design:** Prospective comparative observational clinic-based case series.

**Participants:** One eye each of 77 healthy subjects and 162 patients with primary open-angle glaucoma of Caucasian ethnic origin. Healthy subjects had normal visual fields, healthy-looking optic discs, and intraocular pressures  $\leq 21$  mmHg in both eyes. Glaucoma patients had a reproducible glaucomatous visual field defect and a glaucomatous appearance of the optic disc in at least one eye.

**Methods:** All subjects were measured with the GDx VCC with automated variable corneal compensator. We constructed receiver operating characteristic (ROC) curves for all available parameters. Subsequently, we calculated sensitivity, specificity, and multilevel likelihood ratios for the best discriminating parameter in the entire group. In addition, we calculated sensitivity and specificity in patients with mild, moderate, and severe glaucomatous damage, separately.

**Main outcome measures:** Software-derived parameters 'TSNIT Average', 'Superior Average', 'Inferior Average', 'TSNIT Std. Dev.', and 'Nerve Fiber Indicator' (NFI).

**Results:** The areas under the ROC curves for 'TSNIT Average', 'Superior Average', 'Inferior Average', 'TSNIT Std. Dev.', and NFI were 0.93, 0.94, 0.90, 0.92, and 0.98, respectively. For the best discriminating parameter NFI, the sensitivity and specificity with a cut-off point of  $\geq 40$  were 89.0% and 95.9%, respectively. The multilevel likelihood ratios for glaucoma at NFI values  $< 35$  was 0.07, between 35 and 44, 1.30, and at values  $\geq 44$ , 61.50. At the cut-off level of  $\geq 40$ , the sensitivities of the NFI for correctly identifying glaucoma patients with mild, moderate, and severe damage were 83.8%, 92.9%, and 90.1%, respectively.

**Conclusions:** The GDx VCC allowed easy, rapid, and accurate discrimination between healthy and glaucomatous eyes. The NFI was the best discriminating parameter. We think that the GDx VCC fulfills criteria for a glaucoma screening device. *Ophthalmology* 2004;110:1860-1865.

---

Primary open-angle glaucoma (POAG) is an acquired progressive optic neuropathy, with atrophy of retinal ganglion cells (RGCs) and their axons, leading to loss of visual function.<sup>1</sup> In clinical practice, the diagnosis of POAG is often based on a characteristic appearance of the optic nerve head<sup>2</sup> and typical visual field defects,<sup>3</sup> in addition to open anterior chamber

angles and absence of known other explanations for glaucomatous optic nerve atrophy.<sup>4</sup> Evaluation of the retinal nerve fiber layer (RNFL) may greatly facilitate and support the clinical diagnosis of glaucoma.<sup>5-7</sup> Localized and/or diffuse changes of the RNFL, visible with either ophthalmoscopy or red-free fundus photography, almost always indicate abnormality.<sup>8,9</sup> In addition, RNFL defects have been reported to be one of the earlier signs of glaucoma.<sup>8,10,11</sup> However, the RNFL is not routinely evaluated by clinicians to diagnose glaucoma, as a good view on the RNFL may be difficult to obtain in many patients. In addition, grading the degree of loss may be difficult and highly subjective.<sup>12</sup>

The RNFL may be evaluated more easily with scanning laser polarimetry (SLP). This technique, featured in the GDx VCC (Laser Diagnostic Technologies, Inc., San Diego, CA, USA), estimates the thickness of the peripapillary RNFL by measuring the summed retardation of a polarized scanning laser beam, presumably induced by the form-birefringent microtubules supporting the RGC axons.<sup>13,14</sup> The GDx VCC is equipped with a so-called variable corneal compensator (VCC), allowing eye-specific compensation of the birefringent effects of the cornea and, to a lesser degree, the lens. A previous commercially available scanning laser polarimeter, the GDx NFA (Laser Diagnostic Technologies, Inc., San Diego, CA, USA), was equipped with a fixed corneal compensator (FCC), that sometimes lead to spurious measurements<sup>15</sup> due to incomplete compensation of anterior segment birefringence.<sup>16-18</sup> Equipped with a VCC, however, SLP has been shown to match the appearance of the RNFL by red-free fundus photography.<sup>15</sup> In addition, SLP with a prototype VCC has been shown to discriminate better between healthy subjects and glaucoma patients than SLP with FCC.<sup>19</sup> The commercially available GDx VCC features an automated VCC, a 20° x 20° field of view of the parapapillary RNFL, easy and rapid administration, and easy and objective interpretation of the measurements. In the present study, we determined the accuracy of measurements with the GDx VC for diagnosis of glaucoma.

## Methods

### Subjects

Seventy-seven healthy subjects and 162 glaucoma patients were measured with the GDx VCC (Laser Diagnostic Technologies, Inc., San Diego, CA, USA) between September 2002 and September 2003 by three experienced operators at the Perimetry Department of The Rotterdam Eye Hospital. Healthy subjects were recruited either consecutively from an ongoing longitudinal follow-up study (n=48) or from employees of The Rotterdam Eye Hospital and their spouses and friends (n=29). All healthy subjects had a Glaucoma Hemifield Test of 'Within normal limits' and no nerve fiber bundle abnormalities<sup>3</sup> on the total and/or pattern deviation probability plots with standard automated perimetry (SAP; Humphrey Field Analyzer, 24-2 SITA-Standard test program, Carl Zeiss Meditec, Dublin, CA, USA). In addition, they had healthy-looking optic discs and an intraocular pressure of 21 mmHg or less in both eyes, measured with Goldmann

applanation tonometry. Only subjects with open angles by gonioscopy were entered into the study. Slit lamp examination was unremarkable in all eyes. All subjects were of Caucasian ethnic origin and had a best corrected visual acuity of 20/40 or better. None had any significant history of ocular disease (including posterior segment eye disease and corneal disease), a history of intra-ocular surgery (except for uncomplicated cataract surgery), relatives in the first and/or second degree with glaucoma, systemic hypertension for which medication was used, diabetes mellitus, or any other systemic disease. One eye per subject was randomly chosen for analysis.

Glaucoma patients were recruited consecutively from an ongoing longitudinal follow-up study at The Rotterdam Eye Hospital (n=149) or after referral by a glaucoma specialist (HGL) for clinical reasons (n=13). All glaucoma patients had POAG, i.e. a glaucomatous appearance of the optic disc in at least one eye with a corresponding reproducible glaucomatous nerve fiber bundle abnormality<sup>3</sup> on the total and/or pattern deviation probability plots with SAP, and open angles by gonioscopy. Slit lamp examination was unremarkable in all eyes. All patients were of Caucasian ethnic origin and had a best corrected visual acuity of 20/40 or better. None had any other significant history of ocular disease (including posterior segment eye disease and corneal disease), a history of intra-ocular surgery (except for uncomplicated cataract and glaucoma surgery), systemic hypertension for which medication was used, diabetes mellitus, or any other systemic disease. Only one eye per patient was used for analysis. If both eyes showed glaucomatous damage, the one with the more positive mean deviation (MD) in perimetry was used.

The research followed the tenets of the Declaration of Helsinki. Informed consent was obtained from the subjects after explanation of the nature and possible consequences of the study. The institutional human experimentation committee had approved the research.

### **Measurement protocol**

In all subjects, both eyes were scanned with the GDx VCC, starting with the right eye. The spherical equivalent refractive error of each eye was entered into the software to allow the GDx VCC to focus on the retina. If necessary, the focus was adjusted manually in 0.25 diopters steps. The pupils of the patients were undilated and the room lights were left on. The patient's face was gently placed into the face mask of the GDx VCC. To maintain the same orientation of the slow axes of the birefringent structures in the eye to that of the instrument's compensator, the operator saw to it that patients had their heads as vertical as possible during all measurements. For each scan, the operator aligned the instrument with the cornea and the sclera of the measured eye. First, anterior segment birefringence was assessed for each eye per subject with the method described by Zhou and Weinreb.<sup>20</sup> To this end, the magnitude of the compensator of the GDx VCC was automatically set to zero after which the fundus was scanned. The interaction between the birefringence of the radially oriented axons of the photoreceptors that constitute Henle's fiber layer in the macula, and the anterior segment birefringence, resulted in a bow-tie shaped pattern

on the retardation image. The amount of retardation was measured from within a circular band with an inner diameter of 20 pixels (~0.9 mm in an emmetropic eye) that had been positioned manually at the center of the fovea. A dedicated algorithm, incorporated into the GDx VCC software, then determined the anterior segment birefringence (consisting of corneal polarization magnitude [CPM] and corneal polarization axis [CPA]) from this profile.

The software used these calculations to automatically adjust the anterior segment compensator to each individual eye, and both eyes were scanned again with individualized compensation. Adequate compensation of anterior segment birefringence was verified subjectively by looking at the retardation pattern in the macular region that had to be uniformly weak with a cross- or donut-shaped pattern. The typical time to measure both eyes of a patient was 3 minutes. All scans were of high quality, i.e. with a centered optic disc, well-focused, even and just illuminated throughout the image, and without any motion artifacts. Four of the 77 (5.2%) healthy subjects and 12/162 (7.4%) glaucoma patients were excluded from analysis as their measurements were flagged by the GDx VCC software as 'Results may not be compatible with normative database'. In addition, 4/162 (2.5%) glaucoma patients were excluded because high quality images could not be obtained because of poor fixation (2) or because images were too dark to obtain a good measurement (2). All other measurements passed the four scan quality checks that were automatically performed by the GDx VCC software, i.e. 'Alignment', 'Fixation' (including eye movements), 'Refraction', and 'Other' (including the amount of illumination). Seventy-three of the 77 (94.8%) healthy subjects and 146/162 (90.1%) glaucoma patients were used for analysis in the present study.

### Data analysis

The margin of the optic disc was manually marked with an ellipse on a reflection image of the fundus. The GDx VCC software positioned a circle, 8 pixels wide (~0.4mm in an emmetropic eye) and with an inner diameter of 54 pixels (~2.5mm in an emmetropic eye), centered on the center of the ellipse. Based on the retardation values within this band, the software calculated the following 5 parameters: 'TSNIT Average', 'Superior Average', 'Inferior Average', 'TSNIT Std. Dev.', and 'Nerve Fiber Indicator' (NFI) (Table 3.1.1). A 6th parameter, called 'Inter-Eye Symmetry' that describes the correlation between the two eyes of a subject, could not be calculated in the present study as we included only one eye per patient. Statistical analysis was performed with the computer program SPSS for Windows (release 11.0.1; SPSS, Chicago, IL, USA). We classified the glaucoma patients by the severity of their visual field damage with SAP using the Hodapp-Anderson-Parrish grading scale: 37 patients had a mild glaucomatous defect, 28 a moderate one, and 81 a severe one.<sup>21,22</sup> We constructed receiver operating characteristic (ROC) curves for the 5 GDx VCC parameters. Areas under the ROC curve (AUCs) were classified as follows: >0.9, high accuracy; 0.7-0.9, moderate accuracy; 0.5-0.7, low accuracy; 0.5, chance

Parameter	Description
TSNIT Average	Average retardation beneath the measurement ellipse
Superior Average	Average retardation beneath the measurement ellipse in the superior sector
Inferior Average	Average retardation beneath the measurement ellipse in the inferior sector
TSNIT Std. Dev.	Standard deviation from the average of the retardation beneath the measurement ellipse
Nerve Fiber Indicator	Support vector-machine derived algorithm trained to discriminate between healthy and glaucomatous eyes. Possible values range from 1–100

**Table 3.1.1.** Description of the 5 evaluated GDx VCC parameters.

result.<sup>23</sup> The 95% confidence intervals (CIs) for the AUCs were calculated as the point estimate of the AUC  $\pm 1.96 \cdot$  standard error. Differences in AUCs between the parameter with the highest area and the other parameters were tested for statistical significance with the paired samples test described by DeLong et al.<sup>24</sup> In addition, we determined the sensitivity and specificity of the parameter with the highest AUC for the entire sample and for the subgroups for three different cut-off criteria. The 95% CIs for sensitivity and specificity were approximated with the formula  $p \pm 1.96 \cdot \sqrt{p(1-p)/n}$ , where  $p$  represents either sensitivity or specificity,  $n$  is the sample size, and  $n \times p$  is  $>10$ .<sup>25</sup> In addition to using a single cut-off value to discriminate between healthy and glaucomatous eyes, with potential loss of diagnostic information contained within continuous numeric test results, we determined multilevel likelihood ratios for the best discriminating parameter.<sup>26</sup> To this end, outcome values of this parameter were grouped into three ordinal strata. Subsequently, likelihood ratios (LRs) were calculated for each rank with the formula  $(G_{rank} / G_{total}) / (N_{rank} / N_{total})$ , with  $G_{rank}$  = the number of glaucoma patients in a rank,  $G_{total}$  = the total number of glaucoma patients,  $N_{rank}$  = the number of healthy subjects in a rank, and  $N_{total}$  = the total number of healthy subjects. The 95% CIs for the multilevel likelihood ratios were approximated with the formula  $LR \times e^{\pm 1.96 \cdot \sqrt{(1-p_0)/(n_0p_0) + (1-p_1)/(n_1p_1)}}$ , where  $p_0 = N_{rank} / N_{total}$ ,  $n_0 = N_{total}$ ,  $p_1 = G_{rank} / G_{total}$ , and  $n_1 = G_{total}$ .

## Demographics

The demographics of the healthy subjects and the glaucoma patients have been presented in table 3.1.2. Differences in demographics between the two groups were tested for statistical significance with the unpaired samples  $t$  test.<sup>27</sup> CPM was statistically significantly associated with age in the healthy subjects (Spearman's rank correlation coefficient,  $-0.35$ ;  $P = 0.003$ ). CPA was not statistically significantly associated with age in the healthy subjects (Spearman's rank correlation coefficient,  $-0.067$ ;  $P = 0.57$ ).

The parameters 'Superior Average' and 'TSNIT Std. Dev.' were statistically significantly associated with age in the healthy subjects when described with linear regression analysis (slopes,  $-0.196 \mu\text{m}\cdot\text{year}^{-1}$  [ $P = 0.011$ ] and  $-0.088 \mu\text{m}\cdot\text{year}^{-1}$  [ $P = 0.026$ ], respectively). The parameters 'TSNIT

	Unit	Healthy subjects	Glaucoma patients	<i>P</i>
Age (SD; range)	Years	59 (11; 35 – 82)	61 (10; 30 – 77)	0.11
Gender, men (%)	NA	34 (47)	81 (56)	
Eye, OD (%)	NA	33 (45)	74 (51)	
MD (SD; range)	Decibels	0.39 (1.13; -2.89 – +2.90)	-8.45 (6.81; -29.13 – +1.25)	< 0.001
PSD (SD; range)	Decibels	1.63 (0.40; 1.00 – 3.47)	8.13 (3.88; 1.99 – 16.43)	< 0.001
CPA (median; SD; range)	Degrees	18.5 (15.1; 13.9; -2.3 – +56.5)	18.0 (16.3; 15.7; -12.8 – +75.9)	0.83
CPA, residual (SD; range)	Degrees	7.8 (15.9; -44.9 – +51.3)	10.0 (19.9; -98.5 – +70.0)	0.41
CPM (median; SD; range)	nm	40.3 (39.0; 12.4; 7.0 – 74.0)	36.8 (36.0; 13.2; 9.0 – 77.0)	0.058
CPM, residual (SD; range)	nm	5.9 (2.0; 0.0 – 9.0)	5.8 (2.5; 0.0 – 20.0)	0.67

**Table 3.1.2.** Demographics of healthy subjects (n=73) and glaucoma patients (n=146).

CPA = corneal polarization axis; CPM = corneal polarization magnitude; MD = mean deviation; NA = not applicable; PSD = pattern standard deviation; SD = standard deviation.

Differences between groups were tested for statistical significance with an unpaired samples *t* test.



	Unit	Healthy subjects	Glaucoma patients			
			All	Mild	Moderate	Severe
TSNIT Average	μm	54.8 (53.4-56.1)	40.4 (39.2-41.7)	43.8 (42.0-45.6)	40.4 (37.6-43.2)	38.9 (37.1-40.7)
Superior Average	μm	66.7 (65.0-68.4)	46.1 (44.4-47.9)	51.2 (48.3-54.1)	44.0 (40.5-47.5)	44.5 (42.0-47.1)
Inferior Average	μm	61.5 (59.4-63.6)	44.1 (42.5-45.7)	47.8 (45.4-50.3)	45.2 (41.1-49.2)	42.1 (39.7-44.4)
TSNIT Std. Dev.	μm	20.0 (19.2-20.9)	12.8 (12.2-13.4)	14.6 (13.3-16.0)	11.8 (10.4-13.3)	12.3 (11.5-13.0)
NFI	NA	21.1 (19.2-23.1)	67.3 (63.7-70.8)	55.1 (49.1-61.2)	69.5 (61.0-78.1)	72.0 (67.3-76.7)

**Table 3.1.3.** Mean (95% confidence interval) values of 5 GDx VCC parameters for healthy subjects and glaucoma patients with varying severity of visual field loss (classified with the Hodapp-Anderson-Parrish grading scale).

NA = not applicable; NFI = Nerve Fiber Indicator.

All parameters were statistically significantly different between healthy subjects and glaucoma patients with mild, moderate, and severe loss (unpaired samples *t* test,  $P < 0.001$ ).

Average', 'Inferior Average', and NFI were not statistically significantly associated with age when described with linear regression analysis (slopes  $-0.094 \mu\text{m}\cdot\text{year}^{-1}$  [ $P = 0.13$ ],  $-0.156 \mu\text{m}\cdot\text{year}^{-1}$  [ $P = 0.10$ ], and  $0.172 \mu\text{m}\cdot\text{year}^{-1}$  [ $P = 0.052$ ], respectively).

## Results

The mean values of the 5 evaluated GDx VCC parameters were all statistically significantly different between healthy subjects and glaucoma patients with mild, moderate, and severe loss (Table 3.1.3). The NFI was the best parameter to discriminate between healthy and glaucomatous eyes with a high accuracy (area under the ROC curve, 0.98; standard error [SE], 0.007; 95%

	MD (decibels) (SD)	Area under the ROC curve (SE; 95% CI)	Sensitivity (%) (95% CI)	Specificity (%) (95% CI)
All	-8.45 (6.81)	0.98 (0.007; 0.97-1.00)	89.0 (83.9-94.1)	95.9 (91.4-100.0)
Mild	-2.01 (1.65)	0.96 (0.022; 0.92-1.00)	83.8 (71.9-95.7)	
Moderate	-5.44 (2.30)	0.99 (0.008; 0.97-1.00)	92.9 (83.4-100.0)	
Severe	-12.43 (6.53)	0.99 (0.006; 0.98-1.00)	90.1 (83.6-96.6)	

**Table 3.1.4.** Diagnostic accuracy, expressed as area under the receiver operating characteristic (ROC) curve, sensitivity, and specificity, for the GDx VCC parameter Nerve Fiber Indicator (NFI) for discriminating between healthy eyes and eyes with mild, moderate, and severe glaucomatous damage (classified with the Hodapp-Anderson-Parrish grading scale), at a fixed specificity of 95.9% with a cut-off point of  $\geq 40$ .

CI = confidence interval; MD = mean deviation; SD = standard deviation; SE = standard error.

NFI	Healthy subjects (%)	Glaucoma patients (%)	Multilevel likelihood ratio (95% CI)
<35	67 (92)	10 (7)	0.07 (0.04-0.14)
35-44	5 (7)	13 (9)	1.30 (0.48-3.51)
≥44	1 (1)	123 (84)	61.50 (8.77-431.31)

**Table 3.1.5.** Number of healthy subjects and glaucoma patients and corresponding multilevel likelihood ratios for glaucoma with Nerve Fiber Indicator (NFI) values <35, between 35 and 44, and ≥44. CI = confidence interval.

CI, 0.97-1.00). For the parameters ‘TSNIT Average’, ‘Superior Average’, ‘Inferior Average’, and ‘TSNIT Std. Dev.’, the AUCs (SE; 95% CI) were 0.93 (0.015; 0.90-0.96), 0.94 (0.015; 0.91-0.97), 0.90 (0.020; 0.86-0.94), and 0.92 (0.019; 0.88-0.95), respectively. The AUC of NFI was statistically significantly larger than of the other parameters ( $P < 0.001$ ).

With cut-off points for the NFI of ≥35, ≥40, and ≥44, sensitivities and specificities were 93.2% and 91.8%, 89.0% and 95.9%, and 84.2% and 98.6%, respectively (see also table 3.1.4). The multilevel likelihood ratios for glaucoma at NFI values <35 was 0.07, between 35 and 44, 1.30, and at values ≥44, 61.50 (Table 3.1.5).

For glaucoma patients with mild, moderate, and severe glaucomatous loss, the sensitivities of the NFI with a cut-off point of ≥40 were 83.8%, 92.9%, and 90.1%, respectively, at a specificity of 95.9% (Table 3.1.4)

## Discussion

We found that GDx VCC parameters discriminate well between healthy and glaucomatous eyes. The NFI appeared to be the best parameter in classifying glaucoma. The GDx VCC readily identified glaucoma patients with moderate and severe visual field loss. For patients with mild visual field loss, its sensitivity was somewhat lower.

SLP with a prototype VCC has been shown to have a markedly improved diagnostic accuracy over SLP with fixed corneal compensation. Weinreb et al<sup>19</sup> reported an area under the ROC curve for the parameter ‘Superior Average’ of 0.68 for SLP with fixed compensation. With their prototype VCC, the area under the ROC curve statistically significantly increased to 0.83.<sup>19</sup> The commercially available GDx VCC, with its proprietary parameter NFI, may discriminate even better between healthy and glaucomatous eyes.

In the present study, we assessed the diagnostic accuracy of 5 single parameters. Usually, GDx VCC measurements of a subject’s right and left eye are presented to the clinician on a printout that includes fundus images, color-coded retardation maps, the 5 presently evaluated parameters,

a parameter describing the symmetry between eyes, and a so-called TSNIT graph, representing the retardation beneath the measurement circle. In such a printout, data are presented both as raw measurements and in comparison with a normative database. Colen et al<sup>28</sup> have shown for the GDx NFA that judgment of such a printout as a whole resulted in a better separation between normal and glaucomatous eyes than single parameters. We therefore expect that an assessment of the entire printout will further improve the high accuracy of the GDx VCC.

Diagnostic accuracy is often presented in terms of sensitivity and specificity. Clinically, however, likelihood ratios may be more useful as they provide information about the probability that a patient with a given test result actually has the disease. In the present study, we found a multilevel likelihood ratio for glaucoma of 0.07 with an NFI <35, indicating that an NFI value below 35 occurs 14 times more often in healthy subjects than in glaucoma patients. The multilevel likelihood ratio for glaucoma with an NFI  $\geq 44$  was 61.50, indicating that an NFI value  $\geq 44$  occurs over 60 times more often in glaucoma patients than in healthy subjects. These data suggest that glaucoma subjects rarely have an NFI <35 and healthy subjects will almost never have an NFI  $\geq 44$ . For NFI values between 35 and 44, however, the multilevel likelihood ratio was close to one, indicating that such a test result is almost equally likely to occur among patients with glaucoma as in healthy individuals. In such a case, other data in the GDx VCC printout may be indicative of the diagnosis of glaucoma. Future studies will have to address the accuracy of a subjective interpretation of the entire printout.

We found that the sensitivity of the GDx VCC for detecting severe stages of glaucoma was slightly lower than for detecting moderate stages. In the present study, we classified glaucoma patients using the Hodapp-Anderson-Parrish grading scale.<sup>21,22</sup> This classification takes into account the size of the glaucomatous visual field defect, depth of the defect, and proximity of the defect to fixation, which may closely reflect a clinician's interpretation of visual field loss.<sup>21,22</sup> For example, a patient with a small localized RNFL defect resulting in visual field loss close to fixation will be classified as having severe glaucomatous loss as the threatening loss of central vision calls for more aggressive therapy. However, the localized RNFL defect may be difficult to be identified by the NFI, resulting in a lower sensitivity. If severe damage had been defined as an MD below -12 dB, the sensitivity of the NFI for detecting severe glaucomatous damage would have been 100%. Two of the 5 presently analyzed parameters were statistically significantly associated with age when described with linear regression analysis. However, the slopes of the regression lines were very shallow compared to the values found in healthy subjects and glaucoma patients. Therefore, we speculate that the minor, and not statistically significant, age difference between the two groups was not of any significance to the results of our study.

In the present study, we were unable to assess the influence of clinically significant cataract on the diagnostic accuracy of the GDx VCC, as we did not include subjects with cataract who had a visual acuity below 20/40. However, we speculate that cataract will have little effect as Kremmer et al<sup>29</sup> have shown that useful RNFL measurements can be made with SLP in eyes with cataract down to a visual acuity of approximately 20/160 to 20/125.<sup>29</sup> In addition, possible changes in birefringence of the cataractous lens that could distort RNFL measurements,<sup>29</sup> are presumably neutralized with SLP equipped with a VCC when compensating an eye's anterior segment birefringence.

The overall high diagnostic accuracy of the GDx VCC that we presently found may have been biased by our including patients with relatively moderate to severe glaucomatous damage (mean MD, -8.45 dB). In addition, we analyzed subjects without co-morbidity, which may have increased the diagnostic accuracy somewhat favorably. Furthermore, the validity of our results may be limited to patients with well-defined POAG, as we included only patients with a glaucomatous appearance of their optic nerve heads and corresponding marked visual field losses. In the ocular hypertension treatment study, visual field loss has been reported to sometimes precede prominent glaucomatous changes in the optic nerve head.<sup>30</sup> Patients without apparent structural damage may be more difficult to be identified by the GDx VCC, as SLP evaluates a structural characteristic. The diagnostic accuracy in these patients may be lower than we found in the present study. Conversely, patients with pre-perimetric glaucoma may perhaps be identified more easily.

Approximately 7% of the measured subjects were excluded from analysis as their measurements were deemed by the GDx VCC software not to be compatible with its normative database. In these subjects, an atypical pattern of retardation was apparent on the retardation images. Although the origin of such retardation is unknown, measurements with polarization sensitive OCT suggest that it may originate from subretinal structures (De Boer JF, et al. *IOVS* 2003;44: ARVO E-Abstract 3388). If these subjects had been included in the analysis, the diagnostic accuracy of the NFI with a cut-off point of  $\geq 40$  would have decreased only little. The specificity would have decreased from 95.9% to 92.2%, the sensitivity would have decreased from 89.3% to 88.6%, and the area under the ROC curve would have remained 0.98.

Our present data suggest that the GDx VCC may fulfill all reported non-financial requirements for a screening device for glaucoma.<sup>31</sup> Its accuracy exceeds the required 85% sensitivity and 95% specificity for detecting moderate to severe glaucomatous damage.<sup>31</sup> In addition, the GDx VCC features ease of administration, short testing and processing time, and ease of interpretation of the results. The usefulness of the GDx VCC for screening depends on the positive and negative

predictive values and the costs, not necessarily financial, of false positive and false negative results. Positive and negative predictive values are highly dependent of the prevalence of a disease. The positive predictive value represents the proportion of test positive people who truly have the disease. Conversely, the negative predictive value represents the proportion of test negative people who truly do not have the disease. If our results were applicable to a general Caucasian population, with an estimated prevalence of glaucoma of approximately 2% (range 0.8%-3.2%, depending on the definition),<sup>32</sup> one could calculate that the predictive value of an abnormal GDx VCC scan (NFI  $\geq 40$ ; sensitivity, 89.0%; specificity, 95.9%) would be 31%. These results then indicate that, for every correctly identified glaucoma patient, 3 suspects will have to be evaluated. Because of the low prevalence of glaucoma, the predictive value of a negative test result (NFI  $< 40$ ) would be almost 100%. In different populations, other values may apply. In conclusion, we have shown that the GDx VCC allowed easy, rapid, and accurate discrimination between healthy and glaucomatous eyes. Furthermore, we think that the GDx VCC fulfills all non-financial criteria for a glaucoma screening device.

## References

1. Quigley HA. Neuronal death in glaucoma. *Prog Retin Eye Res* 1999;18:39-57.
2. Jonas JB, Budde WM, Panda-Jonas S. Ophthalmoscopic evaluation of the optic nerve head. *Surv Ophthalmol* 1999;43:293-320.
3. Keltner JL, Johnson CA, Cello KE, et al. Classification of visual field abnormalities in the ocular hypertension treatment study. *Arch Ophthalmol* 2003;121:643-50.
4. American Academy of Ophthalmology. Preferred practice pattern. Primary open angle glaucoma. San Francisco, CA: American Academy of Ophthalmology, 2000.
5. Tuulonen A, Airaksinen PJ, Erola E, et al. The Finnish evidence-based guideline for open-angle glaucoma. *Acta Ophthalmol Scand* 2003;81:3-18.
6. Quigley HA, Miller NR, George T. Clinical evaluation of nerve fiber layer atrophy as an indicator of glaucomatous optic nerve damage. *Arch Ophthalmol* 1980;98:1564-71.
7. Jonas JB, Dichtl A. Evaluation of the retinal nerve fiber layer. *Surv Ophthalmol* 1996;40:369-78.
8. Tuulonen A, Lehtola J, Airaksinen PJ. Nerve fiber layer defects with normal visual fields. Do normal optic disc and normal visual field indicate absence of glaucomatous abnormality? *Ophthalmology* 1993;100:587-97.
9. Jonas JB, Schiro D. Localised wedge shaped defects of the retinal nerve fibre layer in glaucoma. *Br J Ophthalmol* 1994;78:285-90.
10. Sommer A, Katz J, Quigley HA, et al. Clinically detectable nerve fiber atrophy precedes the onset of glaucomatous field loss. *Arch Ophthalmol* 1991;109:77-83.
11. Quigley HA, Katz J, Derick RJ, et al. An evaluation of optic disc and nerve fiber layer examinations in monitoring progression of early glaucoma damage. *Ophthalmology* 1992;99:19-28.

12. Weinreb RN, Zangwill L. Retinal nerve fiber layer evaluation in glaucoma. *J Glaucoma* 2001;10:S56-S58.
13. Weinreb RN, Dreher AW, Coleman A, et al. Histopathologic validation of Fourier-ellipsometry measurements of retinal nerve fiber layer thickness. *Arch Ophthalmol* 1990;108:557-60.
14. Zhou Q, Knighton RW. Light scattering and form birefringence of parallel cylindrical arrays that represent cellular organelles of the retinal nerve fiber layer. *Appl Opt* 1997;36:2273-85.
15. Reus NJ, Colen TP, Lemij HG. Visualization of localized retinal nerve fiber layer defects with the GDx with individualized and with fixed compensation of anterior segment birefringence. *Ophthalmology* 2003;110:1512-6.
16. Greenfield DS, Knighton RW, Huang XR. Effect of corneal polarization axis on assessment of retinal nerve fiber layer thickness by scanning laser polarimetry. *Am J Ophthalmol* 2000;129:715-22.
17. Knighton RW, Huang XR. Linear birefringence of the central human cornea. *Invest Ophthalmol Vis Sci* 2002;43:82-6.
18. Weinreb RN, Bowd C, Greenfield DS, Zangwill LM. Measurement of the magnitude and axis of corneal polarization with scanning laser polarimetry. *Arch Ophthalmol* 2002;120:901-6.
19. Weinreb RN, Bowd C, Zangwill LM. Glaucoma detection using scanning laser polarimetry with variable corneal polarization compensation. *Arch Ophthalmol* 2003;121:218-24.
20. Zhou Q, Weinreb RN. Individualized compensation of anterior segment birefringence during scanning laser polarimetry. *Invest Ophthalmol Vis Sci* 2002;43:2221-8.
21. Anderson DR, Patella VM. Automated Static Perimetry, 2nd ed. St. Louis, MO: Mosby, 1999.
22. Budenz DL, Rhee P, Feuer WJ, et al. Comparison of glaucomatous visual field defects using standard full threshold and Swedish interactive threshold algorithms. *Arch Ophthalmol* 2002;120:1136-41.
23. Swets JA. Measuring the accuracy of diagnostic systems. *Science* 1988;240:1285-93.
24. DeLong ER, DeLong DM, Clarke-Pearson DL. Comparing the areas under two or more correlated receiver operating characteristic curves: a nonparametric approach. *Biometrics* 1988;44:837-45.
25. Harper R, Reeves B. Reporting of precision of estimates for diagnostic accuracy: a review. *BMJ* 1999;318:1322-3.
26. Fischer JE, Bachmann LM, Jaeschke R. A readers' guide to the interpretation of diagnostic test properties: clinical example of sepsis. *Intensive Care Med* 2003;29:1043-51.
27. Altman DG. Comparing groups - continuous data. Practical statistics for medical research, First ed. London: Chapman & Hall, 1991; chap. 9.
28. Colen TP, Lemij HG. Sensitivity and specificity of the GDx: clinical judgment of standard printouts versus the number. *J Glaucoma* 2003;12:129-33.
29. Kremmer S, Garway-Heath DF, De Cilla S, et al. Influence of cataract surgery with implantation of different intraocular lenses on scanning laser tomography and polarimetry. *Am J Ophthalmol* 2003;136:1016-21.
30. Kass MA, Heuer DK, Higginbotham EJ, et al. The Ocular Hypertension Treatment Study: a

randomized trial determines that topical ocular hypotensive medication delays or prevents the onset of primary open-angle glaucoma. *Arch Ophthalmol* 2002;120:701-13.

31. Stamper RL. Glaucoma screening. *J Glaucoma* 1998;7:149-50.
32. Wolfs RC, Borger PH, Ramrattan RS, et al. Changing views on open-angle glaucoma: definitions and prevalences--The Rotterdam Study. *Invest Ophthalmol Vis Sci* 2000;41:3309-21.





## 3.2 Accuracy of GDx VCC, HRT I, and clinical assessment of stereoscopic optic nerve head photographs for diagnosing glaucoma

---

**Purpose:** To determine and compare the accuracy of GDx VCC scanning laser polarimetry (SLP) with variable cornea compensation (VCC), HRT I confocal scanning laser ophthalmoscopy (CSLO), and clinical assessment of stereoscopic optic nerve head (ONH) photographs for diagnosing glaucoma.

**Design:** Prospective comparative observational clinic-based case series.

**Participants and Controls:** One eye each of 40 healthy subjects, 48 glaucoma patients, and 6 patients with ocular hypertension.

**Methods:** All subjects were measured with SLP-VCC and CSLO. In addition, simultaneous stereoscopic ONH photographs were obtained. Sixteen photographs of healthy and glaucomatous eyes were duplicated for assessing intraobserver agreement. Four glaucoma specialists, 4 general ophthalmologists, 4 residents in ophthalmology, and 4 optometrists classified the ONH photographs as normal or glaucomatous. For SLP-VCC, the Nerve Fiber Indicator (NFI) was evaluated. For CSLO, the Moorfields Regression Analysis (MRA) and the Bathija linear discriminant function (LDF) were used.

**Main Outcome Measures:** Sensitivity, specificity, percentage of correctly classified eyes, and intra- and interobserver agreement, expressed as kappa ( $k$ ).

**Results:** SLP-VCC had the highest diagnostic accuracy, with a sensitivity, specificity, and overall correct classification of 91.7%, 95.0%, and 93.2%, respectively. CSLO, expressed as MRA and Bathija LDF, had a similar diagnostic accuracy as glaucoma specialists and general ophthalmologists with an overall accuracy of 89.8%, 86.4%, 86.7%, and 85.2%, respectively. Residents classified the fewest eyes correctly. Intraobserver agreement for classifying the ONH photographs ranged between 0.48 (within residents) and 0.78 (within glaucoma specialists). The interobserver agreement ranged between 0.45 (between residents) and 0.74 (between glaucoma specialists). The agreement between observers and CSLO MRA ( $k$ , 0.68) was statistically significantly higher ( $P < 0.001$ ; paired  $t$  test) than between observers and SLP-VCC NFI ( $k$ , 0.60) and CSLO Bathija LDF ( $k$ , 0.62).

**Conclusions:** Automated analysis of measurements with GDx VCC had a higher diagnostic accuracy for glaucoma than classification of stereoscopic ONH photographs by individual general ophthalmologists, residents in ophthalmology, optometrists, and some glaucoma specialists. The HRT performed about as well as glaucoma specialists and general ophthalmologists. The intra- and

interobserver agreement for ONH analysis was only moderate to good. We think these imaging techniques may assist clinicians in diagnosing glaucoma. *Am J Ophthalmol, submitted.*

---

**T**he ability of eye-care professionals to discriminate between healthy and glaucomatous eyes, based solely on the subjective evaluation of the appearance of the optic nerve head (ONH), is limited;<sup>1-5</sup> even glaucoma specialists do not classify all optic discs correctly. Nonetheless, assessment of the ONH's appearance remains a cornerstone for diagnosing glaucoma in clinical practice.

Various objective imaging techniques, such as scanning laser polarimetry (SLP) and confocal scanning laser ophthalmoscopy (CSLO), have been developed to assess glaucomatous damage to the retinal nerve fiber layer (RNFL) and ONH, respectively. SLP, featured in the commercially available GDx VCC (Carl Zeiss Meditec, Inc., Dublin, CA, USA), estimates the thickness of the RNFL in the peripapillary area. The GDx VCC is the fifth generation of the commercially available instrument and incorporates a variable corneal compensator (VCC) to allow accurate assessment of RNFL morphology. CSLO, featured in the commercially available Heidelberg Retina Tomograph (HRT; Heidelberg Engineering GmbH, Dossenheim, Germany), creates a topography image of the ONH.

The purpose of the present study was to determine whether these imaging techniques may assist clinicians in the management of glaucoma. To this end, we compared the accuracy of SLP-VCC and CSLO for diagnosing glaucoma to that of clinical assessment of stereoscopic ONH photographs by various eye-care professionals.

## **Methods**

### **Subjects**

Forty healthy subjects, 48 glaucoma patients, and 6 patients with ocular hypertension were recruited at The Rotterdam Eye Hospital for the present study. All subjects were imaged with SLP-VCC, CSLO, and stereoscopic ONH photography. In addition, all subjects were measured with standard automated perimetry by means of the Humphrey Field Analyzer II (Carl Zeiss Meditec, Inc., Dublin, CA, USA) 24-2 Full Threshold (FT) or Swedish interactive threshold algorithm (SITA) Standard test program. Visual fields had to be reproducible as well as reliable. Reliability criteria applied were: 1) fixation losses <25% and 2) false-positive and false-negative response rates  $\leq$ 20% for the FT test paradigm and  $\leq$ 7% for the SITA-Standard test program. In glaucomatous eyes with advanced field loss, higher false-negative response rates were accepted: up to 33% for the FT paradigm and up to 12% for the SITA-Standard paradigm.

All healthy subjects had normal visual fields, i.e., a glaucoma hemifield test (GHT) within normal limits and no nerve fiber bundle visual field defects in the total and/or pattern deviation

probability plots. In addition, they were of white ethnic origin and had a best-corrected visual acuity (BCVA) of 20/40 or better. None had a significant history of ocular disease, a history of intraocular surgery (except for any uncomplicated cataract surgery), relatives in the first and/or second degree with glaucoma, any significant coexisting diseases, or systemic diseases with possible ocular involvement, such as diabetes mellitus. Furthermore, slit-lamp examination was unremarkable; they had healthy-looking ONHs (no diffuse or local rim thinning and no optic disc hemorrhages), an IOP of 21 mmHg or less in both eyes, and open angles upon gonioscopy. One eye was randomly selected for analysis.

Glaucoma patients were diagnosed with glaucoma by one of the four glaucoma specialists of The Rotterdam Eye Hospital based on a glaucomatous appearance of at least one of their ONH (with notching or thinning of the neuroretinal rim), a reproducible corresponding nerve fiber bundle visual field defect with SAP, and open angles by gonioscopy. All patients with glaucoma were of white ethnic origin and had a BCVA of 20/40 or better. Patients with any significant coexisting ocular diseases, a history of intraocular surgery (except for any uncomplicated cataract or glaucoma surgery), or systemic diseases with possible ocular involvement, such as diabetes mellitus, were excluded. One eye was randomly selected for analysis if both eyes were eligible.

Subjects with ocular hypertension had an IOP of  $\geq 22$  mmHg and  $\leq 32$  mmHg and normal visual fields on at least two separate occasions. The appearance of the ONH not a selection criterion. All subjects with ocular hypertension were of white ethnic origin and had a BCVA of 20/40 or better. Patients with any significant history of ocular disease (other than ocular hypertension), a history of intraocular surgery (except for any uncomplicated cataract surgery), any significant coexisting diseases or systemic diseases with possible ocular involvement, such as diabetes mellitus, were excluded. Furthermore, all eyes had open angles upon gonioscopy. One eye was randomly selected for analysis.

The research adhered to the tenets of the Declaration of Helsinki. The institutional human experimentation committee had approved the research. Informed consent was obtained from the subjects after explanation of the nature and possible consequences of the study.

### **GDx VCC Scanning Laser Polarimetry**

SLP-VCC measurements were performed with the commercially available GDx VCC (software version 5.4.0). This technique has been described in detail elsewhere.<sup>6</sup> In short, three experienced technicians performed GDx VCC measurements in both eyes of all subjects. Pupils were undilated and the room lights were left on. The spherical equivalent refractive error of each eye was entered into the GDx VCC software to allow the instrument to properly focus on the retina. For each subject, anterior segment birefringence was assessed, after which images were obtained from both eyes with VCC. To maintain the same orientation of the slow axes of the birefringent structures in the eye to that of the instrument's compensator, the operator saw to it that patients had their

heads in the same position during all measurements. All accepted scans were of high quality, i.e. with a centered optic disc, well-focused, evenly and justly illuminated throughout the image, and without any motion artifacts.

### **HRT I Confocal Scanning Laser Ophthalmoscopy**

CSLO measurements were performed with the commercially available HRT I (software version 1.4.0.0). This technique has been described in detail elsewhere.<sup>7</sup> In short, two experienced technicians performed the HRT measurements in both eyes of all subjects. Pupils of subjects were undilated and the room lights were left on. Before each measurement, the subject's corneal curvature radius was entered into the software. The patient's face was then gently placed onto the head-and-chin rest of the HRT and imaging was performed at the 1.5-cm imaging head-eye distance, recommended in the instruction manual, as the subject viewed a distant fixation target. Three high-quality images at a 15° x 15° scanning angle were recorded for each subject. The quality of the images was assessed with the aid of the HRT software and by the technician. All images were of high quality, i.e. with a centered optic disc, with a clear dark-light-dark pattern over the 32 consecutive images, evenly and justly illuminated throughout the individual images, and without any motion artifacts. A mean topography image, computed from the three scans, was used for subsequent analysis with HRT software. Mean images with a mean SD of the height measurements >50 mm were excluded from analysis. The optic disc margin was manually marked at the inner edge of Elschnig's ring by one of the authors (NJR). When in doubt about the position of the optic disc margin, stereoscopic ONH photographs were used to assist. The standard reference plane was used for calculations of optic disc topography with the relative and tilted coordinate system turned on.

### **Optic Nerve Head Stereo Photography**

The ONH in both eyes of all subjects were photographed with a simultaneous stereoscopic camera (TRC-SS2, Topcon Medical Systems, Inc., Paramus, NJ, USA) at a 15° field of view. The perception of depth was achieved by simultaneously obtaining two images of the ONH with a spatial shift in a single frame. All images were of high quality, i.e. with a centered optic disc and evenly and justly illuminated throughout the image. Nine photographs of glaucoma patients and 7 photographs of healthy subjects were duplicated for assessing intraobserver agreement, resulting in 110 stereoscopic ONH photographs. The sequence of the photographs was randomized.

### **Clinical Assessment of Optic Nerve Head Photographs**

Stereoscopic ONH photographs were evaluated by 16 observers: 4 glaucoma specialists, 4 general ophthalmologists, 4 residents in ophthalmology, and 4 optometrists. Participating glaucoma specialists were working at The Rotterdam Eye Hospital. General ophthalmologists were working

either at the Sint Franciscus Gasthuis (2), a hospital affiliated with the Rotterdam Eye Hospital, or at a general hospital in The Netherlands not affiliated with the eye hospital (2). Participating residents were the younger residents in ophthalmology at The Rotterdam Eye Hospital who had been in training for 1-2 years. In The Netherlands, the ophthalmology training lasts 5 years, and follows a medical degree (MD). Optometrists were employed by The Rotterdam Eye Hospital. In The Netherlands, optometrists are a relatively new phenomenon. After their bachelor's degree in optometry, they often work at optician's stores where they may provide primary eye care. With increasing frequency, however, they provide basic patient care in a clinical setting supervised by ophthalmologists.

The graders individually classified the ONHs as either normal or glaucomatous. When in doubt, they were forced to make a classification. All observers classified the set of slides in the same, randomized, order and were instructed not to look back at previously classified photographs. To give a rough estimate of optic disc size, stereoscopic ONH photographs of healthy subjects with a small (5th percentile), a medium (50th percentile), and a large (95th percentile) optic disc were provided.

### Data analysis

The sensitivity (the proportion of glaucomatous eyes that are correctly identified) and specificity (the proportion of healthy eyes that are correctly identified) were calculated for all observers and imaging techniques individually. In addition, we calculated the sensitivity and specificity for each group of observers by averaging the individual sensitivities and specificities. For the GDx VCC, we determined the sensitivity and specificity of the NFI parameter, which has been shown to be its best discriminating parameter.<sup>6</sup> In the present study, we used a cut-off value of 35. For GDx VCC software versions 5.3.1 and higher, we have found the best discriminating cut-off value to be 35 (unpublished data) instead of the previously published value of 40.<sup>6</sup> For the HRT, we calculated the sensitivity and specificity for both the Moorfields regression analysis (MRA)<sup>8</sup> and the Bathija linear discriminant function (LDF).<sup>9</sup> The Bathija LDF has been shown to be the best discriminating parameter of the HRT.<sup>10</sup> The MRA is a parameter that is often used in clinical practice. For MRA, we interpreted the classification of 'Borderline' as 'Outside normal limits'. For the continuous parameters NFI and Bathija LDF, we constructed receiver operating characteristic (ROC) curves. The 95% confidence intervals (CIs) for the areas under the ROC curves (AUCs) were calculated as the point estimate of the AUC  $\pm$  1.96  $\times$  standard error (SE). To explore the agreement in classification between the various observers, SLP-VCC and CSLO, we determined the intraobserver and interobserver agreement, expressed as *k*. The values for *k* were classified as follows:  $\leq 0.2$ , poor; 0.21 to 0.40, fair; 0.41 to 0.60, moderate; 0.61 to 0.80, good; and  $\geq 0.81$ , very good.<sup>11</sup>

Data of ocular hypertensive eyes were not analyzed in the present study as they had merely been added so that the set represented a continuum of glaucomatous damage.

We classified the glaucoma patients by the severity of their visual field damage with standard automated perimetry based on their mean deviation (MD) and with the Hodapp-Anderson-Parrish (HAP) grading scale.<sup>12</sup> This latter classification takes into account the size of the glaucomatous visual field defect, depth of the defect, and proximity of the defect to fixation, which may closely reflect a clinician's interpretation of visual field loss.<sup>12</sup>

We used paired and unpaired t tests to evaluate differences in measurements within and between groups, respectively. For differences in dichotomous variables between groups, we used the Pearson Chi-square test. Differences in AUCs between NFI and Bathija-LDF were tested for statistical significance with the paired-samples test described by DeLong et al.<sup>13</sup> In the present study, a P value of less than 0.05 was considered statistically significant. For paired comparisons, the  $\alpha$  was adjusted to the number of comparisons within each analysis with the Bonferroni correction to allow for multiple testing. Statistical analyses were performed with SPSS for Windows (release 12.0.1, 2003, SPSS Inc., Chicago, IL, USA).

The demographics of the healthy subjects and glaucoma patients have been presented in Table 3.2.1.

## Results

### Diagnostic accuracy

The sensitivity and specificity for discriminating between healthy and glaucomatous eyes by SLP-VCC, CSLO, and evaluation of stereoscopic ONH photographs by glaucoma specialists, general ophthalmologists, residents in ophthalmology, and optometrists have been presented in the figure 3.2 and in Table 3.2.2. Overall, the SLP-VCC NFI parameter appeared to have the highest diagnostic accuracy with a sensitivity, specificity, and overall accuracy of 91.7%, 95.0%, and 93.2%, respectively. The accuracy of CSLO Bathija LDF was slightly lower (Table

	Unit	Healthy Subjects	Glaucoma Patients	<i>P</i>
Age (SD; range)	Years	59 (12)	61 (11)	0.31
Gender (male) (%)	NA	19 (48)	26 (54)	0.53
Randomized eye (right) (%)	NA	21 (53)	18 (38)	0.16
Disc area (SD; range)	mm <sup>2</sup>	1.89 (0.33; 1.29 to 2.97)	2.03 (0.37; 1.47 to 2.90)	0.055
MD (SD; range)	Decibels	0.10 (0.93; -1.55 to 2.04)	-6.56 (6.32; -22.26 to 1.25)	< 0.001
PSD (SD; range)	Decibels	1.64 (0.38; 0.91 to 3.01)	7.71 (4.03; 2.65 to 15.92)	< 0.001

**Table 3.2.1.** Demographics of Healthy Subjects (n = 40) and Glaucoma Patients (n = 48).

Differences between the groups were tested for statistical significance with an independent samples t-test for continuous variables and with the Pearson Chi-Square test for dichotomous variables.

MD = mean deviation; NA = not applicable; PSD = pattern standard deviation; SD = standard deviation

	Sensitivity (%)	Specificity (%)	Correctly classified (%)
SLP-VCC			
<i>NFI</i>	91.7	95.0	93.2
CSLO			
<i>Bathija LDF</i>	85.4	95.0	89.8
<i>MRA</i>	77.1	97.5	86.4
Stereoscopic ONH photographs			
<i>Glaucoma specialists (SD)</i>	80.2 (4.9)	94.4 (5.5)	86.7 (5.0)
<i>General ophthalmologists (SD)</i>	78.7 (9.5)	93.1 (6.3)	85.2 (2.5)
<i>Optometrists (SD)</i>	77.1 (10.5)	86.9 (6.6)	81.5 (4.1)
<i>Ophthalmology residents (SD)</i>	69.3 (9.5)	77.5 (15.9)	73.0 (5.5)

**Table 3.2.2.** Sensitivity and specificity for discriminating between healthy and glaucoma eyes and the percentage of correctly classified eyes by scanning laser polarimetry with variable corneal compensation (SLP-VCC), confocal scanning laser ophthalmoscopy (CSLO), and stereoscopic ONH photography evaluated by 4 glaucoma specialists, 4 general ophthalmologists, 4 optometrists, and 4 junior ophthalmology residents. Bathija LDF = Linear Discriminant Function by Bathija et al;<sup>9</sup> MRA = Moorfields Regression Analysis; NFI = Nerve Fiber Indicator; ONH = optic nerve head; SD = standard deviation.

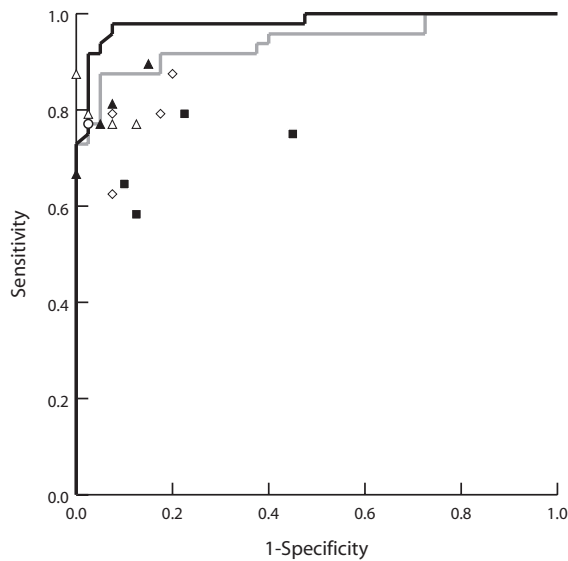


**Figure 3.2.** Receiver operating characteristic curves of the scanning laser polarimetry with variable cornea compensator parameter NFI (solid black line) and the confocal scanning laser ophthalmoscopy (CSLO) linear discriminant function by Bathija (solid grey line) for diagnosing glaucoma in 40 healthy and 48 glaucomatous eyes. In addition, data on evaluation of stereoscopic optic nerve head photographs by 4 glaucoma specialists (open triangles), 4 general ophthalmologists (closed triangles), 4 optometrists (open diamonds), and 4 junior ophthalmology residents (closed squares) as well as the CSLO Moorfields Regression Analysis (open circle) have been presented.

3.2.2). The areas under the ROC curve of the SLP-VCC NFI parameter (0.98; 95% CI, 0.96-1.00) and CSLO Bathija LDF (0.94; 95% CI, 0.89-0.99) were not statistically significantly different ( $P = 0.087$ ; paired  $t$  test). With regard to the graders of stereoscopic ONH photographs, glaucoma specialists had the highest diagnostic accuracy (sensitivity, 80.2%; specificity, 94.4%; overall accuracy, 86.7%), followed subsequently by general ophthalmologists, optometrists, and ophthalmology residents (Table 2). CSLO MRA had a diagnostic accuracy that was similar to that of glaucoma specialists for evaluating stereoscopic ONH photographs (Table 3.2.2).

The sensitivity for correctly classifying glaucomatous eyes stratified for mild, moderate, and severe visual field loss has been presented in Table 3.2.3. Eyes with mild glaucomatous damage were most difficult to correctly classify, for both the imaging techniques and the clinical observers.

### **Intraobserver agreement**

The intraobserver agreement ( $k$ , mean; range) between ophthalmology residents for classifying ONHs was moderate (0.48; 0.13-0.74). The intraobserver agreement for classification by optometrists (0.63; 0.53-0.73), general ophthalmologists (0.71; 0.52-1.00), and glaucoma specialists (0.78; 0.46-1.00) was good.

### **Interobserver agreement**

Considerable variability was apparent in the accuracy of individual observers to classify ONHs as healthy or glaucomatous (Figure 3.2). The average interobserver agreement between glaucoma specialists, general ophthalmologists, optometrists, and ophthalmology residents was 0.74, 0.72, 0.67, and 0.45, respectively (Table 3.2.4).

The agreement between subjective classification of stereoscopic ONH photographs and classification of the ONH by CSLO MRA (mean  $k$ , 0.68) was statistically significantly higher than 1) the agreement between subjective ONH classification and the classification by the SLP-VCC NFI parameter (mean  $k$ , 0.60) ( $P < 0.001$ , paired  $t$  test) and 2) the agreement between subjective ONH classification and classification with CSLO by means of the Bathija LDF (mean  $k$ , 0.62) ( $P < 0.001$ , paired  $t$  test).

The agreement between observers and SLP-VCC NFI was not statistically significantly different from the agreement between observers and the Bathija LDF ( $P = 0.090$ , paired  $t$  test).

## **Discussion**

In the present study, automated analysis of SLP-VCC measurements discriminated better between healthy and glaucomatous eyes than clinical assessment of stereoscopic ONH photographs by general ophthalmologists, junior residents in ophthalmology, optometrists, and even some glaucoma specialists. CSLO measurements classified about as well as did glaucoma specialists



	Specificity (%)	Sensitivity (%)					
		MD			HAP		
		Mild	Moderate	Severe	Mild	Moderate	Severe
<b>SLP-VCC</b>							
NFI	95.0	85.2	100.0	100.0	100.0	76.5	100.0
<b>CSLO</b>							
MRA	97.5	66.7	84.6	100.0	100.0	64.7	95.2
Bathija LDF	95.0	77.8	92.3	100.0	100.0	76.5	95.2
<b>Stereoscopic ONH photographs</b>							
Glaucoma specialists (SD)	94.4 (5.5)	65.8 (8.2)	98.1 (3.8)	100.0 (0.0)	100.0 (0.0)	60.3 (11.2)	98.8 (2.2)
General ophthalmologists (SD)	93.1 (6.3)	63.0 (15.4)	98.1 (3.8)	100.0 (0.0)	100.0 (0.0)	58.8 (14.4)	96.4 (4.6)
Optometrists (SD)	86.9 (6.6)	64.8 (12.3)	90.4 (9.7)	96.9 (6.3)	96.9 (6.3)	66.2 (10.1)	91.7 (6.0)
Ophthalmology residents (SD)	77.5 (15.9)	52.8 (12.6)	86.5 (18.2)	96.9 (6.3)	96.9 (6.3)	54.4 (13.0)	89.3 (6.0)

**Table 3.2.3.** Sensitivity and specificity for discriminating between healthy eyes and eyes with mild, moderate, and severe glaucomatous damage (classified with the Mean Deviation [MD] and the Hodapp-Anderson-Parrish [HAP] grading scales) by scanning laser polarimetry with variable corneal compensation (SLP-VCC), confocal scanning laser ophthalmoscopy (CSLO), and stereoscopic ONH photography evaluated by 4 glaucoma specialists, 4 general ophthalmologists, 4 optometrists, and 4 junior ophthalmology residents.

Bathija LDF = Linear Discriminant Function by Bathija et al.; MRA = Moorfields Regression Analysis; NFI = Nerve Fiber Indicator; ONH = optic nerve head; SD = standard deviation.

**Glaucoma specialists**

	A	B	C	D	SLP-VCC, NFI	CSLO, MRA	CSLO, Bathija LDF
A	-	0.66	0.84	0.70	0.71	0.79	0.73
B	-	-	0.77	0.68	0.59	0.68	0.61
C	-	-	-	0.77	0.82	0.86	0.84
D	-	-	-	-	0.68	0.77	0.66

**General ophthalmologists**

	A	B	C	D	SLP-VCC, NFI	CSLO, MRA	CSLO, Bathija LDF
A	-	0.69	0.79	0.84	0.66	0.75	0.68
B	-	-	0.75	0.58	0.75	0.75	0.68
C	-	-	-	0.68	0.68	0.82	0.75
D	-	-	-	-	0.64	0.76	0.66

**Optometrists**

	A	B	C	D	SLP-VCC, NFI	CSLO, MRA	CSLO, Bathija LDF
A	-	0.66	0.58	0.62	0.63	0.64	0.66
B	-	-	0.68	0.73	0.57	0.66	0.55
C	-	-	-	0.72	0.44	0.55	0.50
D	-	-	-	-	0.66	0.75	0.68

**Ophthalmology residents**

	A	B	C	D	SLP-VCC, NFI	CSLO, MRA	CSLO, Bathija LDF
A	-	0.29	0.33	0.47	0.36	0.34	0.39
B	-	-	0.52	0.51	0.44	0.55	0.45
C	-	-	-	0.60	0.48	0.65	0.59
D	-	-	-	-	0.57	0.57	0.55

**Table 3.2.4.** Agreement (k) between classification of healthy and glaucoma eyes by evaluation of stereoscopic ONH photographs by 4 glaucoma specialists, 4 general ophthalmologists, 4 optometrists, and 4 junior residents in ophthalmology and scanning laser polarimetry with variable corneal compensation (SLP-VCC), confocal scanning laser ophthalmoscopy (CSLO) within various groups.

Bathija LDF = Linear Discriminant Function by Bathija et al;<sup>9</sup> MRA = Moorfields Regression Analysis; NFI = Nerve Fiber Indicator.

and general ophthalmologists. Of all subjective graders of stereoscopic ONH photographs, the glaucoma specialists showed the highest overall diagnostic accuracy. For any technique or grader, eyes with mild glaucomatous loss were more difficult to classify correctly than eyes with more severe damage.

The diagnostic accuracy of the GDx VCC that we found presently was similar to that reported earlier by us,<sup>6</sup> which may be due to our including some of the same eyes in both studies. In a

different sample, Medeiros et al<sup>10</sup> reported the area under the ROC curve for the GDx VCC NFI parameter to be 0.91,<sup>10</sup> which is slightly smaller than what we presently found (i.e., 0.98). This difference may be due to the larger number of glaucomatous eyes with mild visual field loss that Medeiros et al<sup>10</sup> included than we did, which are more difficult to classify correctly. Similarly, we found the ability of the HRT to discriminate between healthy and glaucomatous eyes by means of the Bathija LDF and the MRA to be slightly higher than reported in the literature by Medeiros et al<sup>10</sup> (Bathija LDF) and Ford et al (Bathija LDF and MRA).<sup>14</sup> This difference may again be due to their including more patients with milder glaucomatous damage than we did. The difference in the diagnostic accuracy of the GDx VCC appeared to be higher than that of the HRT, which was also reported by Medeiros et al.<sup>10</sup> However, in neither their study nor ours was this difference statistically significant. A larger sample size might yield a statistically significant difference.

We found that more experienced graders classified ONHs more accurately, i.e., glaucoma specialists and general ophthalmologists had a higher diagnostic accuracy than ophthalmology residents and optometrists. These findings correspond well with findings by Varma et al<sup>1</sup> and Abrams et al<sup>2</sup> in a smaller analysis of 18 glaucomatous discs and 15 healthy ones.

The diagnostic accuracy of glaucoma specialists that we presently found was similar to that found by Greaney et al.<sup>3</sup> In contrast, both Wollstein et al<sup>4</sup> and Girkin et al<sup>5</sup> found a slightly lower sensitivity and specificity for glaucoma specialists than we did, which might be due to their including more glaucoma eyes with milder damage.

In our study, optometrists had a higher accuracy for classifying ONHs correctly than junior ophthalmology residents. By contrast, Abrams et al<sup>2</sup> found that residents classified ONH photographs better than optometrists did. In their study, however, the graders were senior residents, who were more likely to correctly classify ONHs than the junior residents in our study.

Subjective grading of the ONH plays a key role in the clinical evaluation of a patient for glaucoma. However, we have presently shown that automated analysis of measurements with SLP-VCC may be better in discriminating between healthy and glaucomatous eyes than when ophthalmologists merely grade the appearance of ONHs. Therefore, we think that the clinical diagnosis of glaucoma may improve when clinicians use imaging techniques in combination with their assessment of the ONH together with all other available clinical information, such as RNFL appearance, the presence of visual field defects, and any risk factors, such as elevated IOP, older age, high myopia, African ethnic origin, and first- and/or second-degree family members with glaucoma.<sup>15</sup> Furthermore, as SLP-VCC measurements were substantially better in correctly classifying healthy and glaucomatous eyes than the less experienced eye-care professionals, i.e. optometrists and ophthalmology residents, we think that results obtained with this technique

may also train them in assessing glaucomatous losses more accurately.

We found substantial variability in classifying the ONH as normal or glaucomatous both within and between graders. The agreement within an observer and between observers was only moderate to good, which corresponds to previously published data.<sup>1-4</sup> Both intra- and interobserver agreement increased from graders with less experience to those who were well experienced in classifying ONHs. In other words, with more experience, graders more often agreed with themselves and with each other.

Of interest, subjective ONH graders showed better agreement with the Moorfield Regression Analysis than with the other automated analyses, which may not be very surprising because both relate strongly to ONH morphology. This also suggests that the MRA may be of little added diagnostic value to the clinician. Conversely, the NFI parameter relates to only RNFL morphology rather than ONH morphology and the Bathija LDF relates to both, which may perhaps explain the lower agreement between the subjective ONH grading and these instrument based classifiers. Therefore, their classifiers may yield clinicians more additional information on the patient's eyes than does the MRA.

To our knowledge, the present study is the first to compare the diagnostic accuracy for glaucoma of subjective grading of stereoscopic ONH photographs by various eye-care professionals to that of automated analysis by the GDx VCC and the HRT. More research is needed to determine the effect of implementing imaging techniques in routine clinical practice.

In conclusion, we have shown that automated analysis of commercially available imaging techniques, such as the GDx VCC and the HRT I, discriminate well between glaucomatous and healthy eyes compared with eye-care professionals classifying stereoscopic ONH photographs, suggesting that these objective techniques may assist clinicians in glaucoma management. The use of imaging devices has the added benefit of objectively documenting the ONH and/or RNFL for follow-up.

## Acknowledgments

The authors would like to thank the glaucoma specialists, general ophthalmologists, ophthalmology residents, and optometrists who participated in the present study.

## References

1. Varma R, Steinmann WC, Scott IU. Expert agreement in evaluating the optic disc for glaucoma. *Ophthalmology* 1992;99:215-21.
2. Abrams LS, Scott IU, Spaeth GL, et al. Agreement among optometrists, ophthalmologists, and residents in evaluating the optic disc for glaucoma. *Ophthalmology* 1994;101:1662-7.
3. Greaney MJ, Hoffman DC, Garway-Heath DF, et al. Comparison of optic nerve imaging methods to

- distinguish normal eyes from those with glaucoma. *Invest Ophthalmol Vis Sci* 2002;43:140-5.
4. Wollstein G, Garway-Heath DF, Fontana L, Hitchings RA. Identifying early glaucomatous changes. Comparison between expert clinical assessment of optic disc photographs and confocal scanning ophthalmoscopy. *Ophthalmology* 2000;107:2272-7.
  5. Girkin CA, McGwin G, Jr., Long C, et al. Subjective and objective optic nerve assessment in African Americans and whites. *Invest Ophthalmol Vis Sci* 2004;45:2272-8.
  6. Reus NJ, Lemij HG. Diagnostic accuracy of the GDx VCC for glaucoma. *Ophthalmology* 2004;111:1860-5.
  7. Weinreb RN, Dreher AW, Bille JF. Quantitative assessment of the optic nerve head with the laser tomographic scanner. *Int Ophthalmol* 1989;13:25-9.
  8. Wollstein G, Garway-Heath DF, Hitchings RA. Identification of early glaucoma cases with the scanning laser ophthalmoscope. *Ophthalmology* 1998;105:1557-63.
  9. Bathija R, Zangwill L, Berry CC, et al. Detection of early glaucomatous structural damage with confocal scanning laser tomography. *J Glaucoma* 1998;7:121-7.
  10. Medeiros FA, Zangwill LM, Bowd C, Weinreb RN. Comparison of the GDx VCC scanning laser polarimeter, HRT II confocal scanning laser ophthalmoscope, and Stratus OCT optical coherence tomograph for the detection of glaucoma. *Arch Ophthalmol* 2004;122:827-37.
  11. Altman DG. *Practical Statistics for Medical Research*, 1st ed. London: Chapman and Hall, 1991.
  12. Hodapp E, Parrish RK, Anderson DR. *Clinical Decisions in Glaucoma*. St. Louis, MO: Mosby, 1993.
  13. DeLong ER, DeLong DM, Clarke-Pearson DL. Comparing the areas under two or more correlated receiver operating characteristic curves: a nonparametric approach. *Biometrics* 1988;44:837-45.
  14. Ford BA, Artes PH, McCormick TA, et al. Comparison of data analysis tools for detection of glaucoma with the Heidelberg Retina Tomograph. *Ophthalmology* 2003;110:1145-50.
  15. Weinreb RN, Khaw PT. Primary open-angle glaucoma. *Lancet* 2004;363:1711-20.



# 4

## **The relationship between function and structure**





## 4.1 The relationship between standard automated perimetry and GDx VCC measurements

---

**Purpose:** To investigate the relationship between retinal light sensitivity measured with standard automated perimetry (SAP) and retardation of the peripapillary retinal nerve fiber layer (RNFL) measured with the GDx VCC.

**Methods:** Forty-seven healthy subjects and 101 patients with glaucoma were examined with SAP and with the commercially available scanning laser polarimeter GDx VCC, with automated individualized compensation of anterior segment birefringence. Individual visual field test points and peripapillary RNFL retardation measurements were grouped into six corresponding sectors. The correlation between perimetry and GDx VCC measurements was determined, and the relationship between RNFL retardation and perimetry, expressed both in the standard decibel scale and in an unlogged scale, was described with linear regression analysis.

**Results:** A statistically significant correlation was found in most sectors between perimetry and GDx VCC measurements in patients with glaucoma, but not in healthy subjects. A linear relationship was found between the unlogged sensitivities and GDx VCC measurements for the superotemporal and inferotemporal sectors. In the decibel scale, this relationship was curvilinear.

**Conclusions:** GDx VCC measurements of the peripapillary RNFL relate well with functional loss in glaucoma. Based on the observed relationships between function and structure, patients with mild to moderate visual field loss in glaucoma may be better monitored with the GDx VCC and patients who have severe loss, with SAP. *Invest Ophthalmol Vis Sci* 2004;45:840-845.

---

**G**laucoma is an optic neuropathy with loss of retinal ganglion cells (RGCs) and their axons.<sup>1-3</sup> The loss of RGC axons may be apparent structurally as a local and/or a diffuse thinning of the retinal nerve fiber layer (RNFL)<sup>3-6</sup> and of the neuroretinal rim.<sup>5</sup> Functionally, RGC atrophy leads to characteristic visual field defects.<sup>7</sup> In clinical practice, as well as in clinical trials, both structural and functional losses are assessed for the diagnosis and monitoring of glaucoma.<sup>1,8,9</sup>

Functional losses by glaucoma are traditionally evaluated with standard automated perimetry (SAP). Perimetry assesses the differential light sensitivity (unlogged-DLS =  $L_b/(L_t - L_b)$ , where  $L_b$  is background luminance and  $L_t$  the stimulus luminance at threshold)<sup>10</sup> at various locations in

the central retina which is typically expressed in a decibel scale (decibel-DLS =  $10 \cdot \log_{10} L_{max} / (L_t - L_b)$  where  $L_{max}$  is the perimeter's maximum stimulus luminance). The relationship between function and structure has been found to be curvilinear for the relationships between decibel-DLS and number of ganglion cells<sup>11,12</sup> and neuroretinal rim area.<sup>13-15</sup> However, when differential light sensitivity is expressed in the unlogged-DLS scale, function appears to relate linearly to structure, as has been shown by Garway-Heath et al.<sup>11,13,16</sup>

Structural losses of the RNFL can be evaluated with scanning laser polarimetry (SLP). Instruments featuring this technique, such as the GDx nerve fiber analyzer (NFA) and the GDx VCC (both from Laser Diagnostic Technologies, Inc., San Diego, CA), estimate the thickness of the RNFL by measuring the summed retardation of a polarized scanning laser beam, induced by the form-birefringent microtubules that support the RGC axons.<sup>17-19</sup> Retardation in these instruments is usually expressed in micrometers of thickness, based on the relationship between the amount of retardation and the histologically determined RNFL thickness in monkey eyes,<sup>19</sup> although this relationship may vary somewhat per nerve fiber bundle around the optic nerve head (Huang X, et al. *IOVS* 2003;44:ARVO E-Abstract 3363).

Both the GDx NFA and the GDx VCC are equipped with an anterior segment compensator to cancel the birefringent effects of the cornea and, to a lesser degree, the lens. Whereas the compensator of the GDx NFA is fixed, the GDx VCC is equipped with an automated so-called variable corneal compensator (VCC), allowing eye-specific compensation of anterior segment birefringence. Because of large interindividual and intraindividual variability in anterior segment birefringence,<sup>20-22</sup> measurements with the GDx NFA do not always accurately reflect the RNFL<sup>23</sup> and have been reported to have no to only a moderate correlation with perimetry.<sup>24-30</sup> Equipped with a VCC, SLP has been shown to allow objective assessment of localized structural RNFL defects.<sup>23</sup> In addition, using a modified GDx NFA, Bowd et al<sup>24</sup> have shown that SLP measurements with VCC in patients with predominantly mild glaucomatous damage correlate better with perimetry than those with fixed compensation.

The aim of the present study was to investigate the functional-structural relationship between standard automated perimetry and measurements of peripapillary RNFL retardation with the commercially available GDx VCC in healthy subjects and patients with glaucoma.

## Methods

Forty-seven healthy subjects and 101 glaucoma patients were examined with SAP (Humphrey Field Analyzer [HFA] II, 24-2 Full Threshold or Swedish interactive threshold algorithm [SITA] Standard test program, Carl Zeiss Meditec, Dublin, CA) and SLP with individualized compensation of anterior segment birefringence (GDx VCC; Laser Diagnostic Technologies, Inc., San Diego, CA). The research adhered to the tenets of the Declaration of Helsinki. Informed consent was obtained from the subjects after explanation of the nature and possible consequences

of the study. The institutional human experimentation committee had approved the research. Glaucoma patients were recruited consecutively from an ongoing longitudinal follow-up study ( $n = 96$ ) or after referral by a glaucoma specialist (HGL) for clinical reasons ( $n = 5$ ). All glaucoma patients had a reproducible glaucomatous visual field defect with SAP and a glaucomatous appearance of the optic disc. Only one eye per patient was used for analysis. If more than one eye was eligible, the one with the more positive mean deviation (MD) for SAP was used. All glaucoma patients were of white ethnic origin and had a visual acuity of 20/40 or better. Patients with any significant coexisting ocular disease, including posterior segment eye diseases and corneal diseases, or systemic diseases with possible ocular involvement, such as diabetes mellitus, were excluded.

Healthy subjects were recruited either consecutively from an ongoing longitudinal follow-up study or from employees of the Rotterdam Eye Hospital and their spouses and friends. All healthy subjects had a Glaucoma Hemifield Test of 'Within normal limits' for SAP, healthy-looking optic discs, and an intraocular pressure of 21 mmHg or less, measured with Goldmann applanation tonometry. All subjects were of white ethnic origin and had a visual acuity of 20/40 or better. None had any significant history of ocular diseases, including posterior segment eye diseases and corneal diseases, relatives in the first and/or second degree with glaucoma, systemic hypertension for which medication was used, diabetes mellitus, or any other systemic disease.

For SAP, appropriate near refractive correction was used. Reliability criteria applied were: 1) fixation losses less than or equal to 25% and 2) false-positive and false-negative response rates less than or equal to 20% for the Full Threshold test paradigm and less than or equal to 7% for the SITA-Standard test paradigm. In the patients with glaucoma, however, higher false-negative response rates were accepted. The mean period between perimetry and GDx VCC measurements was 0.8 weeks (SD, 2.5; range, 0-12) and 12.2 weeks (SD, 11.0; range, 0-27) in patients with glaucoma and in healthy subjects, respectively.

The mean MD was  $-9.39$  dB (SD 7.45) and  $0.48$  dB (SD 1.22) for patients with glaucoma and healthy subjects, respectively. The mean age of the patients with glaucoma and of the healthy subjects was 62 years (SD 10) and 59 years (SD 13), respectively, which was not statistically significantly different (two-sample  $t$ -test,  $P = 0.10$ ).

In the glaucoma group, 54 of the 101 subjects (54%) were men. Of the healthy subjects, 23 of the 47 (49%) were men. Fifty-two of the 101 eyes (51%) in the glaucoma group were right eyes; in the healthy group, 22 of the 47 (47%) were right eyes.

In all subjects, both eyes were scanned with the GDx VCC, starting with the right eye. The spherical equivalent refractive error of each eye was entered into the software to allow the GDx VCC to properly focus on the retina. The patient's face was gently placed into the face mask of

the GDx VCC. To maintain the same orientation of the slow axes of the birefringent structures in the eye to that of the instrument's compensator, the operator saw to it that patients had their heads as vertical as possible during all measurements. The pupils of the patients were undilated and the room lights were left on. For each scan, the operator aligned the instrument with the cornea and the sclera of the measured eye.

First, anterior segment birefringence was assessed for each eye per subject with the method described by Zhou and Weinreb.<sup>31</sup> To this end, the magnitude of the compensator of the GDx VCC was automatically set to zero, after which the fundus was scanned. The interaction between the birefringence of the radially oriented axons of the photoreceptors that constitute Henle's fiber layer in the macula and the anterior segment birefringence resulted in a bow-tie shaped pattern on the retardation image. A dedicated algorithm, incorporated into the GDx VCC software, determined the anterior segment birefringence (consisting of magnitude and axis) from this profile.

The software then used these calculations to automatically adjust the anterior segment compensator to each individual eye, and both eyes were scanned again with individualized compensation. Adequate compensation of anterior segment birefringence was verified subjectively by looking at the retardation pattern in the macular region that had to be uniformly weak with a cross- or donut-shaped pattern. The typical time to measure both eyes of a patient was 3 minutes. All scans had to be of high quality, i.e. with a centered optic disc, well focused, even and just illuminated throughout the image, and without any motion artifacts. In addition, the measurements had to pass the five scan quality checks that were automatically performed by the GDx VCC software. The margin of the optic disc was manually marked with an ellipse on a reflection image of the fundus. The GDx VCC software positioned a circle, 8 pixels wide ( $\sim 0.4$  mm in an emmetropic eye) and with an inner diameter of 54 pixels ( $\sim 2.5$  mm in an emmetropic eye), centered on the center of the ellipse. The instrument processed the retardation values within this band to give a total of 256 values evenly distributed along the circle. These values were subsequently grouped into 64 sectors and exported by the software.

The relationship between visual field test points and regions of the optic disc as described by Garway-Heath et al<sup>32</sup> was used to correlate the visual fields to the GDx VCC measurements. The 64 peripapillary sectors in the GDx VCC retardation image and the 52 visual field test points were grouped into 6 corresponding sectors (Fig. 4.1.1). Due to the fixed dimensions of the exported sectors in the GDx VCC, the size and orientation of the 6 optic nerve head sectors differed slightly from those presented by Garway-Heath et al, but were consistent with their published relationship between optic nerve head location and visual field test points.<sup>32</sup> The peripapillary measurement circle was divided into one 90° sector (temporally (T)), one 112.5° sector (nasally (N)), and four equally sized sectors of approximately 39.4° (superotemporally

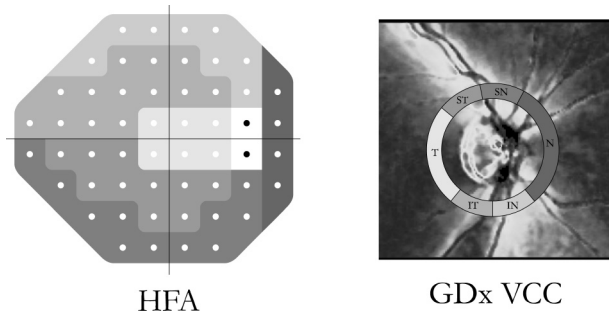


**Figure 4.1.1.** Test pattern of the HFA 24-2 (Carl Zeiss Meditec, Inc.) paradigm for a right eye (*left*) and a GDx VCC (Laser Diagnostic Technologies, Inc.) retardation image of a right eye (*right*), with a measurement circle superimposed. In the present study, visual field test points and peripapillary GDx VCC measurements were grouped in corresponding sectors as suggested by Garway-Heath et al.<sup>32</sup> Corresponding sectors were grayscale and named after the position of the sector in the GDx VCC image in relation to the optic disc.

(ST), superonasally (SN), inferotemporally (IT) and inferonasally (IN)). The average retardation was calculated for each sector.

The differential light sensitivity in each visual field sector was also averaged and expressed in both the typically used decibel scale (decibel-DLS) and in the unlogged DLS scale (unlogged-DLS =  $L_b / (L_t - L_b) = (L_b / L_{max}) \cdot L_{max} / (L_t - L_b) = (L_b / L_{max}) \cdot 10^{DLS_{dB}/10}$ ). For the HFA,  $L_b = 31.6$  asb and  $L_{max} = 10,000$  asb.

To measure the degree of association between SAP and GDx VCC measurements, we calculated Spearman's rank correlation coefficient ( $r_s$ ) for each sector. Subsequently, the relationship between perimetry, expressed in both the decibel-DLS and the unlogged-DLS scale and GDx VCC measurements was described with linear regression analysis.

Sector	Glaucoma patients		Healthy subjects	
	$r_s$	$P$	$r_s$	$P$
Superotemporal	0.77	< 0.001	0.04	0.78
Superonasal	0.52	< 0.001	0.37	0.012
Nasal	0.46	< 0.001	-0.11	0.47
Inferonasal	0.51	< 0.001	0.22	0.13
Inferotemporal	0.38	< 0.001	0.05	0.77
Temporal	0.19	0.059	-0.16	0.29

**Table 4.1.** Correlation between SAP and GDx VCC measurements. Degrees of association, measured with Spearman's rank correlation coefficient ( $r_s$ ;  $P$ ), between SAP differential light sensitivity and GDx VCC measurements in patients with glaucoma ( $n = 101$ ) and healthy subjects ( $n = 47$ ) for the six sectors described in Figure 4.1.1.

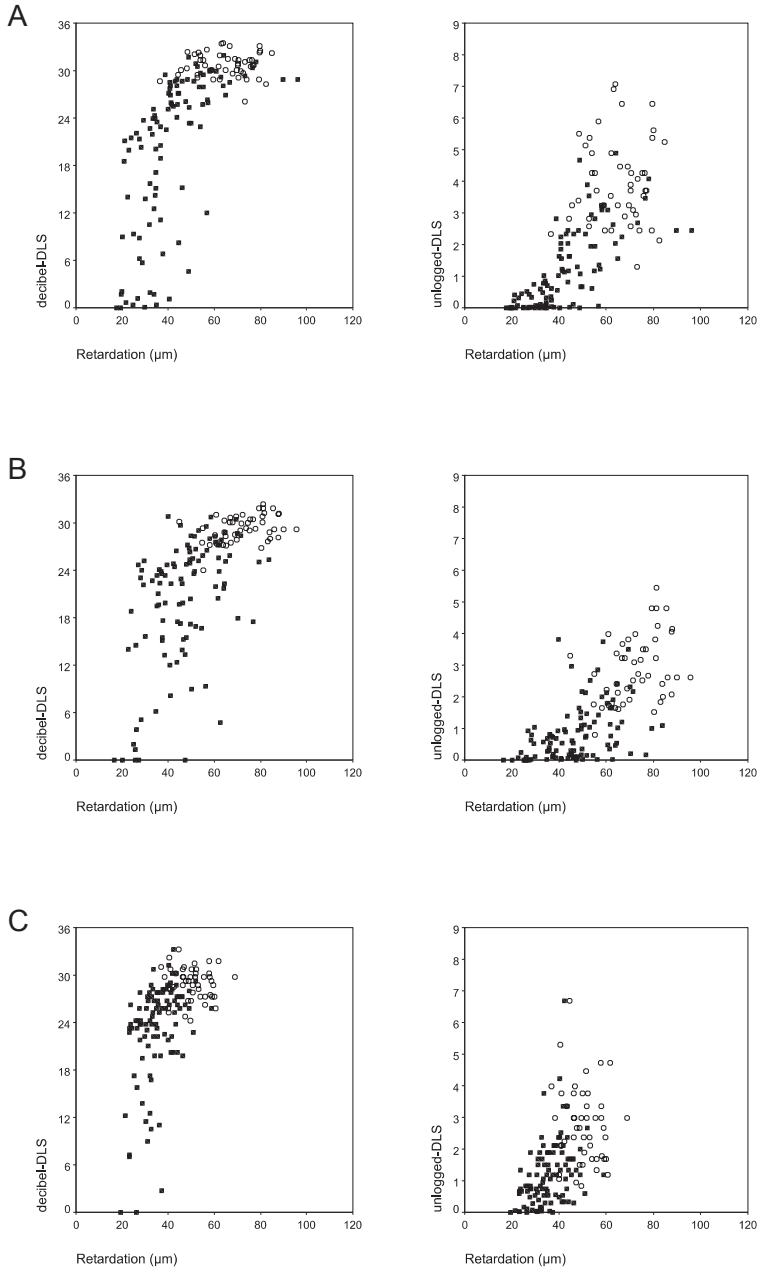


**Figure 4.1.2.** Scatterplots of differential light sensitivity (DLS), expressed as decibel-DLS (*left*) and as unlogged-DLS (*right*), against peripapillary RNFL retardation measured with the GDxVCC (Laser Diagnostic Technologies, Inc.). (○) Healthy subjects; (■) patients with glaucoma. Sectors: (A) superotemporal; (B) superonasal; (C) nasal; (D) inferonasal; (E) inferotemporal; (F) temporal.

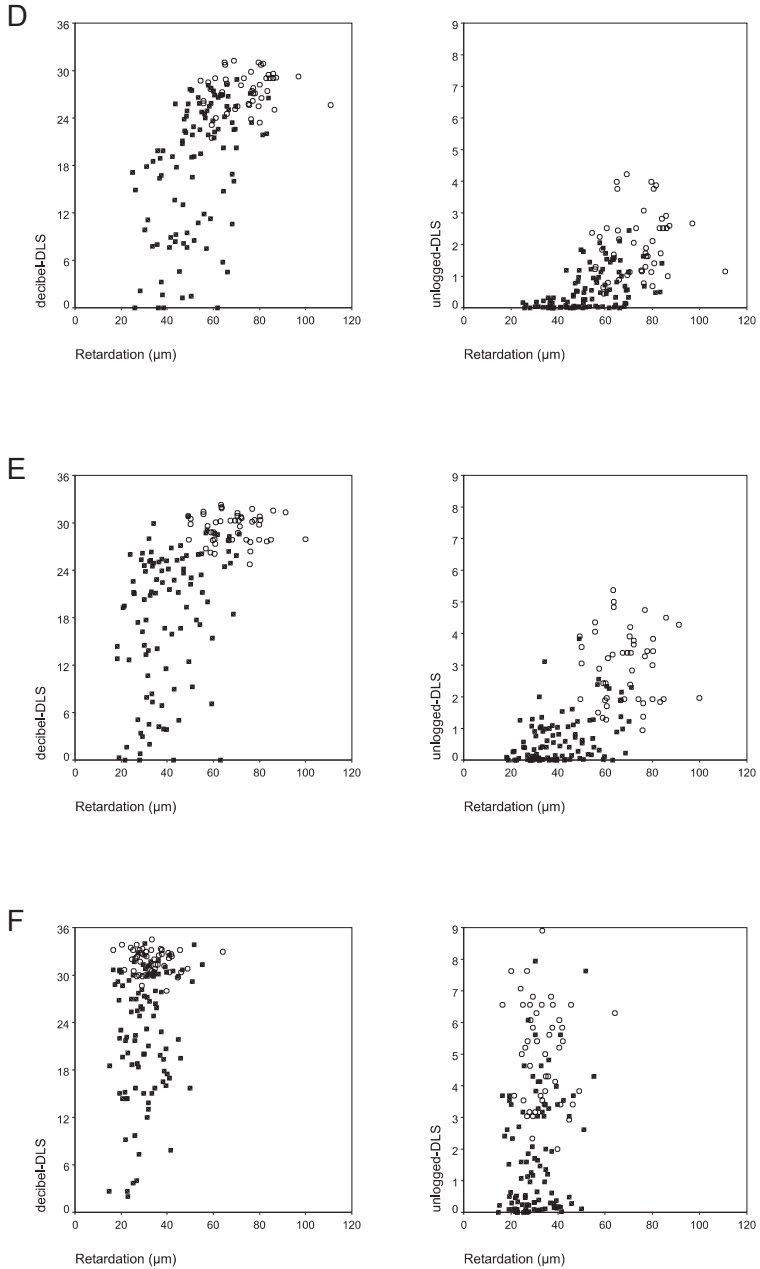


Figure 4.1.2. (Continued)

## Results

The relationship between perimetry and GDx VCC measurements has been graphically presented for all sectors in figure 4.1.2. We found statistically significant correlations between standard automated perimetry and GDx VCC measurements in patients with glaucoma ( $P < 0.001$ ), in all sectors except the temporal one ( $P = 0.059$ ), with  $r_s$  values of 0.77, 0.52, 0.46, 0.51, 0.38, and 0.19 for the sectors ST, SN, N, IN, IT, and T, respectively (Fig. 4.1.2, Table 4.1). In healthy subjects, no statistically significant correlations between perimetry and GDx VCC measurements were found in any sector ( $P > 0.13$ ), except the superonasal one ( $P = 0.012$ ; Fig. 4.1.2, Table 4.1).

When fit with a least-squares linear regression model, the relationship between decibel-DLS and RNFL retardation in healthy subjects and patients with glaucoma yielded  $R^2$  values of 0.48, 0.42, 0.29, 0.37, and 0.35 for the sectors ST, SN, N, IN, and IT, respectively (for slopes,  $P < 0.001$ ). For the unlogged-DLS, the  $R^2$  values of the linear regression models were 0.52, 0.48, 0.26, 0.35, and 0.43, respectively ( $P$  of slopes,  $< 0.001$ ).

For the sectors ST, SN, and IT, linear regression analysis yielded statistically significant better fits for the unlogged-DLS scale than for the decibel-DLS scale (signed rank test,  $P = 0.011$ ,  $P < 0.001$ , and  $P = 0.011$ , respectively). Conversely, for the sectors N and IN, linear regression analysis yielded statistically significant better fits for the decibel-DLS scale (signed rank test,  $P < 0.001$  and  $P = 0.004$ , respectively). We did not fit the relationship between perimetry and GDx VCC measurements for the temporal sector with linear regression analysis, because they did not correlate.

## Discussion

We have shown a correlation between standard automated perimetry and GDx VCC measurements in patients with glaucoma, suggesting that GDx VCC measurements relate well with functional loss in glaucoma. However, in healthy subjects, we found virtually no correlation between perimetry and GDx VCC measurements.

For the sectors ST, IT and SN, the relationship between function and structure was linear in the unlogged-DLS scale. In the standard decibel-DLS scale, a curvilinear relationship was apparent. Because the sectors ST and IT are reportedly most affected by glaucoma<sup>3-5,33</sup> and also because they represent areas of the visual field close to fixation, we think that the differences in linearity in these sectors are clinically important. Figures 4.1.2A and 4.1.2E, relating to these sectors, show that large differences in GDx VCC measurements correlated with only small differences in decibel-DLS in areas with no to moderate functional loss. In more advanced functional loss, the opposite was true. Therefore, SLP appears to be more suited than SAP for monitoring both healthy subjects at risk of contracting glaucoma and patients with glaucoma with mild to



moderate functional damage. In more advanced glaucoma, however, SAP may be more useful than SLP for follow-up. Patients with glaucomatous visual field defects of mixed severity may be best monitored with a combination of SLP and SAP.

This relationship was similar for the SN sector (Fig. 4.1.2B) but less pronounced for the N sector (Fig. 4.1.2C). In the IN sector, however, GDx VCC measurements did not appear to be better at detecting mild glaucomatous loss than perimetry (Fig. 4.1.2D). We would argue, however, that the IN sector, which relates to the uppermost visual field of the HFA 24-2 program, has poor perimetric reproducibility,<sup>34</sup> which limits its clinical usefulness.

The linear relationship that we found between function (unlogged-DLS) and structure was similar to those reported by Garway-Heath et al between unlogged-DLS and the number of RGCs,<sup>11</sup> neuroretinal rim area,<sup>16</sup> and to the theoretically modeled one by Swanson et al (Swanson WH, et al. *IOVS* 2003;44:ARVO E-Abstract 57) between unlogged-DLS and the number of RGCs. In addition, our finding of a curvilinear functional-structural relationship between decibel-DLS and RNFL retardation corresponds with the reported relationships between decibel-DLS and number of RGCs,<sup>11,12</sup> and between decibel-DLS and neuroretinal rim area.<sup>14,15</sup>

Several investigators also studied the relationship between SAP and SLP measurements and reported no correlation or only a mild one in healthy and glaucomatous eyes.<sup>24-30</sup> Their poor correlation may perhaps be attributable to differences in study populations and the use of different parameters. More important, they used SLP with a fixed compensator of anterior segment birefringence, instead of a variable one. Knighton et al<sup>35</sup> reasoned that an individualized anterior segment compensation of birefringence would be necessary for accurate measurement of RNFL retardation.<sup>20,22</sup> Our results support those of Bowd et al,<sup>24</sup> who compared a variable with a fixed anterior segment compensator and found an improved relationship between visual function and structure with VCC. Interestingly, Bowd et al<sup>24</sup> found that the relationship between decibel-DLS and GDx measurements with VCC was better described by a linear model than by a curvilinear one in all sectors. However, their data related to predominantly mild glaucomatous damage (mean MD, -2.74 dB; SD, 3.71 dB), whereas we used a much larger range of glaucomatous eyes and also many healthy eyes. Their smaller range may have precluded the detection of curvilinearity in the relationship between function and structure.

For the sectors ST and IT, the  $R^2$  values of the linear regression models describing the relationship between unlogged-DLS and RNFL retardation were 0.52 and 0.43, respectively. Therefore, 48% to 57% of the variation in unlogged-DLS was not explained by RNFL retardation alone. In the other sectors, 52% to 95% of the variation in this relationship was unexplained. Some of this scatter may be due to retardation originating from axons that had their origin outside the points tested by the HFA. Such axons might relate to areas either between the tested points or

outside the entire test area displayed in figure 4.1.1. In addition, mismatching of the six optic nerve head (ONH) sectors and the visual field test points in the map constructed by Garway-Heath et al<sup>32</sup> may have added to the variation in the correlation between perimetry and GDx VCC measurements. Garway-Heath et al<sup>32</sup> have reported that the range of possible positions at the ONH of RGC axons originating from each visual field test point location covers almost 30°. Factors that contributed to the variation in that study were the intereye variability in position of the ONH in relation to the fovea, inter-eye variability in retinal magnification, and variations in shape, rotation, and tilt of the ONH.<sup>32</sup> Apart from these variations, our data may also have been influenced by variation in the positioning of the head during SLP. Some of the unexplained variation in the relationship between DLS and RNFL retardation may also be attributable to the reproducibility of measurements with SAP and SLP. For example, the variability in DLS within subjects has been shown to be substantial.<sup>34,36,37</sup> Therefore, combining the results of several subsequent visual field tests may improve the relationship between DLS and RNFL retardation. To what extent the variability of GDx VCC measurements has influenced our results is unclear as its reproducibility of measurements has not yet been assessed. Some variation in DLS may also have been due to age-related changes in the ocular media as well as age-related changes of the retina,<sup>38</sup> other than loss of RGCs, and of the central nervous system.

For DLS values near zero, we still measured retardation equivalent to approximately 20  $\mu\text{m}$  or more (Fig. 4.1.2). A possible explanation for this offset is that some RGCs had stopped functioning, but their axons were still present, thus exhibiting birefringence. Axons have been identified in the RNFL that have no demonstrable visual function.<sup>39</sup> Another explanation is that we measured residual retardation from incomplete compensation of anterior segment birefringence or that we measured retardation induced by birefringent structures in the eye other than the RGC axons or anterior segment, as has been suggested by measurements with polarization sensitive optical coherence tomography (De Boer JF, et al. *IOVS* 2003;44:ARVO E-Abstract 3388). It is unclear whether an offset may have been present in the instrument itself. The offset may also have been caused by the retardation originating from axons that had their origin outside the tested points of the HFA 24-2 program (i.e., either between the testing points or outside the tested central 24° area).

In the present study, we found a linear relationship between unlogged-DLS and RNFL retardation and a curvilinear relationship between decibel-DLS and RNFL retardation. This suggests that the unlogged-DLS scale may be more appropriate for comparing structural and functional measurements than the standard dB scale, as suggested earlier by Garway-Heath et al.<sup>13</sup> Clinically, however, the standard decibel scale may be more appropriate, because the variability of perimetric measurements between healthy subjects appears to be less when expressed in the decibel-DLS

scale than in the unlogged-DLS scale (cf. Figs 4.1.2A-F, *right* and *left*). This apparently improved variability may, however, lower its sensitivity to detecting change, notably at the higher end of the decibel-DLS scale. Such change might, as stated earlier, be better monitored with SLP than with SAP.

## Acknowledgment

The authors thank Paul G.H. Mulder, PhD (Department of Epidemiology & Biostatistics, Erasmus MC, Rotterdam, The Netherlands) for valuable discussions.

## References

1. American Academy of Ophthalmology. Preferred practice pattern. Primary open angle glaucoma. San Francisco, CA: American Academy of Ophthalmology; 2000.
2. Kerrigan-Baumrind LA, Quigley HA, Pease ME, Kerrigan DF, Mitchell RS. Number of ganglion cells in glaucoma eyes compared with threshold visual field tests in the same persons. *Invest Ophthalmol Vis Sci* 2000;41:741-8.
3. Quigley HA, Addicks EM, Green WR. Optic nerve damage in human glaucoma. III. Quantitative correlation of nerve fiber loss and visual field defect in glaucoma, ischemic neuropathy, papilledema, and toxic neuropathy. *Arch Ophthalmol* 1982;100:135-46.
4. Jonas JB, Schiro D. Localised wedge shaped defects of the retinal nerve fibre layer in glaucoma. *Br J Ophthalmol* 1994;78:285-90.
5. Tuulonen A, Airaksinen PJ. Initial glaucomatous optic disk and retinal nerve fiber layer abnormalities and their progression. *Am J Ophthalmol* 1991;111:485-90.
6. Quigley HA, Miller NR, George T. Clinical evaluation of nerve fiber layer atrophy as an indicator of glaucomatous optic nerve damage. *Arch Ophthalmol* 1980;98:1564-71.
7. Keltner JL, Johnson CA, Cello KE, et al. Classification of visual field abnormalities in the ocular hypertension treatment study. *Arch Ophthalmol* 2003;121:643-50.
8. Heijl A, Leske MC, Bengtsson B, et al. Reduction of intraocular pressure and glaucoma progression: results from the Early Manifest Glaucoma Trial. *Arch Ophthalmol* 2002;120:1268-79.
9. Gordon MO, Kass MA. The Ocular Hypertension Treatment Study: design and baseline description of the participants. *Arch Ophthalmol* 1999;117:573-83.
10. Greve EL. Single and multiple stimulus static perimetry in glaucoma; the two phases of perimetry. Thesis. *Doc Ophthalmol* 1973;36:1-355.
11. Garway-Heath DF, Caprioli J, Fitzke FW, Hitchings RA. Scaling the hill of vision: the physiological relationship between light sensitivity and ganglion cell numbers. *Invest Ophthalmol Vis Sci* 2000;41:1774-82.
12. Harwerth RS, Carter-Dawson L, Shen F, Smith EL, III, Crawford MLJ. Ganglion Cell Losses Underlying Visual Field Defects from Experimental Glaucoma. *Invest Ophthalmol Vis Sci* 1999;40:2242-50.

13. Garway-Heath DF, Holder GE, Fitzke FW, Hitchings RA. Relationship between electrophysiological, psychophysical, and anatomical measurements in glaucoma. *Invest Ophthalmol Vis Sci* 2002;43:2213-20.
14. Jonas JB, Grondler AE. Correlation between mean visual field loss and morphometric optic disk variables in the open-angle glaucomas. *Am J Ophthalmol* 1997;124:488-97.
15. Airaksinen PJ, Drance SM, Douglas GR, Schulzer M. Neuroretinal rim areas and visual field indices in glaucoma. *Am J Ophthalmol* 1985;99:107-10.
16. Garway-Heath DF, Viswanathan A, Westcott M, et al. Relationship between perimetric light sensitivity and optic disc neuroretinal rim area. In: Wall M, Wild JM, eds. *Perimetry Update 1998/1999*. The Hague, The Netherlands: Kugler Publications; 1999:381-389.
17. Huang XR, Knighton RW. Linear birefringence of the retinal nerve fiber layer measured in vitro with a multispectral imaging micropolarimeter. *J Biomed Opt* 2002;7:199-204.
18. Dreher AW, Bailey ED. Assessment of the retinal nerve fiber layer by scanning-laser polarimetry. *SPIE* 1993;1877:266-71.
19. Weinreb RN, Dreher AW, Coleman A, et al. Histopathologic validation of Fourier-ellipsometry measurements of retinal nerve fiber layer thickness. *Arch Ophthalmol* 1990;108:557-60.
20. Knighton RW, Huang XR. Linear birefringence of the central human cornea. *Invest Ophthalmol Vis Sci* 2002;43:82-6.
21. Weinreb RN, Bowd C, Greenfield DS, Zangwill LM. Measurement of the magnitude and axis of corneal polarization with scanning laser polarimetry. *Arch Ophthalmol* 2002;120:901-6.
22. Greenfield DS, Knighton RW, Huang XR. Effect of corneal polarization axis on assessment of retinal nerve fiber layer thickness by scanning laser polarimetry. *Am J Ophthalmol* 2000;129:715-22.
23. Reus NJ, Colen TP, Lemij HG. Visualization of Localized Retinal Nerve Fiber Layer Defects with the GDx with Individualized and with Fixed Compensation of Anterior Segment Birefringence. *Ophthalmology* 2003;110:1512-6.
24. Bowd C, Zangwill LM, Weinreb RN. Association between scanning laser polarimetry measurements using variable corneal polarization compensation and visual field sensitivity in glaucomatous eyes. *Arch Ophthalmol* 2003;121:961-6.
25. Shields JR, Chen PP, Mills RP. Topographic mapping of glaucomatous visual field defects to scanning laser polarimetry of the peripapillary nerve fiber layer. *Ophthalmic Surg Lasers* 2002;33:123-6.
26. Kwon YH, Hong S, Honkanen RA, Alward WL. Correlation of automated visual field parameters and peripapillary nerve fiber layer thickness as measured by scanning laser polarimetry. *J Glaucoma* 2000;9:281-8.
27. Niessen AG, Van Den Berg TJ, Langerhorst CT, Greve EL. Retinal nerve fiber layer assessment by scanning laser polarimetry and standardized photography. *Am J Ophthalmol* 1996;121:484-93.
28. Chen YY, Chen PP, Xu L, et al. Correlation of peripapillary nerve fiber layer thickness by scanning laser polarimetry with visual field defects in patients with glaucoma. *J Glaucoma* 1998;7:312-6.

29. Tjon-Fo-Sang MJ, Lemij HG. The sensitivity and specificity of nerve fiber layer measurements in glaucoma as determined with scanning laser polarimetry. *Am J Ophthalmol* 1997;123:62-9.
30. Weinreb RN, Shakiba S, Sample PA, et al. Association between quantitative nerve fiber layer measurement and visual field loss in glaucoma. *Am J Ophthalmol* 1995;120:732-8.
31. Zhou Q, Weinreb RN. Individualized compensation of anterior segment birefringence during scanning laser polarimetry. *Invest Ophthalmol Vis Sci* 2002;43:2221-8.
32. Garway-Heath DE, Poinoosawmy D, Fitzke FW, Hitchings RA. Mapping the visual field to the optic disc in normal tension glaucoma eyes. *Ophthalmology* 2000;107:1809-15.
33. Sommer A, Katz J, Quigley HA, et al. Clinically detectable nerve fiber atrophy precedes the onset of glaucomatous field loss. *Arch Ophthalmol* 1991;109:77-83.
34. Heijl A, Lindgren G, Olsson J. Normal variability of static perimetric threshold values across the central visual field. *Arch Ophthalmol* 1987;105:1544-9.
35. Knighton RW, Huang XR, Greenfield DS. Analytical model of scanning laser polarimetry for retinal nerve fiber layer assessment. *Invest Ophthalmol Vis Sci* 2002;43:383-92.
36. Heijl A, Lindgren A, Lindgren G. Test-retest variability in glaucomatous visual fields. *Am J Ophthalmol* 1989;108:130-5.
37. Keltner JL, Johnson CA, Quigg JM, et al. Confirmation of visual field abnormalities in the Ocular Hypertension Treatment Study. Ocular Hypertension Treatment Study Group. *Arch Ophthalmol* 2000;118:1187-94.
38. Gao H, Hollyfield JG. Aging of the human retina. Differential loss of neurons and retinal pigment epithelial cells. *Invest Ophthalmol Vis Sci* 1992;33:1-17.
39. Quigley HA, Dunkelberger GR, Green WR. Retinal ganglion cell atrophy correlated with automated perimetry in human eyes with glaucoma. *Am J Ophthalmol* 1989;107:453-64.



## 4.2 Relationships between standard automated perimetry, HRT confocal scanning laser ophthalmoscopy, and GDx VCC scanning laser polarimetry

---

**Purpose:** To determine and compare the relationships between visual function measured with standard automated perimetry (SAP) and structure, either as neuroretinal rim area measured with confocal scanning laser ophthalmoscopy (CSLO), or as retinal nerve fiber layer (RNFL) thickness determined by scanning laser polarimetry with variable corneal compensation (SLP-VCC).

**Methods:** Forty-six healthy subjects and 76 glaucoma patients were examined with SAP, with CSLO by means of the Heidelberg Retina Tomograph I (HRT; Heidelberg Engineering, Dossenheim, Germany), and with SLP-VCC by means of the GDx VCC (Carl Zeiss Meditec, Inc., Dublin, CA, USA). The relationships between SAP, expressed either in the typically used decibel scale or as number of abnormal points in the total deviation probability plot, and CSLO and between SAP and SLP-VCC were described with linear and logarithmic regression analysis for global data and six individual sectors. The relationship between measurements with CSLO and SLP-VCC was fit with linear regression analysis.

**Results:** The relationship between SAP and CSLO and between SAP and SLP-VCC appeared curvilinear for all sectors except the temporal one between SAP and SLP-VCC. For CSLO, a logarithmic fit was statistically significantly better than a linear one for the global data and in the superotemporal and inferonasal sectors. For SLP-VCC, a curvilinear fit was better for the global data and in the superotemporal, superonasal, and inferonasal sectors. CSLO data correlated linearly with SLP-VCC data in all sectors, except temporally.

**Conclusions:** CSLO and SLP-VCC showed a very similar curvilinear relationship with SAP. The observed curvilinear relationships confirm earlier reports that these imaging devices appear to detect glaucomatous loss earlier than SAP. *Invest Ophthalmol Vis Sci, in press.*

---

**G**laucoma is a progressive optic neuropathy with loss of retinal ganglion cells (RGCs) and their axons, leading to loss of vision.<sup>1</sup> In clinical practice, functional losses are often assessed with standard automated perimetry (SAP). Structural losses may be assessed in a qualitative or semi-quantitative way with (in)direct ophthalmoscopy, stereoscopic optic disc photography, and red-free fundus photography. A more quantitative and objective analysis of structural losses may be performed with confocal scanning laser ophthalmoscopy

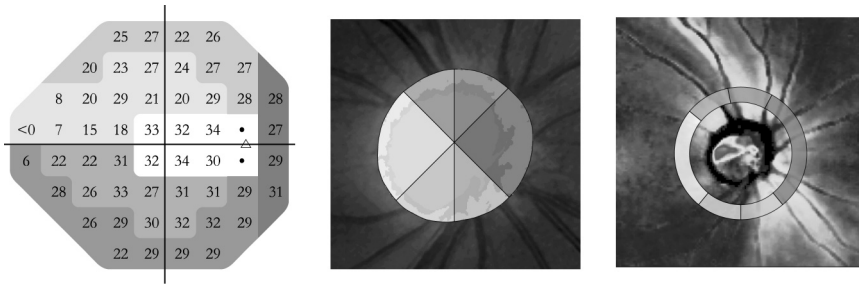


**Figure 4.2.1.** Standard automated perimetry test pattern (*left*), confocal scanning laser ophthalmoscopy (CSLO) topography map (*middle*), and scanning laser polarimetry with variable corneal compensation (SLP-VCC) retardation map (*right*) for a right eye. In the present study, visual field test points, CSLO measurements of rim area, and peripapillary SLP-VCC measurements were grouped in corresponding sectors, which have been grayscaled and named after the position of the sectors in the CSLO and SLP-VCC images relative to the optic disc.

(CSLO) and scanning laser polarimetry with variable corneal compensation (SLP-VCC).<sup>2</sup>

CSLO, featured in the commercially available Heidelberg Retina Tomograph (HRT; Heidelberg Engineering GmbH, Dossenheim, Germany), assesses the topography of the optic disc. It measures the intensity of light reflected off the retinal surface at subsequent depths of focus.<sup>3</sup> The weighted peak reflectance is thought to represent the interface between the retinal surface and the vitreous. The measured depths of peak reflectance at various points in the optic disc are used to construct a topography map of the optic disc (e.g., Fig. 4.2.1, *middle*).

SLP-VCC, featured in the commercially available GDx VCC (Carl Zeiss Meditec, Inc., Dublin, CA, USA), estimates the thickness of the peripapillary retinal nerve fiber layer (RNFL) by measuring the summed retardation of a polarized scanning laser beam, presumably induced by the form-birefringent microtubules that support the RGC axons.<sup>4-6</sup> The amount of retardation is proportional to the thickness of the RNFL and is therefore usually expressed in micrometers of thickness.<sup>6</sup> Retardation measurements at various points around the optic disc are used to construct a thickness map of the RNFL (e.g., Fig. 4.2.1, *right*). Equipped with VCC, SLP measurements have been shown to accurately assess RNFL morphology.<sup>7</sup>

Recently, we found a curvilinear relationship between function by SAP and structure by SLP-VCC in a large cohort of healthy subjects and glaucoma patients, when function was expressed in the standard, logarithmic, decibel scale.<sup>8</sup> When expressed in an unlogged scale, SAP measurements correlated linearly with SLP-VCC measurements.<sup>8</sup> In the present study, we investigated the relationship between function by SAP and structure by CSLO and compared it to the relationship between SAP and SLP-VCC in a single population of healthy subjects and



glaucoma patients. In addition, we compared measurements of neuroretinal rim area by CSLO with measurements of RNFL thickness by SLP-VCC.

## Methods

Forty-six eyes of 46 healthy subjects and 76 eyes of 76 patients with glaucoma were recruited prospectively for the present study. The research adhered to the tenets of the Declaration of Helsinki. The institutional human experimentation committee had approved the research. Informed consent was obtained from the subjects after explanation of the nature and possible consequences of the study.

### Healthy subjects

Healthy subjects of white ethnic origin were recruited either consecutively from an ongoing longitudinal follow-up study (n=28) or from employees of The Rotterdam Eye Hospital and their spouses and friends (n=18). All healthy subjects had a glaucoma hemifield test 'Within normal limits' and no nerve fiber bundle abnormalities, as described by Keltner et al,<sup>9</sup> in the total and/or pattern deviation probability plots with SAP. In addition, they had healthy-looking optic discs, an IOP of 21 mmHg or less in both eyes, and open angles upon gonioscopy. Slit lamp examination was unremarkable in all eyes. All subjects had a best-corrected visual acuity of 20/40 or better. None had any significant history of ocular disease, a history of intra-ocular surgery (except uncomplicated cataract surgery), relatives in the first and/or second degree with glaucoma, systemic hypertension for which medication was used, diabetes mellitus, or any other systemic disease. One eye was randomly selected for analysis.

### Glaucoma patients

Glaucoma patients of white ethnic origin were recruited consecutively from an ongoing longitudinal follow-up study (n=75) or after referral by a glaucoma specialist (HGL) for clinical reasons (n=1). All patients had a glaucomatous appearance of the optic disc (with notching or thinning of the neuroretinal rim),<sup>10</sup> a corresponding nerve fiber bundle visual field defect, as described by Keltner et al,<sup>9</sup> with SAP, and open angles by gonioscopy. Slit lamp examination was unremarkable in all eyes. All patients had a best-corrected visual acuity of 20/40 or better. None had any significant history of ocular disease other than glaucoma, a history of intra-ocular surgery (except any uncomplicated cataract or glaucoma surgery), systemic hypertension for which medication was used, diabetes mellitus, or any other systemic disease. One eye was randomly selected if both were eligible.

### Demographics

The mean age (SD) of the healthy subjects and the patients with glaucoma was 60 years (12) and

62 years (10), respectively, which was not statistically significantly different (two-samples *t*-test,  $P = 0.39$ ). The disc area (SD), derived from the HRT data, was  $1.95 \text{ mm}^2$  (0.35) in the healthy subjects and  $2.00 \text{ mm}^2$  (0.41) in the glaucoma patients, which was not statistically significantly different (two-samples *t*-test,  $P = 0.47$ ). In the healthy group, 23 of the 46 subjects (50%) were men. Of the glaucoma patients, 46 of the 76 (60%) were men. Twenty-five of the 46 randomly selected eyes (54%) in the healthy subjects were right ones; in the glaucoma group, 37 of the 76 eyes (49%) were right eyes.

The mean 'mean deviation' (SD; range) of the visual field was 0.38 dB (0.99; -1.55 to 2.73) in the healthy group and -9.52 dB (8.43; -30.39 to 1.25) in the glaucoma group, respectively. The 'pattern standard deviation' (SD; range) of the visual field was 1.63 dB (0.26; 1.13 to 2.30) in the healthy eyes and 8.35 dB (4.32; 1.99 to 15.92) in the glaucoma eyes, respectively.

The mean period (SD) between measurements with SAP, CSLO, and SLP-VCC was 1 month (6) in healthy subjects and 0 months (1) in glaucoma patients.

### Visual Field Testing

Visual field testing was performed with the Humphrey Field Analyzer II (HFA; Carl Zeiss Meditec, Inc., Dublin, CA, USA) by means of the 24-2 Full-Threshold (FT) or Swedish interactive threshold algorithm (SITA) Standard test program. Twenty-nine of the 46 (63%) healthy subjects and 73/76 (96%) glaucoma patients were tested with the FT paradigm. Visual fields had to be reproducible as well as reliable. Reliability criteria applied were: 1) fixation losses <25% and 2) false-positive and false-negative response rates  $\leq 20\%$  for the FT test paradigm and  $\leq 7\%$  for the SITA-Standard test program. In glaucoma eyes with advanced field loss, higher false-negative response rates were accepted: up to 33% for the FT paradigm and up to 12% for the SITA-Standard paradigm. The two visual field test points nearest to the blind spot were excluded from analysis. The 52 remaining test points were grouped into 6 sectors based on the relationship between visual field test points and regions of the optic disc as described by Garway-Heath et al (Fig. 4.2.1).<sup>11</sup> For each sector, the arithmetic mean differential light sensitivity (DLS) was calculated. DLS was expressed in the typically used decibel scale ( $\text{DLS} = 10 \times \log_{10} L_{\text{max}} / (L_t - L_b)$ ), where  $L_{\text{max}}$  is the perimeter's maximum stimulus luminance,  $L_t$  is the stimulus luminance at threshold, and  $L_b$  is background luminance). For the HFA,  $L_b = 31.6 \text{ asb}$  and  $L_{\text{max}} = 10,000 \text{ asb}$ . Because various large clinical trials, such as the Collaborative Initial Glaucoma Treatment Study (CIGTS)<sup>12</sup> and the Early Manifest Glaucoma Trial (EMGT)<sup>13</sup>, analyze probability plots instead of raw DLS values for evaluating progression of visual field loss, we also calculated a weighted score of the number of abnormal points in the total deviation probability plot with a sensitivity below the 5th percentile for each sector. To this end, we awarded points with a sensitivity at  $p < 5\%$  a score of 1, points at  $p < 2\%$  a score of 2, points at  $p < 1\%$  a score of 3, and points at  $p < 0.5\%$  a score of 4. We then calculated the sum of scores of all points within a sector. For example,

the sector ST with 14 test points could have a minimum score of zero and a maximum score of 56 (i.e.,  $4 \times 14$ ).

### **CSLO Measurements**

CSLO measurements were performed with the Heidelberg Retina Tomograph by three trained and experienced operators. Pupils of subjects were undilated and the room lights were left on. Before each measurement, the subject's corneal curvature radius was entered into the software. The patient's face was then gently placed onto the head-and-chin rest of the HRT and imaging was performed at the 1.5-cm imaging head-eye distance, recommended in the instruction manual, as the subject viewed a distant fixation target. Three high-quality images at a  $15^\circ \times 15^\circ$  scanning angle were recorded for each subject. The quality of the images was judged by the technician with the aid of the HRT software. All images were of high quality, i.e. with a centered optic disc, with a clear dark-light-dark pattern over the 32 consecutive images, even and just illuminated throughout the individual images, and without any motion artifacts. A mean topography image, computed from the three scans, was used for subsequent analysis with HRT software version 1.4.0.0. Mean images with a mean SD of the height measurements  $>50 \mu\text{m}$  were excluded from analysis. The optic disc margin was manually marked at the inner edge of Elschnig's ring by one of the authors (NJR). When in doubt about the position of the optic disc margin, stereoscopic optic disc photographs were examined to assist accurate positioning. The standard reference plane was used for calculations of optic disc topography with the relative and tilted coordinate system turned on. The software calculated the rim area ( $\text{mm}^2$ ) for the whole disc (global) and for 6 individual sectors, i.e. a superotemporal sector (ST; extending from  $45^\circ$  to  $90^\circ$ , relative to the temporal meridian), a superonasal one (SN;  $90^\circ$ - $135^\circ$ ), a nasal one (N;  $135^\circ$ - $225^\circ$ ), an inferonasal one (IN;  $225^\circ$ - $270^\circ$ ), an inferotemporal one (IT;  $270^\circ$ - $315^\circ$ ), and a temporal one (T;  $315^\circ$ - $45^\circ$ ).

### **SLP Measurements**

SLP measurements were performed with the GDx VCC by three trained and experienced technicians. Pupils of subjects were undilated and the room lights were left on. The spherical equivalent refractive error of each eye was entered into the software to allow the GDx VCC to focus on the retina. If necessary, the focus was adjusted manually in 0.25 diopter steps. The patient's face was gently placed into the face mask of the GDx VCC. To maintain the same orientation of the slow axes of the birefringent structures in the eye to that of the instrument's compensator, the operator saw to it that patients had their heads as vertical as possible during all measurements. For each scan, the operator aligned the instrument with the cornea and the sclera of the measured eye. Anterior segment birefringence was assessed<sup>14</sup> for each eye individually after which the eye was scanned with individualized compensation, as has been described previously.<sup>8</sup>

The quality of each scanned image was judged by the technician with the aid of the GDx VCC software. All images were of high quality, i.e. with a centered optic disc, well-focused, even and just illuminated throughout the image, and without any motion artifacts. The margin of the optic disc was manually marked with an ellipse on a reflection image of the fundus. The GDx VCC software positioned a circle, 8 pixels wide ( $-0.4$  mm in an emmetropic eye) and with an inner diameter of 54 pixels ( $-2.5$  mm in an emmetropic eye), centered on the center of the ellipse. The instrument processed the retardation values within this band to give 256 values evenly distributed along the circle, after which they were grouped into 64 sectors and exported by the software (version 5.4.0). These values were subsequently grouped into six sectors with the same dimensions and orientation as for the HRT data (Fig. 4.2.1).

### Data Analysis

To determine any correlation between function and structure, the degree of association between SAP (expressed as DLS and as abnormal number of points) and CSLO measurements and SAP (expressed as DLS and as abnormal number of points) and SLP-VCC measurements was determined with Spearman's rank correlation coefficient ( $r_s$ ) for the global data and for each sector individually.

Then, the relationship between SAP and CSLO measurements and SAP and SLP-VCC measurements was described with a least squares linear ( $y = a + b \times x$ ) and logarithmic ( $y = a + b \times \log_{10} x$ ) regression analysis. We determined this relationship for the healthy subjects who were tested with either the SITA or FT paradigm ( $n = 46$ ) and glaucoma patients who were tested with the FT paradigm ( $n = 73$ ). In addition, we investigated the relationships in two other groups separately: 1) healthy subjects ( $n = 28$ ; 1 subject was excluded for age-matching) and glaucoma patients ( $n = 66$ ; 7 subjects were excluded for age-matching) who were tested with the

Sector	SAP & CSLO		SAP & SLP-VCC	
	$r_s$	$P$	$r_s$	$P$
Global	0.70	< 0.001	0.65	< 0.001
Superotemporal	0.75	< 0.001	0.77	< 0.001
Superonasal	0.56	< 0.001	0.66	< 0.001
Nasal	0.44	< 0.001	0.42	< 0.001
Inferonasal	0.64	< 0.001	0.51	< 0.001
Inferotemporal	0.67	< 0.001	0.57	< 0.001
Temporal	0.50	< 0.001	0.03	0.78

**Table 4.2.1.** Degrees of association, expressed with Spearman's rank correlation coefficient ( $r_s$ ,  $P$ ), between standard automated perimetry (SAP) differential light sensitivity, confocal scanning laser ophthalmoscopy (CSLO), and scanning laser polarimetry with variable corneal compensation (SLP-VCC) in patients with glaucoma ( $n = 73$ ) and healthy subjects ( $n = 46$ ).

Sector	SAP & CSLO		SAP & SLP-VCC	
	$r_s$	$P$	$r_s$	$P$
Global	0.74	< 0.001	0.72	< 0.001
Superotemporal	0.71	< 0.001	0.76	< 0.001
Superonasal	0.53	< 0.001	0.56	< 0.001
Nasal	0.42	< 0.001	0.46	< 0.001
Inferonasal	0.59	< 0.001	0.54	< 0.001
Inferotemporal	0.68	< 0.001	0.60	< 0.001
Temporal	0.56	< 0.001	0.05	0.59

**Table 4.2.2.** Degrees of association, expressed with Spearman's rank correlation coefficient ( $r_s$ ,  $P$ ), between standard automated perimetry (SAP) abnormal number of points in the total deviation probability plot, confocal scanning laser ophthalmoscopy (CSLO), and scanning laser polarimetry with variable corneal compensation (SLP-VCC) in patients with glaucoma ( $n = 73$ ) and healthy subjects ( $n = 46$ ).

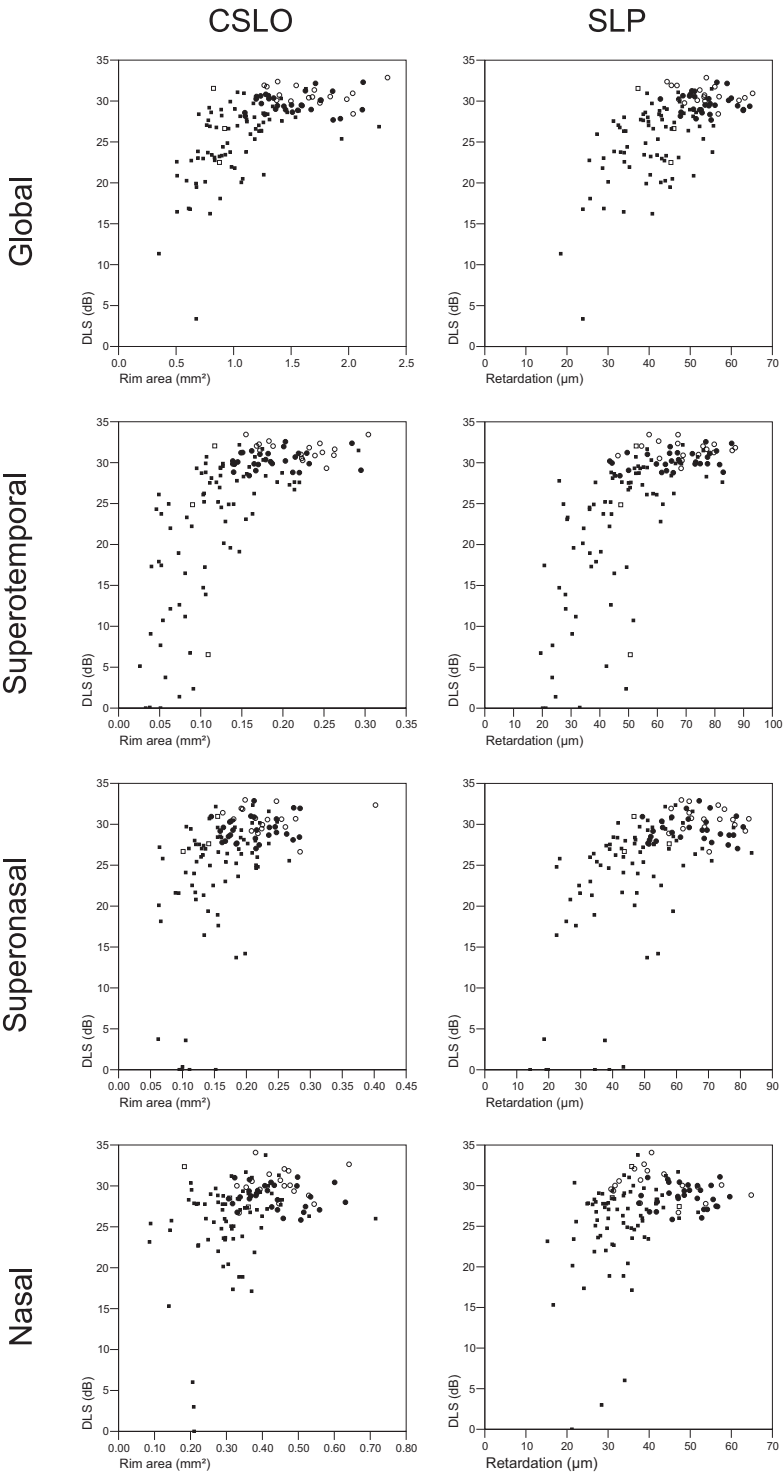
FT paradigm, and 2) glaucoma patients who were tested with the FT paradigm ( $n = 73$ ).

For comparison with a recent study by Schlottmann et al,<sup>15</sup> we used a paired  $t$ -test to evaluate the null hypothesis that the absolute prediction errors (absolute values of the residuals) had the same mean for both models (logarithmic and linear regression). Statistical significance was assumed at  $P < 0.05$ . For comparison, we plotted neuroretinal rim area measured with CSLO against RNFL thickness measured with SLP-VCC for the global data and also for the individual sectors and described their relationship with linear regression analysis.

## Results

The relationships between SAP and CSLO measurements and between SAP and SLP-VCC measurements have been graphically presented in figure 4.2.2. SAP measurements, expressed either as DLS or as abnormal number of points, were statistically significantly correlated with both CSLO and SLP-VCC measurements for the global data as well as for most individual sectors (Fig. 4.2.2, tables 4.2.1 and 4.2.2). In the temporal sector, however, SAP measurements were not statistically significantly correlated with SLP-VCC measurements ( $r_s = 0.003$  with  $P = 0.98$  and  $r_s = 0.03$  with  $P = 0.74$  when SAP was expressed as DLS or abnormal number of points, respectively) (Fig. 4.2.2, tables 4.2.1 and 4.2.2).

The statistically significant relationships between function and structure were curvilinear in appearance (Fig. 4.2.2). Healthy eyes had high DLS values with large rim areas and high retardation values. In general, glaucoma eyes had lower DLS values with smaller rim areas and lower retardation values. However, there was considerable overlap in measurements between the groups.



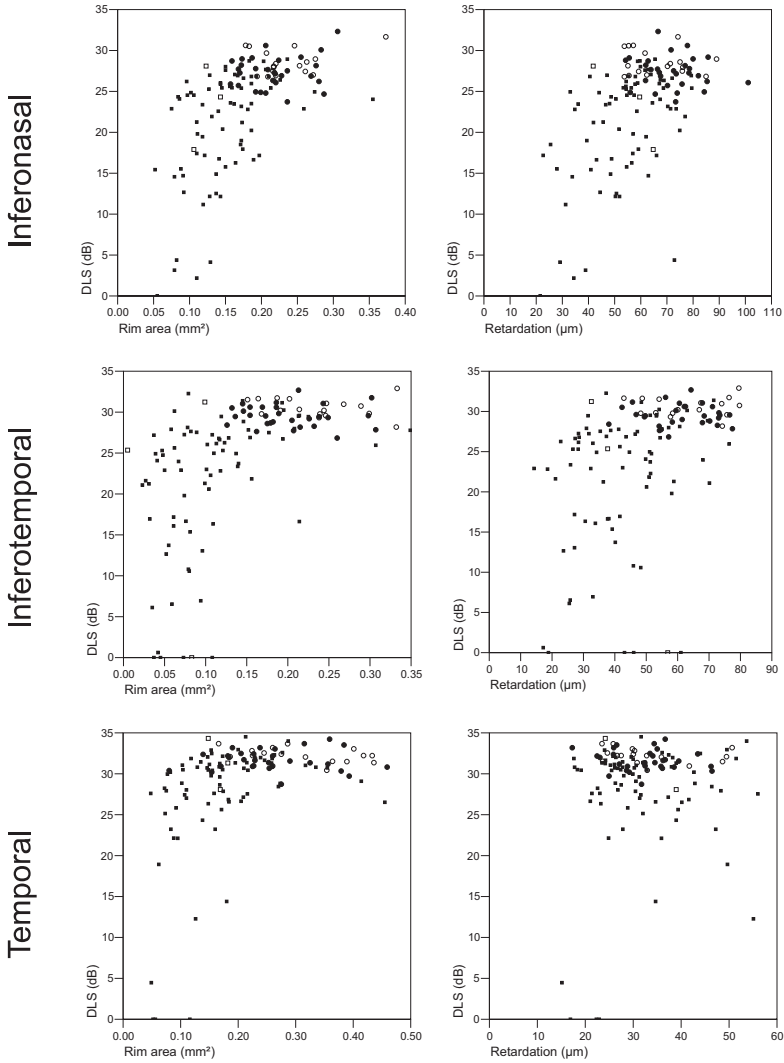


**Figure 4.2.2** (← and ↑). Scatterplots of differential light sensitivity (DLS), expressed in the standard decibel (dB) scale, against confocal scanning laser ophthalmoscopy (CSLO) measurements (*left*) and against scanning laser polarimetry with variable corneal compensation (SLP-VCC) measurements (*right*) for global data and 6 individual sectors. (●) Healthy eyes tested with the FT paradigm; (○) healthy eyes tested with the SITA paradigm; (■) glaucoma eyes tested with the FT paradigm; (□) glaucoma eyes tested with the SITA paradigm.

Sector	Healthy subjects (SITA and FT) and glaucoma patients (FT)			Healthy subjects (FT) and glaucoma patients (FT)			Glaucoma patients (FT)		
	Linear regression ( $R^2$ )	Logarithmic regression ( $R^2$ )	P	Linear regression ( $R^2$ )	Logarithmic regression ( $R^2$ )	P	Linear regression ( $R^2$ )	Logarithmic regression ( $R^2$ )	P
Global	0.42	0.51	0.002	0.36	0.43	0.016	0.28	0.36	0.10
Superotemporal	0.48	0.59	< 0.001	0.45	0.55	0.001	0.41	0.48	0.003
Superonasal	0.26	0.29	0.12	0.21	0.21	0.53	0.19	0.19	0.56
Nasal	0.16	0.16	0.52	0.12	0.14	0.38	0.08	0.08	0.81
Inferonasal	0.36	0.41	0.019	0.29	0.32	0.091	0.22	0.27	0.18
Inferotemporal	0.31	0.35	0.018	0.27	0.31	0.060	0.17	0.18	0.60
Temporal	0.18	0.29	0.061	0.16	0.27	0.14	0.16	0.27	0.11

**Table 4.2.3.** Coefficient of determination ( $R^2$ ) of linear and logarithmic regression analysis between differential light sensitivity, expressed in the standard decibel scale, and CSLO measurements. Data were analyzed separately for 1) healthy subjects tested with the Full-Threshold (FT) or SITA-Standard paradigm ( $n = 46$ ) and patients with glaucoma tested with the FT paradigm ( $n = 73$ ), 2) healthy subjects ( $n = 29$ ) and patients with glaucoma ( $n = 67$ ) tested with the FT paradigm, and 3) patients with glaucoma tested with the FT paradigm ( $n = 73$ ).



Sector	Healthy subjects (SITA and FT) and glaucoma patients (FT)			Healthy subjects (FT) and glaucoma patients (FT)			Glaucoma patients (FT)		
	Linear regression ( $R^2$ )	Logarithmic regression ( $R^2$ )	P	Linear regression ( $R^2$ )	Logarithmic regression ( $R^2$ )	P	Linear regression ( $R^2$ )	Logarithmic regression ( $R^2$ )	P
Global	0.43	0.47	0.006	0.35	0.38	0.082	0.27	0.32	0.049
Superotemporal	0.50	0.57	< 0.001	0.44	0.49	< 0.001	0.43	0.47	0.001
Superonasal	0.37	0.44	< 0.001	0.28	0.34	0.002	0.28	0.34	0.007
Nasal	0.15	0.18	0.31	0.17	0.19	0.20	0.11	0.11	0.67
Inferonasal	0.30	0.35	0.031	0.27	0.30	0.060	0.22	0.25	0.36
Inferotemporal	0.22	0.23	0.18	0.16	0.16	0.94	0.07	0.08	0.55
Temporal	0.01	0.03	0.82	0.00	0.00	0.26	0.02	0.04	0.18

**Table 4.2.4.** Coefficient of determination ( $R^2$ ) of linear and logarithmic regression analysis between differential light sensitivity, expressed in the standard decibel scale, and SLP-VCC measurements. Data were analyzed separately for 1) healthy subjects tested with the Full-Threshold (FT) or SITA-Standard paradigm ( $n = 46$ ) and patients with glaucoma tested with the FT paradigm ( $n = 73$ ), 2) healthy subjects ( $n = 29$ ) and patients with glaucoma ( $n = 67$ ) tested with the FT paradigm, and 3) patients with glaucoma tested with the FT paradigm ( $n = 73$ ).

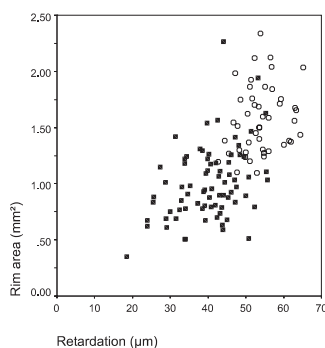


**Figure 4.2.3.** Scatterplot of neuroretinal rim area measured with confocal scanning laser ophthalmoscopy and retinal nerve fiber layer thickness measured with scanning laser polarimetry with variable corneal compensation for global data. (○) Healthy eyes; (■) glaucoma eyes.

With regard to the relationships between SAP and CSLO data with both healthy subjects and glaucoma patients included, logarithmic regression analysis yielded higher coefficients of determination ( $R^2$ ) than linear regression analysis both for the pooled data and for the superotemporal, inferonasal, and inferotemporal sectors (Table 4.2.3). For the other sectors, logarithmic regression analysis was not statistically significantly different from linear regression analysis (Table 4.2.3). When only healthy subjects and patients with glaucoma who were tested with the FT paradigm were analyzed, logarithmic regression analysis yielded statistically significantly higher  $R^2$  values than linear regression analysis for the pooled data and for the superotemporal sector (Table 4.2.3). When only the glaucoma patients tested with the FT paradigm were analyzed, logarithmic regression analysis appeared to yield higher  $R^2$  values than linear regression analysis for the global data as well as for most sectors (Table 4.2.3). However, this difference was only statistically significant for the superotemporal sector (Table 4.2.3).

In the comparisons between SAP and SLP-VCC data with both healthy subjects and glaucoma patients included, we found statistically significantly higher  $R^2$  values with logarithmic regression analysis than with linear regression analysis for the global data and in the superotemporal, superonasal, and inferonasal sectors (Table 4.2.4). When only healthy subjects and patients with glaucoma who were tested with the FT paradigm were included, logarithmic regression analysis yielded statistically higher  $R^2$  values than linear regression analysis for the superotemporal and superonasal sectors (Table 4.2.4). When only glaucoma patients tested with the FT paradigm were included, logarithmic regression analysis appeared to yield higher  $R^2$  values than linear regression analysis for the global data as well as for the individual sectors (Table 4.2.4). However, this difference was only statistically significant for the superotemporal and superonasal sectors (Table 4.2.4).

Sector	$R^2$	Slope ( $\text{mm}^2 \times \mu\text{m}^{-1}$ )	$P$
Global	0.40	$2.71 \times 10^{-2}$	< 0.001
Superotemporal	0.46	$2.50 \times 10^{-3}$	< 0.001
Superonasal	0.34	$2.09 \times 10^{-3}$	< 0.001
Nasal	0.28	$5.86 \times 10^{-3}$	< 0.001
Inferonasal	0.25	$2.01 \times 10^{-3}$	< 0.001
Inferotemporal	0.38	$2.94 \times 10^{-3}$	< 0.001
Temporal	0.04	$2.05 \times 10^{-3}$	0.041

**Table 4.2.5.** Relationship between measurements of neuroretinal rim area with CSLO and measurements of RNFL thickness with SLP-VCC, described with linear regression analysis for global data and 6 individual sectors.

The relationships between SAP and CSLO and between SAP and SLP-VCC appeared very similar (cf. Fig. 4.2.2, *left* and *right*, respectively). Moreover, logarithmic regression analysis of the relationship between SAP and CSLO measurements and between SAP and SLP-VCC measurements did not yield statistically significantly different fits ( $P$  values for global data and the ST, SN, N, IN, IT, and T sectors, 0.20, 0.64, 0.26, 0.73, 0.31, 0.09, and 0.15, respectively).

With regard to healthy subjects, at the higher end of the DLS values in figure 4.2.2, visual function data obtained with the SITA paradigm appeared to be consistently higher than data obtained with the FT paradigm (Fig. 4.2.2). Statistically, DLS values obtained with SITA were statistically significantly higher than DLS values obtained with FT for the pooled data and for the sectors ST, SN, N, IN, and IT ( $P$  values, 0.003, <0.001, 0.011, 0.004, 0.034, 0.011, respectively). For the temporal sector, this difference was not statistically significant ( $P = 0.11$ ).

The CSLO data correlated well with the SLP-VCC data, both for the pooled data (Global; Table 4.2.5, Fig. 4.2.3) and for the individual sectors (Table 4.2.5).

## Discussion

We have presently shown that measurements of neuroretinal rim area assessed with CSLO correlate well with measurements of function by SAP. Their relationship is very similar to the relationship between SAP and measurements of RNFL thickness with SLP-VCC. In addition, we found for both techniques that the relationship between function and structure was curvilinear when function was expressed in the clinically used decibel scale. These findings compare well with other studies on the relationship between perimetry and measurements of neuroretinal rim area by CSLO<sup>16,17</sup> and RNFL thickness by SLP-VCC.<sup>8,15</sup> Furthermore, we found that neuroretinal rim area measured with CSLO correlates linearly with RNFL thickness measured with SLP-VCC.

In clinical practice, differential light sensitivity is expressed in a decibel scale. In this scale, higher values are relatively compressed, as lower values are stretched. As a result, functional damage at higher sensitivities will appear relatively small, whereas progressive damage at lower sensitivities will appear relatively large. In eyes with no or only mild to moderate glaucomatous functional loss, clinically relevant changes in neuroretinal rim area and RNFL thickness, which are expressed in a linear scale, might then occur with only small changes in retinal light sensitivity (e.g., see Fig. 4.2.2). This suggests that a small neuroretinal rim area or a thin RNFL may be detected in eyes with normal visual fields by SAP. In fact, we have recently reported that perimetrically unaffected eyes of glaucoma patients with unilateral field loss on average have a thinner RNFL by SLP-VCC than healthy control eyes.<sup>18</sup> Similarly, Bagga and Greenfield<sup>19</sup> have shown with SLP-VCC and optical coherence tomography (OCT), a technique used to create cross-sectional images of the retina, that in glaucomatous eyes with a normal visual hemifield the corresponding RNFL may be abnormally thin. For the HRT, Wollstein et al<sup>20</sup> have found that thinning of the neuroretinal rim may occur in perimetrically unaffected eyes of normal pressure glaucoma patients with visual field loss in the other eye. For all three techniques, follow-up of these eyes with so-called pre-perimetric glaucoma is indicated to determine whether they will indeed develop glaucomatous visual field loss with SAP. We would like to stress that these results do not indicate that structural losses occur before functional losses per se. In theory, changes in RGC function might even precede structural changes. However, current techniques for assessing structure, such as SLP-VCC and CSLO, appear to be more sensitive for detecting glaucomatous damage than the routinely used SAP. Whether other psychophysical tests, such as frequency-doubling technology (FDT) and short-wavelength automated perimetry (SWAP), may detect functional changes at an earlier stage needs to be explored.

At the other end of the spectrum, SAP may be more sensitive to detecting changes in patients with severe glaucomatous functional loss as functional changes in this part of the decibel scale are maximized. However, the reproducibility of measurements with SAP has been shown to be fairly poor,<sup>21,22</sup> which may limit its sensitivity for detecting more subtle changes. The reproducibility of the HRT<sup>23,24</sup> as well as of the GDx VCC (Bagga H, et al. *IOVS* 2004;45:ARVO E-Abstract 5503) appears to be reasonably good over short periods of time. In the long term, however, the reproducibility of the HRT was reported to be only slightly better than that of SAP by means of the Octopus perimeter.<sup>25</sup> In addition, the dynamic range in these eyes with severe glaucomatous loss is smaller for measurements with CSLO and SLP-VCC than with SAP (e.g., see Fig. 4.2.2), which may limit the number of statistically significant changes that can be detected with CSLO and SLP-VCC. Therefore, whether the HRT I and GDx VCC may be better able to detect subtle changes than SAP in these eyes remains to be investigated.

We presently showed that the relationship between SAP and either CSLO or SLP-VCC was very similar when SAP was expressed as either DLS (dB) or as number of abnormal points in the total deviation probability plot. These data suggest that analyses for detecting progressive visual field loss based on changes in probability plots, such as used in CIGTS, may yield similar results as analyses based on raw DLS values. However, a limitation of using the number of abnormal points analysis may be that when a point has reached a sensitivity below  $p < 0.5\%$ , the depth of the defect is not reflected in this parameter anymore and data will be censored. Therefore, further research is needed to evaluate these two expressions of visual function in detecting progressive visual field loss in long term follow-up studies.

When looking at the data of healthy subjects and patients with glaucoma in figure 4.2.2, a curvilinear relationship between function and structure was apparent in most sectors. This was also true when the relationship between function and structure was analyzed in patients with glaucoma only, indicated by the higher  $R^2$  values found with logarithmic regression analysis over linear regression analysis. However, only few sectors showed a statistically significant better fit with logarithmic than with linear regression analysis. This may have been caused by the size of our sample, which may not have been large enough to detect a statistically significant difference between the two regression analyses. In addition, relatively few data points of patients with glaucoma were present in the lower left part and in the upper right part in the scatter plots of the pooled data and the individual sectors. A more balanced data set with more data points in the lower left as well as, with regard to data of patients with glaucoma, in the upper right part of the scatter plot might have yielded a better curvilinear fit.

CSLO measurements of neuroretinal rim area correlated well with SLP-VCC measurements of RNFL thickness. However, 54% to 96% of the variation in the relationship between CSLO and SLP-VCC was not explained. A good correlation between the techniques would have been intuitive. However, SLP-VCC and CSLO assess different aspects of axonal tissue, using different properties of light, and with different sources of error. Nevertheless, Medeiros et al<sup>26</sup> recently reported that the diagnostic accuracy for detecting glaucomatous visual field loss was similar for the HRT and GDx VCC at a specificity of 96% and slightly lower for the HRT at a specificity of 80%. Whether CSLO and SLP-VCC are equally good at monitoring glaucomatous functional loss needs to be investigated.

The relationships between SAP and CSLO and between SAP and SLP-VCC were very similar, both at a glance in figure 4.2.2 and by analysis of the residuals of linear regression analysis. For both techniques, 41% up to 97% of the variation in the relationship between function and structure was not explained. In a recent paper on the relationship between SAP and SLP-VCC,<sup>8</sup>

we have extensively discussed possible sources of scatter in this relationship. For example, some of it may be due to measurements of axonal tissue that had their origin outside the 54 relatively small areas tested by the HFA 24-2 test program. By contrast, both CSLO and SLP-VCC measure axonal tissue that originates from the entire retina. Furthermore, some of the scatter may have been induced by mismatching of the six optic nerve head sectors and the visual field test points, variation in the positioning of the head during measurements with either CSLO or SLP-VCC, and the reproducibility of measurements with all three techniques.

In the CSLO data, some of the scatter may also have been due to the inter-eye variation in the total volume occupied by the blood vessels in the optic nerve head, especially in the nasal regions. These blood vessels are erroneously measured by CSLO as part of the neuroretinal rim. In addition, the standard reference plane that we presently used to calculate rim area may have increased the scatter in the relationship between SAP and CSLO.<sup>27</sup> Furthermore, some variability may have been induced by drawing of the contour line to outline the optic disc, although its reproducibility has been reported to be quite good for a single observer.<sup>23</sup>

We did not find a statistically significant relationship between SAP and SLP-VCC in the temporal sector, which is similar to our previous findings.<sup>8</sup> Conversely, a curvilinear relationship was apparent between SAP and CSLO. In the temporal sector, SLP-VCC measured low amounts of retardation in comparison to the amount of retardation measured in other sectors. This may have yielded a low signal-to-noise ratio that possibly obscured a correlation. In addition, the form-birefringence of the axons in this sector may have been different from that in other sectors (Huang X, et al. *IOVS* 2003;44:ARVO E-Abstract 3363), with a different relationship between the amount of retardation and thickness of the RNFL and a different relationship with SAP.

In conclusion, we have presently shown that measurements of neuroretinal rim area with CSLO compare well with measurements of RNFL thickness with SLP-VCC. In addition, measurements with these two distinct techniques relate moderately well with retinal ganglion cell function assessed with standard automated perimetry. We think that the curvilinearity of the relationship between function and structure is mainly due to the standard decibel scale in SAP. This scale will probably lead to underestimating early glaucomatous damage by SAP. SLP-VCC and CSLO may better reflect this early damage. In more advanced glaucoma, the standard decibel scale in SAP is likely to overestimate progressive damage. Again, structural assessment with these imaging techniques may then better reflect any truly progressive damage.

The implications of the present findings for clinical glaucoma management, as well as the limitations of the imaging devices, need to be further explored. Furthermore, comparisons between functional measurements with psychophysical tests other than SAP and structural

measurements with CSLO and SLP-VCC may be of interest to further explore the relationship between function and structure.

## References

1. Quigley HA. Neuronal death in glaucoma. *Prog Retin Eye Res.* 1999;18:39-57.
2. Greenfield DS. Optic nerve and retinal nerve fiber layer analyzers in glaucoma. *Curr Opin Ophthalmol.* 2002;13:68-76.
3. Weinreb RN, Dreher AW, Bille JF. Quantitative assessment of the optic nerve head with the laser tomographic scanner. *Int Ophthalmol.* 1989;13:25-9.
4. Huang XR, Knighton RW. Linear birefringence of the retinal nerve fiber layer measured in vitro with a multispectral imaging micropolarimeter. *J Biomed Opt.* 2002;7:199-204.
5. Dreher AW, Bailey ED. Assessment of the retinal nerve fiber layer by scanning-laser polarimetry. *SPIE.* 1993;1877:266-71.
6. Weinreb RN, Dreher AW, Coleman A, et al. Histopathologic validation of Fourier-ellipsometry measurements of retinal nerve fiber layer thickness. *Arch Ophthalmol.* 1990;108:557-60.
7. Reus NJ, Colen TP, Lemij HG. Visualization of localized retinal nerve fiber layer defects with the GDx with individualized and with fixed compensation of anterior segment birefringence. *Ophthalmology.* 2003;110:1512-6.
8. Reus NJ, Lemij HG. The relationship between standard automated perimetry and GDx VCC measurements. *Invest Ophthalmol Vis Sci.* 2004;45:840-5.
9. Keltner JL, Johnson CA, Cello KE, et al. Classification of visual field abnormalities in the ocular hypertension treatment study. *Arch Ophthalmol.* 2003;121:643-50.
10. Jonas JB, Budde WM, Panda-Jonas S. Ophthalmoscopic evaluation of the optic nerve head. *Surv Ophthalmol.* 1999;43:293-320.
11. Garway-Heath DF, Poinosawmy D, Fitzke FW, Hitchings RA. Mapping the visual field to the optic disc in normal tension glaucoma eyes. *Ophthalmology.* 2000;107:1809-15.
12. Gillespie BW, Musch DC, Guire KE, et al. The collaborative initial glaucoma treatment study: baseline visual field and test-retest variability. *Invest Ophthalmol Vis Sci.* 2003;44:2613-20.
13. Leske MC, Heijl A, Hyman L, Bengtsson B. Early Manifest Glaucoma Trial: design and baseline data. *Ophthalmology.* 1999;106:2144-53.
14. Zhou Q, Weinreb RN. Individualized compensation of anterior segment birefringence during scanning laser polarimetry. *Invest Ophthalmol Vis Sci.* 2002;43:2221-8.
15. Schlottmann PG, De Cilla S, Greenfield DS, Caprioli J, Garway-Heath DF. Relationship between visual field sensitivity and retinal nerve fiber layer thickness as measured by scanning laser polarimetry. *Invest Ophthalmol Vis Sci.* 2004;45:1823-9.
16. Garway-Heath DF, Holder GE, Fitzke FW, Hitchings RA. Relationship between electrophysiological,

psychophysical, and anatomical measurements in glaucoma. *Invest Ophthalmol Vis Sci.* 2002;43:2213-20.

17. Garway-Heath DE, Viswanathan A, Westcott M, et al. Relationship between perimetric light sensitivity and optic disc neuroretinal rim area. In: Wall M, Wild JM, eds. *Perimetry Update 1998/1999*. The Hague, The Netherlands: Kugler Publications; 1999:381-389.
18. Reus NJ, Lemij HG. Scanning laser polarimetry of the retinal nerve fiber layer in perimetrically unaffected eyes of glaucoma patients. *Ophthalmology.* 2004.
19. Bagga H, Greenfield DS. Quantitative assessment of structural damage in eyes with localized visual field abnormalities. *Am J Ophthalmol.* 2004;137:797-805.
20. Wollstein G, Garway-Heath DE, Poinosawmy D, Hitchings RA. Glaucomatous optic disc changes in the contralateral eye of unilateral normal pressure glaucoma patients. *Ophthalmology.* 2000;107:2267-71.
21. Heijl A, Lindgren G, Olsson J. Normal variability of static perimetric threshold values across the central visual field. *Arch Ophthalmol.* 1987;105:1544-9.
22. Heijl A, Lindgren A, Lindgren G. Test-retest variability in glaucomatous visual fields. *Am J Ophthalmol.* 1989;108:130-5.
23. Miglior S, Albe E, Guareschi M, Rossetti L, Orzalesi N. Intraobserver and interobserver reproducibility in the evaluation of optic disc stereometric parameters by Heidelberg Retina Tomograph. *Ophthalmology.* 2002;109:1072-7.
24. Rohrschneider K, Burk RO, Kruse FE, Volcker HE. Reproducibility of the optic nerve head topography with a new laser tomographic scanning device. *Ophthalmology.* 1994;101:1044-9.
25. Funk J, Mueller H. Comparison of long-term fluctuations: laser scanning tomography versus automated perimetry. *Graefes Arch Clin Exp Ophthalmol.* 2003;241:721-4.
26. Medeiros FA, Zangwill LM, Bowd C, Weinreb RN. Comparison of the GDx VCC scanning laser polarimeter, HRT II confocal scanning laser ophthalmoscope, and Stratus OCT optical coherence tomograph for the detection of glaucoma. *Arch Ophthalmol.* 2004;122:827-37.
27. Tan JC, Garway-Heath DE, Fitzke FW, Hitchings RA. Reasons for rim area variability in scanning laser tomography. *Invest Ophthalmol Vis Sci.* 2003;44:1126-31.







# 5

**Scanning laser polarimetry of  
the retinal nerve fiber layer  
in perimetrically unaffected  
eyes of glaucoma patients**



---

**Purpose:** To compare scanning laser polarimetry (SLP) measurements of retinal nerve fiber layer (RNFL) thickness in perimetrically unaffected eyes of glaucoma patients to their fellow eyes with field loss and to eyes of healthy subjects.

**Design:** Observational case-control study.

**Participants and controls:** Twenty-three glaucoma patients with a reproducible visual field defect in one eye (mean 'mean deviation' [MD], -5.71 decibels [dB]) and a normal visual field in the other one, i.e.  $\geq 1$  visual field test point below the 5% probability level (mean MD, -0.01 dB), and 73 control eyes of as many age-matched healthy subjects (mean MD, 0.39 dB). The MD and pattern standard deviation of the glaucoma patients' eyes with normal visual fields and the control eyes were not statistically significantly different (independent samples *t* test,  $P = 0.15$  and  $P = 0.61$ , respectively).

**Methods:** All subjects were measured in both eyes with the GDx VCC, a commercially available instrument featuring SLP with automated variable corneal compensation (VCC). Standard automated perimetry (SAP) was assessed by means of the Humphrey Field Analyzer, 24-2 Full Threshold or SITA-Standard achromatic test program.

**Main outcome measures:** The standard GDx VCC parameters 'TSNIT Average', 'Superior Average', 'Inferior Average', 'TSNIT Std. Dev.', and 'Nerve Fiber Indicator' (NFI) were determined. We also assessed the thickness values in 6 parapapillary sectors. In addition, we calculated the proportion of eyes per group with an NFI  $\geq 40$ .

**Results:** GDx VCC measurements showed more RNFL thinning in the perimetrically unaffected eyes of glaucoma patients than in the healthy control eyes. The RNFL in the perimetrically unaffected eyes of glaucoma patients was thicker than in their fellow eyes with field loss. The NFI had a value  $\geq 40$  in 11/23 (47.8%) perimetrically unaffected eyes of glaucoma patients, 19/23 (82.6%) eyes with visual field loss of glaucoma patients, and 3/73 (4.1%) healthy control eyes.

**Conclusion:** With the GDx VCC, thinning of the RNFL may be detected in perimetrically unaffected eyes of glaucoma patients with field loss in their fellow eyes. *Ophthalmology* 2004;111:2199-2203.

---

In glaucoma, abnormalities of the optic disc and the retinal nerve fiber layer (RNFL) have been shown to precede the development of visual field loss with standard automated perimetry (SAP);<sup>1-4</sup> clinically detectable visual field defects develop only when significant numbers of retinal ganglion cells have been lost.<sup>5</sup>

The neuroretinal rim in perimetrically unaffected eyes of glaucoma patients with unilateral field loss has been reported to be thinner than the rim in eyes of healthy subjects, despite normal results with perimetry.<sup>6,7</sup> In addition, perimetrically unaffected eyes have been shown to have an increased risk of developing defects with SAP.<sup>8-10</sup>

Scanning laser polarimetry (SLP) with variable corneal compensation (VCC), featured in the commercially available GDx VCC (Laser Diagnostic Technologies, Inc., San Diego, CA, USA),

allows accurate, objective, and rapid assessment of the RNFL.<sup>11</sup> Some of our earlier data on eyes with established glaucomatous visual field loss and healthy eyes suggest that a mildly to moderately thin RNFL, measured by SLP with VCC, may not necessarily be associated with functional loss by SAP.<sup>12</sup> To test this hypothesis, we currently assessed the thickness of the RNFL with SLP-VCC in perimetrically unaffected eyes of patients with contralateral visual field loss from primary open-angle glaucoma (POAG). We compared the results to those of their fellow eyes with field loss and to eyes of healthy control subjects.

## Methods

### Subjects

Twenty-three glaucoma patients and 73 age-matched healthy subjects were measured with the GDx VCC between September 2002 and September 2003 by three experienced operators at the Perimetry Department of The Rotterdam Eye Hospital. Glaucoma patients were recruited consecutively from an ongoing longitudinal follow-up study, which they had entered between January 1998 and November 2000. All glaucoma patients had POAG in one eye, i.e. a glaucomatous appearance of the optic disc (with notching or thinning of the neuroretinal rim),<sup>13</sup> a corresponding nerve fiber bundle visual field defect, as described by Keltner et al,<sup>14</sup> with SAP (Humphrey Field Analyzer, 24-2 SITA-Standard or Full Threshold test program, Carl Zeiss Meditec, Dublin, CA, USA), and open angles by gonioscopy. Visual fields had to be reproducible as well as reliable. Reliability criteria applied were: 1) fixation losses  $\leq 25\%$  and 2) false-positive and false-negative response rates  $\leq 20\%$  for the Full Threshold (FT) test paradigm and  $\leq 7\%$  for the SITA-Standard test paradigm. In the eyes with advanced visual field loss, however, higher false-negative response rates were accepted: up to 33% for the FT paradigm and up to 12% for the SITA-Standard paradigm. None of the fellow eyes in these patients showed any significant abnormality with SAP, i.e. their visual fields had  $\leq 1$  visual field test point below the 5% probability level in either the total or pattern deviation probability plots. In addition, all these visual fields had a glaucoma hemifield test result classified as 'Within normal limits' and a mean deviation (MD) and a pattern standard deviation (PSD) better than the 5% probability level. For these eyes, the appearance of the optic disc was not a selection criterion. However, they had to have open angles upon gonioscopy. All patients were of Caucasian ethnic origin and had a best corrected visual acuity of 20/40 or better. None had any other significant history of ocular disease (including posterior segment eye disease and corneal disease), a history of intra-ocular surgery (except for uncomplicated cataract and glaucoma surgery), systemic hypertension for which medication was used, diabetes mellitus, or any other systemic disease. Slit lamp examination was unremarkable in all eyes (except for signs of glaucomatous optic neuropathy).

Healthy subjects were recruited either consecutively from an ongoing longitudinal follow-up study (n=46) or from employees of The Rotterdam Eye Hospital and their spouses and friends

(n=27). All healthy subjects had a glaucoma hemifield test 'Within normal limits' and no nerve fiber bundle abnormalities, as described by Keltner et al,<sup>14</sup> in the total and/or pattern deviation probability plots with SAP. In addition, they had healthy-looking optic discs and an IOP of 21 mmHg or less in both eyes. Only subjects with open angles upon gonioscopy were entered into the study. Slit lamp examination was unremarkable in all eyes. All subjects were of Caucasian ethnic origin and had a best corrected visual acuity of 20/40 or better. None had any significant history of ocular disease (including posterior segment eye disease and corneal disease), a history of intra-ocular surgery (except for uncomplicated cataract surgery), relatives in the first and/or second degree with glaucoma, systemic hypertension for which medication was used, diabetes mellitus, or any other systemic disease. One eye per subject was randomly selected for analysis with a custom-made algorithm in Microsoft Excel 97 (Microsoft Corporation, Redmond, WA, USA).

Twenty-two of the 23 glaucoma eyes with field loss and 47 of the healthy eyes were part of a previous study describing the relationship between SAP and SLP with VCC.<sup>12</sup> The presently studied perimetrically unaffected fellow eyes of the 23 glaucoma patients were not part of that study.

The research followed the tenets of the Declaration of Helsinki. Informed consent was obtained from the subjects after explanation of the nature and possible consequences of the study. The institutional human experimentation committee had approved the research.

### **Demographics**

The demographics of the 23 glaucoma patients with unilateral field loss and the 73 healthy subjects have been presented in table 1. The mean (SD; range) intraocular pressure (IOP) of the 23 perimetrically unaffected eyes at the time of inclusion for the present study was 15.4 mmHg (2.74; 11-21), measured with Goldmann applanation tonometry. Twenty-one of the 23 perimetrically unaffected eyes received treatment for lowering the IOP in both eyes. The other 2 only received treatment for the eye that showed field loss.

### **Measurement protocol**

In all subjects, both eyes were scanned with the GDx VCC, starting with the right eye. The spherical equivalent refractive error of each eye was entered into the software to allow the GDx VCC to focus on the retina. If necessary, the focus was adjusted manually in 0.25 diopters steps. The pupils of the patients were undilated and the room lights were left on. The patient's face was gently placed into the face mask of the GDx VCC. To maintain the same orientation of the slow axes of the birefringent structures in the eye to that of the instrument's compensator, the operator saw to it that patients had their heads as vertical as possible during all measurements. For each scan, the operator aligned the instrument with the cornea and the sclera of the measured eye.

	Glaucoma patients			Healthy subjects	Significance ( <i>P</i> value)
	<i>Perimetrically affected eyes</i>	<i>Perimetrically unaffected eyes</i>			
Age (years) (SD; range)		61 (9; 44-75)		59 (11; 35-82)	0.28
Gender (male) (%)		14 (61)		34 (47)	NA
Eye (right) (%)	12 (52%)		11 (48%)	33 (45)	NA
MD (dB) (SD; range)	-5.72 (4.11; -16.75 to -0.09)	-0.01 (1.15; -1.43 to +3.07)		0.39 (1.14; -2.89 to +2.90)	0.15
PSD (dB) (SD; range)	7.08 (3.87; 2.65-17.09)	1.59 (0.20; 1.23-1.94)		1.63 (0.40; 1.00-3.47)	0.61

**Table 5.1.** Demographics of both eyes of 23 glaucoma patients with unilateral field loss and 73 eyes of as many healthy subjects. dB = decibels; MD = mean deviation; NA = not applicable; PSD = pattern standard deviation; SD = standard deviation. Differences between perimetrically unaffected eyes of glaucoma patients and healthy eyes were tested for statistical significance with an independent samples *t* test.



First, anterior segment birefringence was assessed for each eye per subject with the method described by Zhou and Weinreb.<sup>15</sup> To this end, the magnitude of the compensator of the GDx VCC was automatically set to zero after which the fundus was scanned. The interaction between the birefringence of the radially oriented axons of the photoreceptors that constitute Henle's fiber layer in the macula, and the anterior segment birefringence, resulted in a bow-tie shaped pattern on the retardation image. The amount of retardation was measured from within a circular band with an inner diameter of 20 pixels (~0.9 mm in an emmetropic eye) that had been positioned manually with the fovea at its center. A dedicated algorithm, incorporated in the GDx VCC software, then determined the anterior segment birefringence (consisting of a polarization magnitude and a polarization axis) from this profile.

The software used these calculations to automatically adjust the anterior segment compensator to each individual eye, and both eyes were scanned again with individualized compensation. Adequate compensation of anterior segment birefringence was verified subjectively by looking at the retardation pattern in the macular region that had to be uniformly weak with a cross- or donut-shaped pattern. The typical time to measure both eyes of a patient was 3 minutes. All accepted scans were of high quality, i.e. with a centered optic disc, well focussed, even and just illuminated throughout the image, and without any motion artifacts. In addition, all measurements passed the scan quality checks that were automatically performed by the GDx VCC software.

### Data analysis

The margin of the optic disc was manually marked with an ellipse on a reflection image of the fundus. The GDx VCC software (version 5.1.0) positioned a circle, 8 pixels wide (~0.4mm in an emmetropic eye) and with an inner diameter of 54 pixels (~2.5mm in an emmetropic eye), centered on the center of the ellipse. Based on the retardation values within this band, the software calculated the following 6 parameters: 'TSNIT Average', 'Superior Average', 'Inferior Average', 'TSNIT Std. Dev.', 'Inter-Eye Symmetry', and 'Nerve Fiber Indicator' (NFI). The parameter 'Inter-Eye Symmetry' that describes the correlation in retardation measurements between the two eyes of a subject, was not used for analysis because of possible bias in glaucoma patients due to RNFL thinning in the eye with clinically significant visual field loss. The retardation values within the measurement band were grouped and averaged into 6 sectors that were described earlier by Garway-Heath et al:<sup>16</sup> a superotemporal one (ST; extending from 39.4° to 78.8°, relative to the temporal meridian), a superonasal one (SN; 78.8°-118.1°), a nasal one (N; 118.1°-230.6°), an inferonasal one (IN; 230.6°-270°), an inferotemporal one (IT; 270°-309.4°), and a temporal one (T; 309.4°-39.4°). We then compared differences between parameters and sectoral retardation values between the perimetrically unaffected eyes of the glaucoma patients and the eyes of the healthy controls with independent samples *t* tests. We also compared differences in the parameters and the sectoral retardation measurements between the fellow eyes of the

	Glaucoma patients			Significance of differences ( <i>P</i> )	
	Perimetrically affected eyes	Perimetrically unaffected eyes	Healthy subjects	Between fellow eyes of glaucoma patients	Between perimetrically unaffected eyes and healthy eyes
TSNIT Average (mm)	39.9 (36.4-43.4)	48.2 (45.7-50.7)	54.8 (53.4-56.1)	< 0.001	< 0.001
Superior Average (mm)	45.7 (40.4-50.9)	58.5 (54.3-62.6)	66.7 (65.0-68.4)	< 0.001	< 0.001
Inferior Average (mm)	44.6 (40.2-49.1)	53.4 (49.3-57.5)	61.5 (59.4-63.6)	0.001	< 0.001
TSNIT Std. Dev. (mm)	13.8 (11.4-16.1)	17.0 (14.9-19.1)	20.0 (19.2-20.9)	0.002	0.002
NFI	65.4 (54.4-76.5)	36.9 (29.0-44.8)	21.1 (19.2-23.1)	< 0.001	< 0.001
Superotemporal (mm)	43.0 (35.5-50.4)	61.6 (55.5-67.7)	65.4 (62.5-68.2)	< 0.001	0.22
Superonasal (mm)	47.8 (40.7-54.8)	59.8 (53.8-65.7)	70.4 (68.0-72.9)	< 0.001	< 0.001
Nasal (mm)	35.9 (32.5-39.3)	41.2 (38.5-43.9)	49.6 (47.8-51.5)	0.001	< 0.001
Inferonasal (mm)	54.7 (49.0-60.4)	62.4 (56.8-67.9)	72.5 (69.7-75.2)	0.005	0.001
Inferotemporal (mm)	43.9 (37.2-50.6)	57.2 (51.0-63.5)	67.7 (64.9-70.6)	0.002	0.001
Temporal (mm)	28.7 (25.0-32.5)	32.6 (29.9-35.2)	33.1 (31.0-35.2)	0.046	0.79

**Table 5.2.** Mean (95% confidence interval) values of 5 GDx VCC parameters and 6 parapapillary measurement sectors for both eyes of 23 glaucoma patients with unilateral field loss and 73 eyes of as many healthy subjects.

NFI = Nerve Fiber Indicator; TSNIT = temporal, superior, nasal, inferior, temporal.

Differences between parameters have been tested for statistical significance with a paired samples *t* test and an independent samples *t* test between fellow eyes of the glaucoma patients and between perimetrically unaffected eyes of glaucoma patients and healthy subjects, respectively.

glaucoma patients with paired samples  $t$  tests. In addition, we determined the number of eyes with an NFI  $\geq 40$  for each group. The cut-off value of  $\geq 40$  for this parameter has been shown to reach a sensitivity and specificity of 83.8% and 95.9%, respectively, for detecting mild functional glaucomatous loss.<sup>17</sup> Statistical analysis was performed with the computer program SPSS for Windows (release 11.0.1; SPSS, Chicago, IL, USA).

The amount of retardation measured by scanning laser polarimetry is usually expressed in micrometers of thickness based on the relationship between the amount of retardation and the histologically determined RNFL thickness in monkey eyes,<sup>18</sup> although this relationship may vary somewhat per nerve fiber bundle around the optic nerve head (Huang X, et al. *IOVS* 2003;44: ARVO E-Abstract 3363). For simplicity, we will use the term 'thickness' as a surrogate for 'retardation' in the present study

## Results

For most sectors, the RNFL was thinner in the perimetrically unaffected eyes of the glaucoma patients than in the healthy subjects (independent samples  $t$  tests;  $P$  values  $\leq 0.001$ ) (Table 2). In the superotemporal and temporal sectors, however, the average thickness was not statistically significantly different between the two groups (independent samples  $t$  tests;  $P$  values, 0.22 and 0.79, respectively) (Table 2). All GDx VCC parameters were statistically significantly different between the perimetrically unaffected eyes of the glaucoma patients and the healthy eyes (independent samples  $t$  test;  $P$  value  $\leq 0.002$ ) (Table 2).

The RNFL in the perimetrically unaffected eyes of the glaucoma patients was statistically significantly thicker than in their fellow eyes with field loss (paired samples  $t$  tests; all sectors, except the temporal one,  $P$  values  $\leq 0.005$ ; temporal sector,  $P$  value = 0.046) (Table 2). In addition, all standard GDx VCC parameters showed a statistically significantly thicker RNFL in the perimetrically unaffected eyes compared to their fellow eyes with visual field loss (paired samples  $t$  tests,  $P$  values  $\leq 0.002$ ) (Table 2).

The mean magnitudes of both the parapapillary thickness measurements and the summary parameters of the perimetrically unaffected eyes of the glaucoma patients fell between those of the control eyes and the glaucomatous eyes with field loss (Table 2).

The NFI had a value of 40 or higher in 11/23 (47.8%) perimetrically unaffected eyes of glaucoma patients. In the perimetrically affected eyes of the glaucoma patients and in the healthy eyes, 19/23 (82.6%) eyes and 3/73 (4.1%) eyes had a value  $\geq 40$ , respectively. The NFI in the perimetrically unaffected eyes of the glaucoma patients was statistically significantly correlated with the MD of their fellow eyes (Spearman's rank correlation coefficient ( $r_s$ ), -0.50;  $P$  value, 0.016). In the healthy control eyes, the NFI was not correlated with the MD of the fellow eyes ( $r_s$ , -0.01;  $P$  value, 0.91)

## Discussion

We have shown that the RNFL in perimetrically unaffected eyes of patients with asymmetric open-angle glaucoma is thinner than in eyes of healthy subjects as measured by SLP with VCC. These data support our recent findings that suggest that a mildly to moderately thin RNFL may not necessarily be associated with field loss by standard automated perimetry.<sup>12</sup> Compared to their fellow eyes with visual field defects, the perimetrically unaffected eyes of glaucoma patients had a thicker RNFL. We speculate that if further loss of nerve fibers in these perimetrically unaffected eyes were prevented, these eyes might retain their full fields.

Susanna Jr. and Galvao-Filho found similar results,<sup>19</sup> although they used a previous version of the GDx, viz. one with a fixed corneal compensation (FCC). SLP with FCC has been shown to sometimes yield spurious measurements of the RNFL.<sup>11,20,21</sup> Conversely, SLP with VCC, which we currently used, has been shown to allow objective assessment of RNFL morphology.<sup>11</sup>

In the superotemporal and temporal sectors, measurements of RNFL thickness in the perimetrically unaffected eyes of glaucoma patients were somewhat lower than in healthy control eyes, albeit not statistically significant, which agrees with findings by Garway-Heath and Hitchings,<sup>22</sup> who found that the superotemporal area of the neuroretinal rim is less affected in early glaucoma than other areas.

In the present study, we found that the NFI in perimetrically unaffected eyes of glaucoma patients was correlated with the severity of visual field loss in their fellow eyes. These results are comparable to the finding by Fontana et al<sup>10</sup> in patients with normal tension glaucoma and unilateral visual field loss that the severity of field damage in the contralateral eye is a risk factor for developing a field defect in the perimetrically unaffected eye. Between 7% and 26% of perimetrically unaffected eyes of glaucoma patients will develop visual field defects during a follow up period of 4 to 5 years.<sup>8-10,23</sup> In the present study, approximately one half of the eyes with normal perimetry had a thin RNFL, when abnormality was defined as an NFI  $\geq 40$ . Whether these eyes are the ones that will eventually develop glaucomatous visual field defects, and if so, how long that would take, remains to be investigated. If SLP with VCC were indeed a more sensitive technique for detecting early glaucomatous damage, so-called pre-perimetric glaucoma might perhaps be quantified and even defined, as SLP is a quantitative technique. To date, we believe that the notion of pre-perimetric glaucoma is poorly defined and therefore loosely used. By defining it, earlier detection and earlier treatment of glaucoma, with a potentially better prognosis might be in the offing. We found that a single parameter, the NFI, classified approximately half of the perimetrically unaffected eyes as glaucomatous. This parameter has been shown to have a high diagnostic accuracy for classifying glaucomatous and normal eyes.

Such a parameter may be the first step towards a working definition of pre-perimetric glaucoma. A working definition of pre-perimetric glaucoma is unlikely to entail critical measures of RNFL thickness per se due to its large variation across individuals. We think that a working definition of pre-perimetric glaucoma would probably also include the rate of change over time, which would not be detected by perimetry.

It is yet unclear whether other forms of perimetry, such as frequency doubling technology (FDT) and short-wavelength automated perimetry (SWAP), which have been shown to detect glaucoma earlier than SAP,<sup>24-27</sup> are abnormal in the perimetrically unaffected eyes in our study. Such a study is under way. Several studies have suggested that glaucomatous thinning of the RNFL may precede changes in the optic nerve head.<sup>28,29</sup> A limitation of the present study may be that we did not evaluate the appearance of the optic disc in the perimetrically unaffected eyes of glaucoma patients and relate them to SLP measurements.

In conclusion, we have presently shown that perimetrically unaffected eyes of glaucoma patients, with a high risk of developing glaucomatous visual field loss,<sup>8-10</sup> have a statistically significantly thinner RNFL than healthy eyes, measured with the GDx VCC. As the GDx VCC has a high diagnostic accuracy for diagnosing glaucoma<sup>17</sup> and allows rapid and objective assessment of the RNFL,<sup>11</sup> we think that evaluation of the RNFL with the GDx VCC may assist clinicians in making decisions in the management of glaucoma.

## References

1. Johnson CA, Sample PhD PA, Zangwill LM, et al. Structure and function evaluation (SAFE): II. Comparison of optic disk and visual field characteristics. *Am J Ophthalmol* 2003;135:148-54.
2. Tuulonen A, Airaksinen PJ. Initial glaucomatous optic disk and retinal nerve fiber layer abnormalities and their progression. *Am J Ophthalmol* 1991;111:485-90.
3. Sommer A, Katz J, Quigley HA, et al. Clinically detectable nerve fiber atrophy precedes the onset of glaucomatous field loss. *Arch Ophthalmol* 1991;109:77-83.
4. Airaksinen PJ, Drance SM, Douglas GR, et al. Visual field and retinal nerve fiber layer comparisons in glaucoma. *Arch Ophthalmol* 1985;103:205-7.
5. Kerrigan-Baumrind LA, Quigley HA, Pease ME, et al. Number of ganglion cells in glaucoma eyes compared with threshold visual field tests in the same persons. *Invest Ophthalmol Vis Sci* 2000;41:741-8.
6. Caprioli J, Miller JM, Sears M. Quantitative evaluation of the optic nerve head in patients with unilateral visual field loss from primary open-angle glaucoma. *Ophthalmology* 1987;94:1484-7.
7. Zeyen TG, Raymond M, Caprioli J. Disc and field damage in patients with unilateral visual field loss from primary open-angle glaucoma. *Doc Ophthalmol* 1992;82:279-86.

8. Chen PP, Park RJ. Visual field progression in patients with initially unilateral visual field loss from chronic open-angle glaucoma. *Ophthalmology* 2000;107:1688-92.
9. Susanna R, Drance SM, Douglas GR. The visual prognosis of the fellow eye in unioocular chronic open-angle glaucoma. *Br J Ophthalmol* 1978;62:327-9.
10. Fontana L, Armas R, Garway-Heath DF, et al. Clinical factors influencing the visual prognosis of the fellow eyes of normal tension glaucoma patients with unilateral field loss. *Br J Ophthalmol* 1999;83:1002-5.
11. Reus NJ, Colen TP, Lemij HG. Visualization of localized retinal nerve fiber layer defects with the GDx with individualized and with fixed compensation of anterior segment birefringence. *Ophthalmology* 2003;110:1512-6.
12. Reus NJ, Lemij HG. The relationship between standard automated perimetry and GDx VCC measurements. *Invest Ophthalmol Vis Sci* 2004;45:840-5.
13. Jonas JB, Budde WM, Panda-Jonas S. Ophthalmoscopic evaluation of the optic nerve head. *Surv Ophthalmol* 1999;43:293-320.
14. Keltner JL, Johnson CA, Cello KE, et al. Classification of visual field abnormalities in the ocular hypertension treatment study. *Arch Ophthalmol* 2003;121:643-50.
15. Zhou Q, Weinreb RN. Individualized compensation of anterior segment birefringence during scanning laser polarimetry. *Invest Ophthalmol Vis Sci* 2002;43:2221-8.
16. Garway-Heath DF, Poinosawmy D, Fitzke FW, Hitchings RA. Mapping the visual field to the optic disc in normal tension glaucoma eyes. *Ophthalmology* 2000;107:1809-15.
17. Reus NJ, Lemij HG. Diagnostic accuracy of the GDx VCC for glaucoma. *Ophthalmology*. In press.
18. Weinreb RN, Dreher AW, Coleman A, et al. Histopathologic validation of Fourier-ellipsometry measurements of retinal nerve fiber layer thickness. *Arch Ophthalmol* 1990;108:557-60.
19. Susanna R, Jr., Galvao-Filho RP. Study of the contralateral eye in patients with glaucoma and a unilateral perimetric defect. *J Glaucoma* 2000;9:34-7.
20. Knighton RW, Huang XR, Greenfield DS. Analytical model of scanning laser polarimetry for retinal nerve fiber layer assessment. *Invest Ophthalmol Vis Sci* 2002;43:383-92.
21. Greenfield DS, Knighton RW, Huang XR. Effect of corneal polarization axis on assessment of retinal nerve fiber layer thickness by scanning laser polarimetry. *Am J Ophthalmol* 2000;129:715-22.
22. Garway-Heath DF, Hitchings RA. Quantitative evaluation of the optic nerve head in early glaucoma. *Br J Ophthalmol* 1998;82:352-61.
23. Zeyen TG, Caprioli J. Progression of disc and field damage in early glaucoma. *Arch Ophthalmol* 1993;111:62-5.
24. Johnson CA, Adams AJ, Casson EJ, Brandt JD. Blue-on-yellow perimetry can predict the development of glaucomatous visual field loss. *Arch Ophthalmol* 1993;111:645-50.
25. Sample PA, Taylor JD, Martinez GA, et al. Short-wavelength color visual fields in glaucoma suspects at risk. *Am J Ophthalmol* 1993;115:225-33.

26. Polo V, Larrosa JM, Pinilla I, et al. Predictive value of short-wavelength automated perimetry: a 3-year follow-up study. *Ophthalmology* 2002;109:761-5.
27. Sample PA, Bosworth CF, Blumenthal EZ, et al. Visual function-specific perimetry for indirect comparison of different ganglion cell populations in glaucoma. *Invest Ophthalmol Vis Sci* 2000;41:1783-90.
28. Tuulonen A, Lehtola J, Airaksinen PJ. Nerve fiber layer defects with normal visual fields. Do normal optic disc and normal visual field indicate absence of glaucomatous abnormality? *Ophthalmology* 1993;100:587-97.
29. Quigley HA, Katz J, Derick RJ, et al. An evaluation of optic disc and nerve fiber layer examinations in monitoring progression of early glaucoma damage. *Ophthalmology* 1992;99:19-28.





# 6

**The prevalence of  
glaucomatous defects with  
short-wavelength automated  
perimetry in patients with  
elevated intraocular pressures**



---

**Purpose:** To determine the prevalence of abnormal short-wavelength automated perimetry (SWAP) visual fields in subjects with elevated intraocular pressures (IOP) for 7 existing definitions of mild glaucomatous loss, and to explore the agreement between them.

**Patients and Methods:** Seven hundred and forty-four eyes of 379 subjects with an IOP  $\geq 22$  and  $\leq 32$  mmHg and normal visual fields with standard automated perimetry (SAP) were tested with SWAP on three separate occasions, of which the second and third visual field were used for analysis. The appearance of the optic disc was not an eligibility criterion. We determined the number of visual fields classified as abnormal on two successive occasions by 7 existing definitions. In addition, we explored the agreement between the various definitions.

**Results:** The proportion of eyes with a glaucomatous visual field with SWAP ranged between 0% and 9.9%, depending on the criterion used to define abnormality. A pair-wise comparison of the various definitions showed that several definitions classified different eyes as having an abnormal field.

**Conclusions:** We found a large variation in the proportion of visual fields with SWAP classified as abnormal by the various definitions. More importantly, various definitions identified different individuals to have an abnormal field with SWAP. Therefore, the diagnostic accuracy and clinical significance of all definitions need to be determined before SWAP is used in routine clinical care.

*J Glaucoma 2005;14:26-29.*

---

Short-wavelength automated perimetry (SWAP) has been reported to show glaucomatous visual field loss in subjects with ocular hypertension (OH) 3 to 5 years earlier than standard automated perimetry (SAP).<sup>1-3</sup> The proportion of eyes in OH subjects with a SWAP defect ranges between 0.4% and 36.0% across studies.<sup>3-5</sup> It is unclear why there is such a large variation. For instance, it might be due to differences in used definitions of ocular hypertension, studied populations, different testing procedures, and different criteria for abnormality of visual fields. Other factors might also contribute to the large variation. To clarify the variation, we explored how much different definitions of abnormality could contribute to it in patients with elevated intraocular pressure (IOP). In addition, we explored the agreement between the various definitions.

## Methods

Four hundred and nine subjects with elevated IOP, recruited consecutively between November 1997 and March 2001, were tested with both SAP and SWAP (Humphrey Field Analyzer II [HFA], Carl Zeiss Meditec, Dublin, CA, USA) by means of the 24-2 Full Threshold test paradigm.

All patients had an intraocular pressure (IOP) of  $\geq 22$  mmHg and  $\leq 32$  mmHg by Goldmann applanation tonometry in both eyes and normal visual fields with SAP on at least two separate

occasions. The appearance of the optic disc was not a selection criterion. A normal field by SAP was defined as having a glaucoma hemifield test of 'Within normal limits' and no nerve fiber bundle abnormalities, as described by Keltner et al,<sup>6</sup> in the total and/or pattern deviation probability plots. In addition, patients were deemed eligible if they were of white ethnic origin, had a best corrected Snellen visual acuity of at least 20/40, and in whom slit lamp examination was unremarkable, including open angles on gonioscopy. All subjects had recently performed SAP and SWAP (on average 1.5 months [SD 1.1] prior to the current study), to minimize the influence of any subject's experience.<sup>7</sup>

Subjects with any significant coexisting ocular disease, or systemic diseases known to possibly affect the visual field (e.g. diabetes mellitus), a history of intraocular surgery (except for uncomplicated cataract surgery), arterial hypertension for which medication was used, or any previous use of IOP-lowering agents within 3 months before measurements, were excluded. A family history of glaucoma was not a selection criterion.

All subjects were to enter a, currently running, double masked placebo-controlled study on the effect of beta-blockers on the development of glaucomatous retinal nerve fiber layer defects and visual field loss in subjects with elevated IOP.

The research followed the tenets of the Declaration of Helsinki and was approved by the institutional human experimentation committee. Written informed consent was obtained from the subjects after extensive explanation of the nature and possible consequences of the study.

For perimetry, appropriate refractive correction was used for the viewing distance of the perimeter and the patient's age. All subjects were adapted to the background light for at least 5 minutes before testing. Each subject was given the same instructions for the examination, regardless of perimetric experience, in order to minimize the effects of operator bias. Resting periods of 2 to 3 minutes were given prior to each examination and at 5 to 7 minutes intervals during the examination of each eye. Visual field tests for SWAP were not corrected for possible lens transmission losses. All visual fields that were used for analysis satisfied the following reliability criteria: fixation losses  $\leq 25\%$ , and false-positive and false-negative responses  $\leq 20\%$ . None of the visual fields showed a 'Generalized depression of sensitivity' on the Glaucoma Hemifield Test (GHT). The values of the total and pattern deviation probability plot, the GHT, the mean deviation (MD), the pattern standard deviation (PSD), and the corrected pattern standard deviation (CPSD) were derived from the standard HFA STATPAC print-out and entered into a database.

We determined the number of eyes and number of subjects with SWAP fields classified as abnormal for the following optimum definitions designed to identify glaucomatous visual field loss with SWAP:

1. A cluster of  $\geq 3$  points with a sensitivity lower than the 5% probability level, or a cluster of  $\geq 2$  points with a sensitivity lower than the 2% probability level, or an MD lower than the 2%

- probability level, or a CPSD lower than the 2% probability level ( $C3_{p<5\%} | C2_{p<2\%} | MD_{p<2\%} | CPSD_{p<2\%}$ ).<sup>3</sup>
2. A cluster of  $\geq 4$  points with a sensitivity lower than the 5% probability level ( $S4_{p<5\%}$ ).<sup>8</sup>
  3. A cluster of  $\geq 3$  points with a sensitivity lower than the 1% probability level ( $C3_{p<1\%}$ ).<sup>8</sup>
  4. A PSD lower than the 1% probability level ( $PSD_{p<1\%}$ ).<sup>5</sup>
  5. A GHT of 'Outside normal limits' ( $GHT_{ONL}$ ).<sup>5</sup>
  6.  $\geq 4$  Single points with a sensitivity lower than the 5% probability level ( $S4_{p<5\%}$ ).<sup>5</sup>
  7.  $\geq 5$  Single points with a sensitivity lower than the 5% probability level ( $S5_{p<5\%}$ ).<sup>5</sup>

Points were located on the pattern deviation probability plot. All abnormalities had to be confirmed on a subsequent test within one year (mean period between tests: 6.6 months [SD 1.2; right-censored at 12 months]). The definitions were analyzed with custom-made algorithms in Microsoft Access 97 (Microsoft Corporation, Redmond, WA, USA).

Of the 818 eyes of the 409 eligible subjects, 74 eyes were excluded from analysis for the following reasons: no prior experience with SWAP (30), no SWAP available to confirm an abnormal test result (34), the time to confirmation of a defect was longer than 1 year (8), a cholesterol crystal was present in a retinal artery causing a visual field defect (1), or presence of a choroidal nevus with corresponding visual field loss (1). Therefore, 744 eyes of 379 subjects with elevated IOP were analyzed for the present study.

The mean age of the subjects was 57 years (SD 11). One hundred and seventy-nine of the 379 subjects (47%) were men. Three hundred and seventy-three of the 744 eyes (50%) were right ones. The mean IOP in the analyzed eyes was 25.6 mmHg (SD 2.3).

## Results

Between 0% and 9.9% of the eyes with elevated IOP had a visual field defect with SWAP, depending on the definition of abnormality (Table 6.1). The proportion of subjects with an abnormal field in at least one of their eyes ranged between 0.0% and 15.8% (Table 6.1). The definitions  $S4_{p<5\%}$  and  $C3_{p<5\%} | C2_{p<2\%} | MD_{p<2\%} | CPSD_{p<2\%}$  classified the largest number of visual fields as abnormal. The definition  $PSD_{p<1\%}$  did not classify any visual field as abnormal.

A pair-wise comparison of the various definitions in their classification of individual visual fields as normal or abnormal has been presented in table 6.2 (the definition  $PSD_{p<1\%}$  has been omitted as it did not classify any field as abnormal). For 8 pairs of definitions, all fields that were classified as abnormal by the stricter definition were also classified as abnormal by the laxer one, indicating a high degree of overlap. Conversely, for the other 7 pairs of definitions, the overlap in classification was only moderate as both definitions of each pair classified different fields as abnormal. For example, the definitions  $S4_{p<5\%}$  and  $C3_{p<5\%} | C2_{p<2\%} | MD_{p<2\%} | CPSD_{p<2\%}$  agreed on 57 fields to be abnormal, but classified 16 and 17 fields differently, respectively.

## Discussion

All seven definitions of an abnormal SWAP visual field that we explored in the present study have been published as definitions that identify glaucomatous visual field loss with SWAP. However, we have shown a large variation in the proportion of subjects with elevated IOP classified to have functional glaucomatous loss by the various definitions. More importantly, various definitions identified different individuals to have an abnormal SWAP field, and thus identified different individuals to be possibly at risk of developing glaucomatous field defects with SAP.

The proportions of abnormal fields that we found for the definitions  $PSD_{p<1\%}$ ,  $S4_{p<5\%}$ , and  $S5_{p<5\%}$  were similar to those reported by Johnson et al.<sup>5,9</sup> However, we found considerably fewer abnormal tests for the definitions  $GHT_{ONL}$  and  $C3_{p<5\%} | C2_{p<2\%} | MD_{p<2\%} | CPSD_{p<2\%}$  (1.3% and 9.9%, respectively) than reported in the literature (6.9% and 36%, respectively).<sup>3,5,9</sup> A possible explanation for these differences is that both Johnson et al<sup>5</sup> and Polo et al<sup>3</sup> used their own normative values, which may have been more liberal than the normative database of the HFA that we used in the present study. In addition, any differences in the studied populations may also have contributed. For example, in the studies by Johnson et al<sup>5</sup> and Polo et al<sup>3</sup> and the present one, the appearance of the optic disc was not a selection criterion. Therefore, all three studies may have included patients with a normal optic disc, normal visual fields, and a high IOP, i.e. patients with ‘pure’ ocular hypertension, as well as patients with a glaucomatous optic disc and a normal visual field, i.e. patients with so-called pre-perimetric glaucoma. Different proportions of patients with structural glaucomatous loss may have yielded different prevalences of glaucomatous defects

Definition of abnormality	Abnormality with SWAP	
	Eyes (%)	Subjects (%)
$PSD_{p<1\%}$	0 (0)	0 (0)
$C3_{p<1\%}$	6 (0.8)	6 (1.6)
$GHT_{ONL}$	10 (1.3)	9 (2.4)
$S5_{p<5\%}$	41 (5.5)	33 (8.7)
$C4_{p<5\%}$	43 (5.8)	35 (9.2)
$S4_{p<5\%}$	73 (9.8)	57 (15.0)
$C3_{p<5\%}   C2_{p<2\%}   MD_{p<2\%}   CPSD_{p<2\%}$	74 (9.9)	60 (15.8)

**Table 6.1.** Number (percentage) of eyes and subjects with an abnormal visual field with short-wavelength automated perimetry (SWAP) in 744 eyes of 379 subjects with ocular hypertension for various definitions of abnormality as found in the present study as well as in other published reports;  $Cn_{p<1\%}$ , cluster of n points with a sensitivity lower than the i% probability level;  $MD_{p<2\%}$ , mean deviation lower than the 2% probability level;  $CPSD_{p<2\%}$ , corrected pattern standard deviation lower than the 2% probability level;  $PSD_{p<1\%}$ , pattern standard deviation lower than the 1% probability level;  $GHT_{ONL}$ , Glaucoma Hemifield Test of ‘Outside normal limits’;  $Sn_{p<1\%}$ , n single points with a sensitivity lower than the i% probability level.

	C3 <sub>p&lt;1%</sub>		GHT <sub>ONL</sub>		S5 <sub>p&lt;5%</sub>		C4 <sub>p&lt;5%</sub>		S4 <sub>p&lt;5%</sub>	
	Normal	Abnormal	Normal	Abnormal	Normal	Abnormal	Normal	Abnormal	Normal	Abnormal
GHT <sub>ONL</sub>										
	Normal	732	2							
	Abnormal	6	4							
S5 <sub>p&lt;5%</sub>	Normal	703	0	700	3					
	Abnormal	35	6	34	7					
C4 <sub>p&lt;5%</sub>	Normal	701	0	699	2	694	7			
	Abnormal	37	6	35	8	9	34			
S4 <sub>p&lt;5%</sub>	Normal	671	0	670	1	671	0	671	0	
	Abnormal	67	6	64	9	32	41	30	43	
C3 <sub>p&lt;5%</sub>   C2 <sub>p&lt;2%</sub>   MD <sub>p&lt;2%</sub>   CPSD <sub>p&lt;2%</sub>	Normal	670	0	670	0	667	3	670	0	654
	Abnormal	68	6	64	10	36	38	31	43	17

**Table 6.2.** Cross-tabulation of the number of short-wavelength automated perimetry visual fields classified as normal and abnormal in eyes of subjects with ocular hypertension by various definitions of abnormality; see Table 6.1 for abbreviations.

with SWAP. A limitation of the current study may be then that we did not prospectively collect data on the appearance of the optic nerve head and therefore could not relate the presence or absence of a glaucomatous optic neuropathy to the prevalence of abnormalities with SWAP.

With regard to the definitions  $C3_{p<1\%}$  and  $C4_{p<5\%}$ , they have only been reported as criteria to distinguish between glaucoma patients and healthy subjects.<sup>8</sup> To our knowledge, the proportion of abnormal fields by these two criteria in subjects with OH have not been reported yet.

In the present study, we did not correct for possible losses of lens transmission, which Johnson et al<sup>5</sup> and Polo et al<sup>3</sup> did. Losses in lens transmission cause a generalized depression of sensitivity with SWAP.<sup>10</sup> However, none of the eyes that we studied showed a 'generalized depression of sensitivity' with the glaucoma hemifield test. In addition, only 20/744 (2.7%) had an MD  $p<5\%$  with SWAP at both visits, which is less than would have been expected by chance alone. More importantly, all used criteria related to points in the pattern deviation probability plot, which was already corrected for any generalized reductions in sensitivity. Therefore, we suspect that age-related lens transmission losses did not influence our results.

SWAP has been reported to identify functional glaucomatous loss at a stage when SAP does not detect a defect yet.<sup>1-3</sup> Clinically, one would like to know how many people with an abnormal SWAP field, irrespective of its definition, would eventually progress to having an abnormal SAP field. Put differently, the clinician would be interested in how well an abnormal SWAP field predicted further future loss to assist in better managing glaucoma. To our knowledge, the diagnostic accuracy, i.e. the sensitivity and specificity, for predicting glaucomatous defects with SAP has been assessed in a reasonably large population for only one definition: in 160 eyes of 83 subjects with OH, Polo et al<sup>3</sup> determined that the sensitivity and specificity of  $C3_{p<5\%} \mid C2_{p<2\%} \mid MD_{p<2\%} \mid CPSD_{p<2\%}$  for predicting abnormalities with SAP in 3 years time was 73% and 68%, respectively. We suspect that the specificity will increase with a follow-up longer than 3 years. For the other definitions, the diagnostic accuracy for predicting future glaucomatous SAP defects still has to be determined. Based on the large variation in the proportion of eyes with abnormally classified fields between the various definitions, we speculate that the accuracy of the various definitions in predicting future development of SAP abnormalities will vary substantially.

Johnson et al<sup>5</sup> have reported for SAP that the specificity of definitions using single or scattered abnormal points for classifying a visual field as abnormal was similar to that of definitions using clustered points. They extrapolated this result to SWAP and assessed the proportion of abnormal fields with SWAP in subjects with OH only for scattered points, and not for clusters.<sup>5</sup> However, we found that the number of abnormal visual fields decreased by 41% using a definition of clustered points as compared to scattered points (cf.  $S4_{p<5\%}$  and  $C4_{p<5\%}$ , table 6.1). This confirms



the suggestion by Polo et al<sup>8</sup> that optimum definitions based on SAP data can not merely be transferred to SWAP.

In conclusion, several cases have been reported in the literature in which SWAP was able to correctly predict the development of defects with SAP.<sup>1-3</sup> In addition, several definitions have recently been presented for identifying glaucomatous visual field loss with SWAP.<sup>3,5,8</sup> In the present study, we found that various of these definitions identify different individuals to have an abnormal field and also classify different numbers of eyes having abnormalities with SWAP. Our findings may partly explain the large variation in abnormal SWAP fields in OH reported across studies.<sup>3,5</sup>

Although these results may not be entirely unexpected, they underline the importance of well-described criteria for identifying subjects with mild glaucomatous damage. Therefore, we feel that, before SWAP is to be used routinely in clinical care, the diagnostic accuracy of these definitions for predicting the development of glaucomatous functional defects with SAP has to be explored empirically in follow-up studies.

## References

1. Johnson CA, Adams AJ, Casson EJ, Brandt JD. Blue-on-yellow perimetry can predict the development of glaucomatous visual field loss. *Arch Ophthalmol* 1993;111:645-50.
2. Sample PA, Taylor JD, Martinez GA, et al. Short-wavelength color visual fields in glaucoma suspects at risk. *Am J Ophthalmol* 1993;115:225-33.
3. Polo V, Larrosa JM, Pinilla I, et al. Predictive value of short-wavelength automated perimetry: a 3-year follow-up study. *Ophthalmology* 2002;109:761-5.
4. Medeiros FA, Sample PA, Weinreb RN. Corneal thickness measurements and visual function abnormalities in ocular hypertensive patients. *Am J Ophthalmol* 2003;135:131-7.
5. Johnson CA, Sample PA, Cioffi GA, et al. Structure and function evaluation (SAFE): I. criteria for glaucomatous visual field loss using standard automated perimetry (SAP) and short wavelength automated perimetry (SWAP). *Am J Ophthalmol* 2002;134:177-85.
6. Keltner JL, Johnson CA, Cello KE, et al. Classification of visual field abnormalities in the ocular hypertension treatment study. *Arch Ophthalmol* 2003;121:643-50.
7. Wild JM. Short wavelength automated perimetry. *Acta Ophthalmol Scand* 2001;79:546-59.
8. Polo V, Larrosa JM, Pinilla I, et al. Optimum criteria for short-wavelength automated perimetry. *Ophthalmology* 2001;108:285-9.
9. Johnson CA, Sample PhD PA, Zangwill LM, et al. Structure and function evaluation (SAFE): II. Comparison of optic disk and visual field characteristics. *Am J Ophthalmol* 2003;135:148-54.
10. Sample PA, Martinez GA, Weinreb RN. Short-wavelength automated perimetry without lens density testing. *Am J Ophthalmol* 1994;118:632-41.



# 7

## General discussion



In the present thesis, measurements of function and structure in glaucoma by various clinically used techniques have been evaluated. The main findings will now be summarized and discussed in the light of present knowledge.

### 7.1 Assessment of RNFL morphology with SLP

SLP-VCC was developed to allow a more accurate evaluation of the RNFL than with SLP-FCC. In **chapter 2.1**, we demonstrated that SLP-VCC measurements indeed yielded images that better reflected RNFL structure than did SLP-FCC. The SLP-VCC images clearly showed RNFL defects and even physiological striations of the RNFL similar to red-free fundus photographs. SLP-FCC images, however, resembled red-free fundus photographs considerably less, notably when the anterior segment birefringence mismatched the FCC more, both in magnitude and in axis. To our knowledge, our report was the first to show that SLP equipped with VCC was able to allow assessment of RNFL morphology similar to that with red-free fundus photography. Weinreb et al<sup>1</sup> reported to have found similar results when comparing SLP-VCC measurements and stereoscopic photographs of the RNFL in monkey eyes. Furthermore, Medeiros et al<sup>2</sup> showed that RNFL measurements with SLP-VCC compared moderately well with clinical interpretation of red-free fundus photographs. Of note, Medeiros et al<sup>2</sup> also found that automated analysis of SLP-VCC measurements was more accurate in discriminating between healthy and glaucomatous eyes than clinical assessment of red-free fundus photographs.

We performed our study with a GDx NFA that was modified with a manually adjustable VCC. In the commercial GDx VCC, however, the compensator is set automatically. In addition, the GDx VCC has a lower resolution compared to the GDx NFA: 128 x 128 pixels at a 20° x 20° scanning field versus 256 x 256 pixels at a 15° x 15° field of view. Despite these differences, we found similar results in RNFL assessment compared to red-free fundus photography for the two instruments (Reus, NJ, et al. *IOVS* 2003;44:ARVO E-Abstract 3354), although the lower sampling density might limit the detection of physiological RNFL striations to some extent.

In some areas of the images, the agreement between SLP and red-free fundus photography was poor, illustrating that, ultimately, the two techniques examine different aspects of the RNFL, i.e., birefringence and specular reflectivity. Recent studies comparing SLP measurements with OCT data similarly showed that SLP and OCT assess different properties of the RNFL as axonal birefringence (i.e., the ratio of retardation over thickness) was shown to vary around the ONH.<sup>3,4</sup> As the GDx VCC uses a fixed factor of 0.67 nm/mm to convert the measured amount of retardation to a thickness value, it thereby ignores regional differences in birefringence. Van Koolwijk et al (*IOVS* 2005;46:ARVO E-Abstract 2527) recently found that the birefringence of the RNFL is even less in glaucomatous eyes than in healthy ones, suggesting that the RNFL not

only thins in glaucoma, but also that the physical properties, such as the birefringence, of the remaining RNFL change.

### 7.2 The effect of improper anterior segment compensation with SLP

In **chapter 2.2**, we illustrated the effect of improper anterior segment compensation on SLP measurements. With varying amounts of anterior segment birefringence compensation, a healthy eye could appear glaucomatous whereas a glaucomatous eye could appear to have a thicker and healthier RNFL. The results may show clinicians who use the GDx NFA how much incomplete compensation of anterior segment birefringence may yield spurious results in an individual eye. In addition, the examples show that, when switching from GDx NFA to GDx VCC for monitoring patients, large changes in RNFL pattern may be expected in any individual and a new baseline image will have to be made.

With the currently available GDx VCC, anterior segment birefringence is neutralized for each individual eye. This might falsely suggest that artifacts due to incomplete compensation of anterior segment birefringence do not occur in GDx VCC measurements. However, even small variations in corneal compensation, e.g., due to slight head tilt, resulted in apparent changes in RNFL morphology. At the Rotterdam Eye Hospital, we therefore ask patients to keep their heads in the same position on the GDx VCC face mask between measurements of anterior segment birefringence and subsequent assessment of RNFL birefringence. In addition, as small variations in RNFL appearance due to incomplete corneal compensation may mimic or mask glaucomatous progression, we determine an eye's anterior segment birefringence at every visit. However, when a change in RNFL appearance is suspected, one should ascertain that such a change is not due to incomplete compensation artifacts, which may appear as a rotated RNFL pattern (e.g., see Fig. 2.3.1). SLP measurements with enhanced variable corneal compensation (ECC), presented in **chapter 2.3**, may eliminate the effect of head tilt because excess birefringence is removed mathematically after the eye has been measured.

In this study, we only qualitatively assessed the effects of varying amounts of incomplete anterior segment compensation. Future studies with a larger sample may also quantitatively assess the effect of residual anterior segment birefringence in an individual eye. In addition, such an analysis might be useful for evaluating the accuracy of eliminating residual anterior segment birefringence caused by head tilt by SLP-ECC.

### 7.3 Enhanced variable corneal compensation with SLP

Although VCC adequately canceled anterior segment birefringence in SLP measurements in most eyes, we noticed that some eyes still showed some residual birefringence. In addition, about 7%

of eyes had atypical patterns of retardation in their SLP-images.<sup>5</sup> In **chapter 2.3**, a new algorithm to improve assessment of RNFL morphology with SLP-VCC was presented and evaluated.

Measurements obtained with this so-called enhanced cornea compensation (ECC) appeared to represent the expected RNFL morphology better than or otherwise as well as those made with standard VCC. This may have been largely due to the improved compensation of anterior segment birefringence with ECC over VCC. A more accurate assessment of RNFL morphology may then improve the detection and follow-up of glaucomatous damage. However, more research is needed to determine the reproducibility of SLP-ECC in neutralizing anterior segment birefringence. Furthermore, longitudinal follow-up of eyes with various stages of glaucoma may show whether the detection of progressive damage has improved with ECC over VCC.

Atypical patterns were less frequent in measurements with SLP-ECC. The source of this atypical retardation is still unknown, although it appears to occur more frequently in eyes with lightly pigmented fundi, in myopes, and in eyes of elderly subjects in which the signal-to-noise ratio of the SLP images is relatively poor. By introducing a preset measurement bias that was afterwards mathematically removed from the measurements, birefringence measurements were shifted into a more sensitive detection range of the instrument. This may explain why atypical retardation is reduced with ECC. In some eyes, atypical patterns were still apparent in SLP-ECC images, possibly limiting the detection of glaucomatous RNFL loss. Therefore, other sources of these patterns will need to be investigated with, e.g., techniques such as polarization sensitive optical coherence tomography (PS-OCT).<sup>3</sup>

In the nasal and temporal regions around the ONH, no differences in RNFL retardation were detected with SLP-ECC between healthy and glaucomatous eyes. Especially in the temporal sector, the amount of retardation was expected to be smaller in glaucomatous eyes. If the source of retardation in these eyes were due to a low signal-to-noise ratio, the sensitivity to detecting retardation in this segment may perhaps be increased by introducing a bias retardation in not just the vertical axis, as is done with ECC, but in the horizontal axis as well.

#### 7.4 Diagnostic accuracy for glaucoma

For every new diagnostic technique, its accuracy for discriminating between healthy and diseased needs to be determined. Therefore, in **chapter 3.1**, we determined the accuracy of the GDx VCC for classifying glaucoma in patients ranging widely in disease severity. For the best discriminating parameter, i.e., NFI, the sensitivity and specificity were 89% and 96%, respectively. Medeiros et al<sup>6</sup> found a lower sensitivity of 61% at a similar specificity of 97%, which may be due to their including a larger number of glaucomatous eyes with only mild visual field loss than we did, which are more difficult to classify correctly.

In assessing the usefulness of a new technique in clinical care, the question should be whether

such a technique may improve the care that is being provided today under current conditions.<sup>7</sup> To compare the diagnostic accuracy with currently used techniques in glaucoma detection, we subsequently determined the accuracy of automated classification by the GDx VCC and the HRT I and the accuracy of clinicians for classifying glaucoma on stereoscopic ONH photographs alone (**chapter 3.2**). We found that automated analysis of SLP-VCC measurements discriminated better between healthy and glaucomatous eyes than clinical assessment of stereoscopic ONH photographs by general ophthalmologists, junior residents, optometrists, and even some glaucoma specialists. CSLO measurements classified about as well as did glaucoma specialists and general ophthalmologists. More experienced graders classified ONHs more accurately than did graders with less experience, i.e., glaucoma specialists and general ophthalmologists had a higher diagnostic accuracy than ophthalmology residents and optometrists.

For the HRT parameters MRA and Bathija LDF, the sensitivity and specificity were 77% and 98% and 85% and 95%, respectively. These results are slightly higher than reported in the literature by Ford et al (Bathija LDF and MRA)<sup>8</sup> and by Medeiros et al<sup>6</sup> (Bathija LDF). This difference may be due to their including more patients with milder glaucomatous damage than we did.

When comparing the diagnostic accuracies of the GDx VCC and the HRT with each other, the GDx VCC appeared to discriminate better between healthy and glaucomatous eyes than the HRT. However, this difference was not statistically significant. In a study by Medeiros et al,<sup>6</sup> the GDx VCC was found to have a statistically significantly higher diagnostic accuracy for glaucoma than the HRT at a specificity of 80%. However, at specificities of at least 95%, no statistically significant differences were found. Larger sample sizes in the study by Medeiros et al<sup>6</sup> and in ours might have yielded a statistically significant difference at higher specificities.

In another study, Medeiros et al<sup>2</sup> showed that the diagnostic accuracy of the GDx VCC for glaucoma was higher than that of subjective assessment of red-free photographs of the RNFL.<sup>2</sup> Taking all this information together, imaging techniques may assist clinicians in improving their accuracy for diagnosing glaucoma in clinical practice. Obviously, they will then have to combine the imaging information with all other available clinical information, such as the appearance of the ONH and/or RNFL, the presence of visual field defects, and any risk factors, such as elevated IOP, older age, high myopia, African ethnic origin, and first- and/or second-degree family members with glaucoma.

In the presented studies, the diagnostic accuracy of the two imaging methods was assessed for single parameters. In clinical practice, measurements of the GDx VCC and the HRT are presented in a printout containing additional information, such as raw measurements of RNFL retardation or ONH topography and various parameters describing the RNFL and ONH, many of which are compared to normative data. Subjective analysis of the entire printout has been shown to



have a higher diagnostic accuracy than automated analysis of single parameters.<sup>9,10</sup> Therefore, subjective analysis of these print-outs might improve the clinical use of these techniques even further. However, adequate subjective analysis does require additional training. Although such training is widely available for clinicians (e.g., at the annual meetings of the American Academy of Ophthalmology, the European Glaucoma Society, and the Dutch Ophthalmic Society), general ophthalmologists may not reach similar accuracies for diagnosing glaucoma as specialists who regularly work with these imaging techniques. Furthermore, the diagnostic accuracy may also be lower than what we found because of patient selection in our studies.

Recently, more emphasis has been put on the progression of axonal loss in the definition of glaucoma.<sup>11</sup> In the studies presented in the current thesis, the accuracy for diagnosing glaucoma was determined cross-sectionally. Future studies may determine the accuracy for diagnosing progressive and, perhaps equally important, stable glaucomatous loss over time.

### 7.5 Relationship between function and structure

Both functional (e.g., SAP, SWAP, and FDT) and structural (e.g., stereoscopic ONH assessment, SLP-VCC, CSLO, OCT) measurements may be used in clinical practice for detecting and monitoring glaucoma. As the sensitivity for detecting and monitoring glaucomatous damage at different stages may vary between these techniques, understanding the relationships between the various functional and structural measurements may improve their combined use in clinical practice.

In **chapters 4.1 and 4.2**, we showed that measurements of RNFL morphology with SLP-VCC and of neuroretinal rim area with CSLO, respectively, correlate well with measurements of function by SAP. The shape of the relationship between function, when expressed in the clinically used dB scale, and structure, expressed as RNFL thickness by GDx VCC or neuroretinal rim area by HRT, was curvilinear for many sectors. When DLS was expressed in an unlogged-scale, the relationship between function and structure was linear. These results compare well with other studies into the relationship between perimetry and RNFL morphology by SLP-VCC<sup>12,13</sup> and measurements of neuroretinal rim area by CSLO<sup>14,15</sup>.

The curvilinear appearance of the relationship between function by SAP and structure by SLP or CSLO may be due, at least partly, to the use of a decibel scale for expressing DLS. In this scale, higher values are relatively compressed, as lower values are stretched. As a result, functional damage at higher sensitivities will appear relatively small, whereas progressive damage at lower sensitivities will appear relatively large. In eyes with no or only mild to moderate glaucomatous functional loss, clinically relevant changes in neuroretinal rim area and RNFL thickness, which are expressed in a linear scale, might then occur with only small changes in retinal light sensitivity. This suggests that a pathologically reduced neuroretinal rim area or a thinned RNFL may be detected in eyes with normal SAP visual fields (also see **chapter 5**).

At the other end of the spectrum, SAP may be more sensitive to detecting changes in patients with severe glaucomatous functional loss as functional changes in this part of the decibel scale are maximized. However, the reproducibility of measurements with SAP has been shown to be fairly poor, notably at lower retinal sensitivities, which may limit its sensitivity for detecting more subtle changes. The reproducibility of measurements of both the HRT and the GDx VCC appears to be reasonably good over short periods of time.<sup>16-18</sup> In the long term, however, the reproducibility of the HRT was reported to be only slightly better than that of SAP by means of the Octopus perimeter.<sup>19</sup> The long-term reproducibility of measurements with the GDx VCC has not been determined yet. In addition, the dynamic range in eyes with severe glaucomatous loss is smaller for measurements with CSLO and SLP-VCC than with SAP, which may limit the number of statistically significant changes that can be detected with CSLO and SLP-VCC. Therefore, whether the HRT I and GDx VCC may be better at detecting subtle changes than SAP in eyes with advanced glaucomatous loss remains to be investigated.

The present results do not indicate that structural losses occur before functional losses per se. In principle, changes in RGC function might even precede structural changes. However, current techniques for assessing structure, such as SLP-VCC and CSLO, appear to be more sensitive for detecting glaucomatous damage than the routinely used SAP.

We presently determined the relationship between function and structure cross-sectionally. Only longitudinal studies assessing the relationship between function and structure by various techniques over time may determine which ones show any progressive change earlier than others, at various stages of the disease. Such studies may indicate if and when any of these techniques are best used in clinical practice.

## 7.6 Pre-perimetric glaucoma

The studies in the previous chapter suggested that early detection were possible with SLP-VCC. Without longitudinal follow-up studies with SLP-VCC in which eyes with early SLP abnormalities but normal visual fields later showed perimetric defects, we resorted to investigating the RNFL in the perimetrically unaffected eyes of glaucoma patients who had visual field defects in only their fellow eyes (**chapter 5**). The eyes without visual field defects are at an especially high risk for developing field loss: between 7% and 26% of them will develop visual field defects by SAP during a follow-up period of 4 to 5 years.<sup>20-23</sup> We showed that the RNFL in perimetrically unaffected eyes of patients with asymmetric open-angle glaucoma is thinner than the RNFL in eyes of healthy subjects as measured by SLP with VCC. Recently, Henderson et al<sup>24</sup> demonstrated that ocular hypertension patients with thinner corneas, who also have an increased risk of developing glaucomatous field loss, had a statistically significantly thinner RNFL than those with thicker

corneas and healthy control subjects. These data support our findings presented in **chapter 4** that suggest that a mildly to moderately thin RNFL may not necessarily be associated with field loss by SAP.

It is yet unclear whether other forms of perimetry, such as FDT and SWAP, which have been shown to detect glaucoma earlier than SAP,<sup>25-28</sup> are abnormal in the perimetrically unaffected eyes in our study. Such a study is under way.

The present study was a first step towards investigating whether SLP-VCC measurements may precede functional deficits by SAP. Whether the eyes with an abnormal GDx VCC result are the ones that will eventually develop glaucomatous visual field defects and, if so, how long that would take, is being investigated in follow-up studies.

The few studies that investigated the predictive value of CSLO measurements for the development of visual field defects by SAP, showed that CSLO by means of the HRT may indeed predict the development of glaucomatous visual field loss in patients with OH.<sup>29-32</sup> Similarly, one recent study showed that OH patients with a thin RNFL, as measured with the GDx NFA, have an increased risk of developing glaucomatous visual field loss.<sup>33</sup> However, only one study<sup>30</sup> determined the proportion of eyes in which functional defects by SAP preceded structural defects by SLP or CSLO and vice versa. Future studies will have to address this issue in more detail. In addition, in clinical practice, it would be important to be able to identify individual eyes that will later develop visual field loss with SAP.

## 7.7 SWAP

SWAP has been reported to show glaucomatous visual field loss in ocular hypertensive subjects 3 to 5 years earlier than SAP. In **chapter 6**, we determined the prevalence of abnormal SWAP visual fields in subjects with elevated IOP for 7 existing definitions of mild glaucomatous loss, and explored the agreement between them. We found a large variation in the proportion of these subjects classified as having glaucomatous field loss across the various definitions. More importantly, various definitions identified different individuals as having an abnormal SWAP field, and thus identified different individuals to be possibly at risk of developing glaucomatous field defects with SAP. We therefore speculate that a SWAP field classified as abnormal may vary considerably in its power to predict the occurrence of an abnormal SAP field, depending on the definition that is used.

Our results may partly explain the large variation in abnormal SWAP fields in OH reported across studies.<sup>27,34</sup> Although these results may not be entirely unexpected, they underline the importance of well-described criteria for identifying subjects with mild glaucomatous damage. Therefore, we feel that before SWAP is to be used routinely in clinical care, the diagnostic accuracy

of these definitions for predicting the development of glaucomatous functional defects with SAP must be explored empirically in follow-up studies.

These recommendations also apply to other techniques, such as the GDx VCC and the HRT. For both techniques, various criteria have been reported to have a moderate to high accuracy for discriminating between healthy and glaucomatous eyes. However, criteria that have a high accuracy for discriminating between healthy and glaucomatous eyes may not be of much value for predicting future changes. Therefore, imaging techniques such as the GDx VCC and the HRT should be used with caution in clinical practice when used for monitoring glaucoma patients. However, when used in addition to SAP field testing they may be advantageous.

### 7.8 Future developments in clinical care and research

Recently, OCT has developed into an increasingly promising technology for evaluating glaucoma. This technique has been shown to discriminate well between healthy and glaucomatous eyes.<sup>6</sup> Whether its measurements are reproducible enough for clinical follow-up of patients over time remains to be investigated. However, as stated before, such studies are also required for measurements with SLP-VCC, CSLO, and SWAP.

Furthermore, the various OCT-related techniques such as PS-OCT,<sup>3</sup> ultrahigh-resolution OCT,<sup>35</sup> and Fourier-domain OCT (De Boer, JF, et al. *IOVS* 2004;45:ARVO E-Abstract 1139; Leitgeb, RA, et al. *IOVS* 2004;45:ARVO E-Abstract 2201) all of which are still in their infancy, may assess different aspects of glaucomatous optic neuropathy and may prove to be valuable tools for diagnosing and monitoring glaucoma.

In addition, clinically useful assets of the GDx VCC, such as ease of use, a color-coded map of RNFL morphology in a large area around the ONH, together with matching probability maps and an automated classifier for separating glaucomatous from healthy eyes, may be developed for the OCT.

Moreover, healthy subjects, glaucoma patients and patients at high risk of developing glaucoma may be monitored with various perimetric and imaging techniques to determine their ability to detecting glaucomatous changes over time. In addition, the relationship between each other to detecting changes in individual eyes should also be investigated. However, as glaucoma is a slowly progressing disease, large samples of patients may need to be followed for several years to acquire a reasonably sized sample of eyes showing glaucomatous progression. Recently, Vermeer et al (Vermeer, KA, et al. *IOVS* 2005;46:ARVO E-Abstract 2533) developed a model to simulate progression in SLP images while retaining the important statistical properties of empirical data. With this model, an algorithm for detecting progression, including an optimal frequency of measurements and number of measurements needed to confirm progression, may be determined and subsequently validated in clinical trials.

## 7.9 Conclusions

In this thesis, several diagnostic modalities for managing glaucoma have been explored and discussed. They entailed both imaging and perimetry. Although perimetry, notably SAP, ranks among the more traditional diagnostic modalities, imaging devices such as the GDx VCC, OCT, and the HRT will, without doubt, become increasingly important in the clinical management of glaucoma. They allow objective and quantitative assessment, as well as documentation of the ONH and/or the RNFL. More traditional methods, such as measuring the IOP, examining the ONH and SAP, have ever more established limitations that call for adjunctive diagnostic techniques that are potentially offered by the imaging devices.

I have shown in this thesis that SLP-VCC may provide a view of the RNFL similar to that obtained with red-free fundus photography. Furthermore, the GDx VCC may provide an easy and rapid evaluation of the RNFL in a wide range of subjects. With ECC, even more patients may be assessed reliably. In addition, I have shown that both the GDx VCC and HRT discriminate well between healthy and glaucomatous eyes. What is more, automated analysis of GDx VCC and HRT measurements compared favorably to subjective analysis of stereoscopic ONH photographs by general ophthalmologists in classifying healthy and glaucomatous eyes. Furthermore, measurements with both GDx VCC and HRT were shown to correlate well with those by SAP. Moreover, many eyes of glaucoma patients with normal function by SAP had abnormal GDx VCC measurements, suggesting that the GDx VCC may detect so-called pre-perimetric glaucoma.

The imaging techniques evaluated in this thesis, however, also have their limitations. For example, the curvilinear relationship between function and structure, presented in **chapter 4**, suggested that glaucomatous changes may be difficult to detect in more advanced stages, in which few nerve fibers are left. In addition, movements of the eye during image acquisition with either the GDx VCC or the HRT may produce measurement artifacts, significantly limiting reliable interpretation of the results. With regard to measurements with the GDx VCC, atypical RNFL retardation patterns and artifacts due to parapapillary atrophy may limit its use in clinical care, although I have shown in this thesis that these artifacts may occur less often with ECC. A limitation of the HRT may be that the ONH has to be outlined manually in the topography image, limiting a truly objective analysis. Furthermore, when comparing the HRT with the GDx VCC, measurements with the former instrument may be more degraded by media opacities, such as cataract, due to its shorter wavelength of 670 nm versus that of the GDx VCC, i.e., 785 nm.

Nonetheless, when used sensibly, imaging techniques may support clinicians in their management of glaucoma. To this end, clinicians should know which aspect of glaucomatous optic neuropathy is being evaluated by each technique, know how to judge the quality of the images, and, above all, be able to adequately differentiate between normal and abnormal measurements. Therefore,

continuing education on these imaging techniques of clinicians is of utmost importance. In the end, however, an abnormal measurement does not necessarily indicate disease. Clinicians should therefore also be able to interpret measurements, be it that of the GDx VCC, HRT, perimetry, or applanation tonometry, in relation to other findings. After all, supported by imaging techniques, it should be the clinician who makes a diagnosis of glaucoma or judges whether any progression has taken place.

## References

1. Weinreb RN, Bowd C, Zangwill LM. Scanning Laser Polarimetry in Monkey Eyes using Variable Corneal Polarization Compensation. *J Glaucoma* 2002;11:378-84.
2. Medeiros FA, Zangwill LM, Bowd C, et al. Comparison of scanning laser polarimetry using variable corneal compensation and retinal nerve fiber layer photography for detection of glaucoma. *Arch Ophthalmol* 2004;122:698-704.
3. Cense B, Chen TC, Park BH, et al. Thickness and birefringence of healthy retinal nerve fiber layer tissue measured with polarization-sensitive optical coherence tomography. *Invest Ophthalmol Vis Sci* 2004;45:2606-12.
4. Huang XR, Bagga H, Greenfield DS, Knighton RW. Variation of peripapillary retinal nerve fiber layer birefringence in normal human subjects. *Invest Ophthalmol Vis Sci* 2004;45:3073-80.
5. Reus NJ, Lemij HG. Diagnostic accuracy of the GDx VCC for glaucoma. *Ophthalmology* 2004;111:1860-5.
6. Medeiros FA, Zangwill LM, Bowd C, Weinreb RN. Comparison of the GDx VCC scanning laser polarimeter, HRT II confocal scanning laser ophthalmoscope, and Stratus OCT optical coherence tomograph for the detection of glaucoma. *Arch Ophthalmol* 2004;122:827-37.
7. Lee PP. The value of guidelines and consensus and the reality of clinical practice. In: Weinreb RN, Greve EL, eds. *Glaucoma diagnosis. Structure and function*. The Hague, The Netherlands: Kugler Publications, 2004.
8. Ford BA, Artes PH, McCormick TA, et al. Comparison of data analysis tools for detection of glaucoma with the Heidelberg Retina Tomograph. *Ophthalmology* 2003;110:1145-50.
9. Colen TP, Lemij HG. Sensitivity and specificity of the GDx: clinical judgment of standard printouts versus the number. *J Glaucoma* 2003;12:129-33.
10. Nicoleta MT, Martinez-Bello C, Morrison CA, et al. Scanning laser polarimetry in a selected group of patients with glaucoma and normal controls. *Am J Ophthalmol* 2001;132:845-54.
11. Bathija R, Gupta N, Zangwill L, Weinreb RN. Changing definition of glaucoma. *J Glaucoma* 1998;7:165-9.
12. Reus NJ, Lemij HG. The relationship between standard automated perimetry and GDx VCC measurements. *Invest Ophthalmol Vis Sci* 2004;45:840-5.
13. Schlottmann PG, De Cilla S, Greenfield DS, et al. Relationship between visual field sensitivity and

- retinal nerve fiber layer thickness as measured by scanning laser polarimetry. *Invest Ophthalmol Vis Sci* 2004;45:1823-9.
14. Garway-Heath DF, Viswanathan A, Westcott M, et al. Relationship between perimetric light sensitivity and optic disc neuroretinal rim area. In: Wall M, Wild JM, eds. *Perimetry Update 1998/1999*. The Hague, The Netherlands: Kugler Publications, 1999.
  15. Garway-Heath DF, Holder GE, Fitzke FW, Hitchings RA. Relationship between electrophysiological, psychophysical, and anatomical measurements in glaucoma. *Invest Ophthalmol Vis Sci* 2002;43:2213-20.
  16. Rohrschneider K, Burk RO, Kruse FE, Volcker HE. Reproducibility of the optic nerve head topography with a new laser tomographic scanning device. *Ophthalmology* 1994;101:1044-9.
  17. Miglior S, Albe E, Guareschi M, et al. Intraobserver and interobserver reproducibility in the evaluation of optic disc stereometric parameters by Heidelberg Retina Tomograph. *Ophthalmology* 2002;109:1072-7.
  18. Frenkel S, Slonim E, Horani A, et al. Operator learning effect and interoperator reproducibility of the scanning laser polarimeter with variable corneal compensation. *Ophthalmology* 2005;112:257-61.
  19. Funk J, Mueller H. Comparison of long-term fluctuations: laser scanning tomography versus automated perimetry. *Graefes Arch Clin Exp Ophthalmol* 2003;241:721-4.
  20. Chen PP, Park RJ. Visual field progression in patients with initially unilateral visual field loss from chronic open-angle glaucoma. *Ophthalmology* 2000;107:1688-92.
  21. Susanna R, Drance SM, Douglas GR. The visual prognosis of the fellow eye in unocular chronic open-angle glaucoma. *Br J Ophthalmol* 1978;62:327-9.
  22. Fontana L, Armas R, Garway-Heath DF, et al. Clinical factors influencing the visual prognosis of the fellow eyes of normal tension glaucoma patients with unilateral field loss. *Br J Ophthalmol* 1999;83:1002-5.
  23. Zeyen TG, Caprioli J. Progression of disc and field damage in early glaucoma. *Arch Ophthalmol* 1993;111:62-5.
  24. Henderson PA, Medeiros FA, Zangwill LM, Weinreb RN. Relationship between central corneal thickness and retinal nerve fiber layer thickness in ocular hypertensive patients. *Ophthalmology* 2005;112:251-6.
  25. Johnson CA, Adams AJ, Casson EJ, Brandt JD. Blue-on-yellow perimetry can predict the development of glaucomatous visual field loss. *Arch Ophthalmol* 1993;111:645-50.
  26. Sample PA, Taylor JD, Martinez GA, et al. Short-wavelength color visual fields in glaucoma suspects at risk. *Am J Ophthalmol* 1993;115:225-33.
  27. Polo V, Larrosa JM, Pinilla I, et al. Predictive value of short-wavelength automated perimetry: a 3-year follow-up study. *Ophthalmology* 2002;109:761-5.
  28. Sample PA, Bosworth CF, Blumenthal EZ, et al. Visual function-specific perimetry for indirect comparison of different ganglion cell populations in glaucoma. *Invest Ophthalmol Vis Sci* 2000;41:1783-

90.

29. Kamal DS, Viswanathan AC, Garway-Heath DF, et al. Detection of optic disc change with the Heidelberg retina tomograph before confirmed visual field change in ocular hypertensives converting to early glaucoma. *Br J Ophthalmol* 1999;83:290-4.
30. Chauhan BC, McCormick TA, Nicoleta MT, LeBlanc RP. Optic disc and visual field changes in a prospective longitudinal study of patients with glaucoma: comparison of scanning laser tomography with conventional perimetry and optic disc photography. *Arch Ophthalmol* 2001;119:1492-9.
31. Tan JC, Hitchings RA. Approach for identifying glaucomatous optic nerve progression by scanning laser tomography. *Invest Ophthalmol Vis Sci* 2003;44:2621-6.
32. Tan JC, Hitchings RA. Optimizing and validating an approach for identifying glaucomatous change in optic nerve topography. *Invest Ophthalmol Vis Sci* 2004;45:1396-403.
33. Mohammadi K, Bowd C, Weinreb RN, et al. Retinal nerve fiber layer thickness measurements with scanning laser polarimetry predict glaucomatous visual field loss. *Am J Ophthalmol* 2004;138:592-601.
34. Johnson CA, Sample PA, Cioffi GA, et al. Structure and function evaluation (SAFE): I. criteria for glaucomatous visual field loss using standard automated perimetry (SAP) and short wavelength automated perimetry (SWAP). *Am J Ophthalmol* 2002;134:177-85.
35. Wollstein G, Paunescu LA, Ko TH, et al. Ultrahigh-resolution optical coherence tomography in glaucoma. *Ophthalmology* 2005;112:229-37.







# 8

## Summary & Samenvatting



## 8.1 Summary

---

**G**laucoma is a heterogeneous group of optic nerve diseases sharing an accelerated degeneration of retinal ganglion cells (RGCs) that, if untreated, leads to progressive and irreversible loss of visual function. Worldwide, glaucoma is the second leading cause of blindness. Of the many types of glaucoma, primary open-angle glaucoma (POAG) is probably the most common one in Western countries. Probably less than half of all people who have the disease are aware of it.

Traditionally, the diagnosis of POAG is based on characteristic appearances of the optic nerve head (ONH), retinal nerve fiber layer (RNFL), and visual field (by standard automated perimetry [SAP]). There is, however, no consistent and generally approved acceptance of the diagnostic criteria. In addition, the diagnostic techniques that are being used routinely in clinical practice are subjective, have a poor reproducibility of measurements, and may not detect glaucoma at an early stage. Therefore, various techniques have been developed to better detect glaucomatous optic neuropathy.

The aim of the research presented in this thesis was to evaluate some of these techniques in their ability to assess structure and function in glaucoma. To this end, we evaluated scanning laser polarimetry (SLP), confocal scanning laser ophthalmoscopy (CSLO), and short-wavelength automated perimetry (SWAP).

SLP allows evaluation of the RNFL by assessing the amount of retardation exhibited by this birefringent structure, which is proportional to its thickness. Two structures in the anterior segment, i.e., the cornea and, to a lesser extent, the lens, are also birefringent. A previously commercially available instrument featuring SLP, the GDx NFA, was equipped with a so-called fixed corneal compensator (FCC) to cancel a fixed amount of retardation. When corneal birefringence was shown to vary significantly between individuals, so-called variable corneal compensation (VCC), available in the GDx VCC, was introduced to allow an individualized compensation of anterior segment retardation.

CSLO, available in the Heidelberg Retina Tomograph (HRT), assesses the topography of the ONH by measuring, at various points in the ONH, the intensity of light that is reflected off the retinal surface at subsequent depths of focus. The depth of peak reflectance represents the interface between the retinal surface and the vitreous.

SWAP is a perimetric test that assesses the function of a RGC subset, i.e., the small bistratified cells. By assessing only a proportion of the RGCs, loss of just a few cells might be detected by SWAP allowing earlier detection of glaucoma than with SAP.

In **chapter 2**, we evaluated recent developments in SLP. More specifically, in **chapter 2.1**, we compared the assessment of RNFL morphology with SLP-VCC and SLP-FCC to that with red-free fundus photography, a standard for evaluating the RNFL. We showed that measurements with VCC compared very well with red-free fundus photography and reflected RNFL morphology better than with FCC.

We investigated in **chapter 2.2** the extent to which various amounts of incomplete compensation of anterior segment birefringence could distort RNFL measurements by SLP. We showed that even relatively small amounts of residual anterior segment birefringence, which may occur by slight head tilt of a measured subject during routine use of SLP, can have a clinically significant effect on the appearance of the RNFL by SLP-VCC. Clinicians as well as GDx VCC operators should therefore be aware of such artifacts as they may mask or mimic glaucomatous progression.

In **chapter 2.3**, we described and evaluated a new method, called enhanced variable corneal compensation (ECC). Measurements with ECC appeared to represent the expected RNFL morphology often better than or otherwise as well as those made with VCC. This may have been largely due to a better compensation of anterior segment birefringence with ECC over VCC. In addition, atypical patterns of retardation, especially apparent in SLP-VCC images of eyes with lightly pigmented fundi, in myopes, and in eyes of elderly subjects, were less frequent with ECC. We suspected that ECC may enhance the clinical utility of SLP in glaucoma management.

In **chapter 3**, we determined the accuracy of various techniques for detecting glaucoma. In **chapter 3.1**, we assessed the diagnostic accuracy of the GDx VCC for various severities of glaucoma. We showed that the NFI, a support-vector machine derived parameter, had a high accuracy for diagnosing glaucoma. Overall, its sensitivity and specificity were 89% and 96%, respectively. Furthermore, in **chapter 3.2** we compared the diagnostic accuracy of clinical assessment of stereoscopic ONH photographs by various ophthalmic care providers with that of CSLO (HRT I) and SLP-VCC (GDx VCC) in a single population. We showed that automated analysis of GDx VCC and, to a lesser extent, HRT measurements compared well to subjective analysis of stereoscopic ONH photographs by general ophthalmologists, junior residents, optometrists, and even some glaucoma specialists in classifying healthy and glaucomatous eyes. More experienced

graders classified ONHs more accurately than did graders with less experience. We concluded that imaging techniques such as the GDx VCC and HRT may assist clinicians in their glaucoma management.

In **chapter 4.1** and **4.2**, we evaluated the relationships between function by SAP and structure by SLP-VCC and CSLO, respectively. We showed that measurements of function correlated well with measurements of structure assessed with both imaging techniques. In addition, we found the relationship between function and structure to be curvilinear. We suspected that the shape of this relationship may be of clinical significance as large differences in structural measurements correlated with only small differences in function in areas with no to moderate glaucomatous loss. In more advanced glaucomatous loss, the opposite was true. We inferred that imaging techniques may be better used in mild to moderately severe stages and SAP in moderate to severe stages.

Subsequently, in **chapter 5**, we evaluated the RNFL with SLP-VCC in perimetrically unaffected fellow eyes of glaucoma patients with glaucomatous field loss by SAP in only one eye. These perimetrically unaffected eyes run an especially high risk of losing visual function. We showed that many of these eyes already had a thinner RNFL compared to healthy age-matched control eyes. Their RNFL was still thicker than in their fellow eyes with field loss. These data supported our findings in **chapter 4** that a mildly to moderately thin RNFL may not necessarily be associated with field loss by SAP. They further suggested that SLP-VCC may detect so-called pre-perimetric glaucoma.

In **chapter 6**, the prevalence of glaucomatous defects with SWAP in subjects with an elevated intraocular pressure was determined for various published definitions of glaucomatous loss. In addition, the agreement between these definitions was explored. We showed that the prevalence of glaucomatous defects with SWAP varied significantly in eyes with elevated IOP depending on the definitions of field loss. More importantly, various definitions identified different individuals to have an abnormal field with SWAP. Therefore, we concluded that the diagnostic accuracy and clinical significance of all definitions must be determined before SWAP is to be used in routine clinical care.

In summary, we evaluated various techniques that are being used in clinical practice for assessing structure and function in glaucoma. Imaging techniques such as the GDx VCC and HRT may provide objective and quantitative assessment, as well as documentation of the ONH and/or the RNFL. In addition, they have a high diagnostic accuracy for classifying healthy and glaucomatous eyes and may allow detection of glaucoma at an early stage. Standard automated perimetry may be of more use in later stages of the disease. With regard to SWAP, we think that more research is

required before it may be used routinely in clinical practice. Taken together (**chapter 7**), we think that the judicious use of imaging techniques such as the GDx VCC and the HRT may greatly benefit clinicians in their management of glaucoma.



## 8.2 Samenvatting

---

**G**laucoom is een heterogene groep van aandoeningen van de oogzenuw die gekenmerkt wordt door een versnelde degeneratie van retinale ganglion cellen (RGCs) die, onbehandeld, leidt tot een progressief en onomkeerbaar verlies van visuele functie. Wereldwijd is glaucoom de op één na belangrijkste oorzaak van blindheid. In Westerse landen is primair open kamerhoek glaucoom (primary open-angle glaucoma, POAG) waarschijnlijk één van de meest voorkomende typen glaucoom. Vermoedelijk is minder dan de helft van alle mensen die deze aandoening hebben zich hiervan bewust.

Van oudsher wordt de diagnose POAG gesteld op basis van een karakteristiek aspect van de papil, de retinale zenuwvezellaag (RZVL) en het gezichtsveld (zoals gemeten met standaard geautomatiseerde perimetrie [standard automated perimetry, SAP]). Er zijn echter geen consistente en algemeen aanvaarde diagnostische criteria. De technieken die in de klinische praktijk gebruikt worden voor de diagnostiek van glaucoom zijn bovendien subjectief, hebben een slechte meetreproduceerbaarheid en zijn hoogst waarschijnlijk niet in staat glaucoom in een vroeg stadium op te sporen. Daarom zijn er diverse technieken ontwikkeld om glaucoom beter op te kunnen sporen.

Het doel van de onderzoeken die beschreven zijn in dit proefschrift was om enkele van deze technieken te evalueren in hun vermogen om structuur en functie bij glaucoom patiënten te meten. Wij onderzochten scanning laser polarimetrie (SLP), confocale scanning laser ophthalmoscopie (CSLO), en *short-wavelength automated perimetry* (SWAP, in Nederland vaak blauw-geel perimetrie genoemd).

SLP maakt het mogelijk de RZVL te bestuderen door te meten hoeveel retardatie deze dubbelbrekende structuur veroorzaakt in gepolariseerd laserlicht; de hoeveelheid retardatie is proportioneel aan zijn dikte. Twee structuren in het voorsegment (de cornea en, in mindere mate, de lens) zijn ook dubbelbrekend. Een voorheen commercieel verkrijgbaar instrument met SLP, de GDx NFA, was uitgerust met een zogenaamde *fixed corneal compensator* (FCC) die een vaste

(fixed) hoeveelheid retardatie neutraliseerde. Toen ontdekt was dat corneale dubbelbreking sterk varieerde tussen individuen werd variabele cornea compensatie (VCC) geïntroduceerd waarmee een individuele compensatie van retardatie van het voorsegment mogelijk is. Deze techniek is commercieel verkrijgbaar in de GDx VCC.

CSLO, beschikbaar in de Heidelberg Retina Tomograph (HRT), bepaalt de topografie van de papil. Op diverse plaatsen binnen de papil meet deze techniek op opeenvolgende focusdiepten de intensiteit van teruggekaatst licht. Het niveau met de hoogste reflectie wordt beschouwd als de interface tussen het netvlies oppervlak en het glasvocht.

SWAP is een gezichtsveldonderzoek dat de functie van een subpopulatie van de RGCs bepaalt: de kleine dubbelgelaagde (*bistratified*) cellen. Omdat SWAP slechts de functie van een deel van de RGCs meet zou het verlies van slechts enkele cellen al gedetecteerd kunnen worden. Zodoende kan glaucoom mogelijk eerder opgespoord worden met SWAP dan met SAP.

In **hoofdstuk 2** onderzochten we recente ontwikkelingen in SLP. Zo vergeleken wij in **hoofdstuk 2.1** het beoordelen van RZVL morfologie met behulp van SLP-VCC en SLP-FCC met die bepaald met roodvrije fundus fotografie, een standaard voor het evalueren van de RZVL. Wij toonden aan dat metingen met VCC zeer goed vergelijkbaar waren met roodvrije fundus fotografie. Metingen met VCC toonden de RZVL morfologie zelfs beter dan met FCC.

In **hoofdstuk 2.2** onderzochten wij de mate waarin RZVL metingen met SLP verstoord konden worden door incomplete compensatie van dubbelbreking van het voorsegment. Wij toonden aan dat zelfs relatief kleine hoeveelheden niet-gecompenseerde dubbelbreking van het voorsegment, wat voor kan komen bij normaal klinisch gebruik van SLP doordat het hoofd een klein beetje schuin gehouden wordt, een klinisch significant effect kunnen hebben op het aspect van de RZVL gemeten met SLP-VCC. Clinici en GDx VCC operators dienen gespist te zijn op zulke artefacten aangezien ze progressie van glaucoom zowel kunnen verhullen als kunnen nabootsen. Wij beschreven en onderzochten in **hoofdstuk 2.3** een nieuwe methode genaamd *enhanced variable corneal compensation* (ECC). Metingen met ECC leken de verwachte RZVL morfologie vaak beter dan of anders zo goed als metingen met VCC te bepalen. Mogelijk is dit grotendeels te danken aan een betere compensatie van voorsegment dubbelbreking met ECC dan met mogelijk was met VCC. Atypische retardatie patronen, m.n. zichtbaar in SLP-VCC foto's van ogen met licht gepigmenteerde fundi, myope ogen en ogen van oudere mensen, kwamen bovendien minder vaak voor met ECC. Wij vermoedden dat ECC de klinische bruikbaarheid van SLP in glaucoomzorg kan vergroten.

In **hoofdstuk 3** bepaalden we de nauwkeurigheid van verscheidene technieken om glaucoom op te sporen. In **hoofdstuk 3.1** bepaalden we de diagnostische nauwkeurigheid van de GDx VCC voor diverse stadia van glaucoom. Wij toonden aan dat de NFI, een parameter getraind met

behelp van een *support-vector machine*, een hoge nauwkeurigheid had voor het diagnosticeren van glaucoom. Globaal waren de sensitiviteit en specificiteit respectievelijk 89% en 96%. In **hoofdstuk 3.2** vergeleken wij de diagnostische nauwkeurigheid van de klinische beoordeling van papil stereofoto's door diverse zorg professionals met de nauwkeurigheid van CSLO (HRT I) en SLP-VCC (GDx VCC) in dezelfde populatie. Wij toonden aan dat geautomatiseerde analyse van GDx VCC metingen en, in mindere mate, van HRT metingen goed overeen kwamen met classificatie tussen gezonden en glaucomateuze ogen op basis van subjectieve analyse van papil stereofoto's door algemene oogartsen, junior assistenten in opleiding tot oogarts, optometristen en zelfs enkele glaucoomspecialisten. Meer ervaren beoordelaars classificeerden papillen nauwkeuriger dan beoordelaars met minder ervaring. Wij concludeerden dat beeldvormende technieken zoals de GDx VCC en de HRT klinici kunnen ondersteunen in glaucoomzorg.

In **hoofdstuk 4.1** en **4.2** evalueerden we de relatie tussen functie gemeten met SAP en structuur gemeten met respectievelijk SLP-VCC en CSLO. Wij toonden aan dat metingen van functie goed overeen kwamen met metingen van structuur (zowel met SLP-VCC als met CSLO). Bovendien vonden we dat de relatie tussen functie en structuur curvilineair was. Wij meenden dat de vorm van deze relatie klinisch van belang kan zijn aangezien grote veranderingen in structuur gecorreleerd waren met slechts kleine verschillen in functie in gebieden met geen tot matig ernstig functioneel glaucomateus verlies. In meer gevorderd glaucoom was het omgekeerde waar. Wij concludeerden dat beeldvormende technieken mogelijk beter gebruikt kunnen worden in stadia van milde en matig ernstige glaucomateuze schade en SAP in matig ernstige tot ernstige stadia.

Vervolgens evalueerden wij in **hoofdstuk 5** de RZVL in het bij gezichtsveldonderzoek niet-aangedane andere oog van glaucompatiënten met glaucomateus gezichtsveldverlies (met SAP) in slechts één oog. Deze perimetrisch onaangetaste ogen lopen een hoog risico om hun visuele functie te verliezen. Wij toonden aan dat veel van deze ogen een dunnere RZVL hadden dan gezonde controle ogen van vergelijkbare leeftijd. De RZVL was dikker in het niet-aangedane oog dan die in hun andere oog met gezichtsvelduitval. Deze data bevestigden onze bevindingen in **hoofdstuk 4** dat een milde tot matig dunne RZVL niet noodzakelijk geassocieerd is met een gezichtsveldverlies bepaald met SAP. Tevens suggereerden deze data dat SLP-VCC in staat zou kunnen zijn zogenaamd pre-perimetrisch glaucoom op te kunnen sporen.

In **hoofdstuk 6** bepaalden wij bij mensen met een verhoogde oogdruk de prevalentie van glaucomateuze defecten met SWAP voor verscheidene gepubliceerde definities van glaucomateus gezichtsveldverlies. Bovendien onderzochten wij de overeenkomst tussen deze definities. Wij toonden aan dat de prevalentie van glaucomateuze defecten met SWAP sterk wisselde in ogen

met een verhoogde oogdruk afhankelijk van de definitie van gezichtsveldverlies. Bovendien wezen verschillende definities verschillende individuen aan een abnormaal gezichtsveld te hebben met SWAP. Daarom concludeerden wij dat de diagnostische nauwkeurigheid en klinische betekenis van alle definities bepaald dienen te worden voordat SWAP gebruikt kan worden in routine klinische zorg.

Samenvattend evalueerden wij diverse technieken die in de klinische praktijk worden gebruikt voor de beoordeling van structuur en functie in glaucoom. Beeldvormende technieken zoals de GDx VCC en de HRT kunnen een objectieve en kwantitatieve beoordeling en documentatie van de papil en/of zenuwvezellaag geven. Bovendien hebben zij een hoge diagnostische nauwkeurigheid voor het classificeren van gezonde en glaucomateuze ogen en kan met behulp van deze technieken glaucoom waarschijnlijk in een vroeg stadium worden opgespoord. Standaard geautomatiseerde perimetrie kan meer nut hebben in latere stadia van de aandoening. Met betrekking tot SWAP denken wij dat meer onderzoek nodig is voordat het routinematig gebruikt zou kunnen worden in de kliniek.

Al met al (**hoofdstuk 7**) denken wij dat een deskundig gebruik van beeldvormende technieken zoals de GDx VCC en de HRT zeer ten goede kan komen aan klinici in door hen geleverde glaucoomzorg.





# Dankwoord

---

**P**romoveren betekent in de praktijk een lange weg op eigen kracht afleggen. Tijdens het afleggen van dit pad hebben echter vele mensen mij gesteund, die ik daarvoor dank. Enkele mensen wil ik in het bijzonder danken.

Graag dank ik professor Van Rij voor zijn inzet als promotor. Uw hulp verlichtte de laatste moeilijke stappen van het traject.

Bijzondere dank gaat uit naar Hans Lemij, mijn co-promotor. Jouw creativiteit, veelzijdigheid, enthousiasme, kennis, humor en kritische blik hebben mij de afgelopen jaren geïnspireerd. Onder jouw bezielende leiding heb ik geleerd mijn eigen onderzoekspad te kiezen. Met genoegen denk ik terug aan de rebuttals die we samen hebben geschreven als een reviewer het weer eens niet begrepen had.

De leden van de kleine promotiecommissie, professor Avezaat, professor De Zeeuw en professor Sterk, wil ik danken voor hun kritische bestudering van mijn proefschrift. It truly is an honor for me to have Mr. Garway-Heath on the plenary committee for my PhD defence. Ted, I would like to thank you for having shared your knowledge, including how to operate the HRT.

Ik dank mijn directe voorganger, Thomas Colen. In mijn onderzoek heb ik veel kunnen putten uit de lange termijn studie die jij hebt opgezet. Tevens gaat mijn dank uit naar Koen Vermeer. Jouw Delftse blik over onderzoek vond ik heel verfrissend in de medische wereld. Ik dank je dat je tevens mijn paranimf wilt zijn. Leonieke van Koolwijk, jij kwam toen ik bijna ging. Ik ben blij dat er iemand met jouw enthousiasme en inzicht het onderzoek heeft overgenomen.

Het enthousiasme van de medewerkers van de afdeling Perimetrie, in het bijzonder Marjo van der Horst, Joyce Hitalessy, Mieke Triesscheijn, Melania Simileer en Sophie Jaakke is uitzonderlijk. Dames, hartelijk dank voor jullie inzet. Ook dank ik alle medewerkers van de afdeling Fotografie

voor hun hulp. Daarnaast dank ik de medewerkers van de afdeling ERG voor hun goede zorgen tijdens de afronding van mijn onderzoek.

I would like to thank Dr. Zhou for her excellent support of my research. Dear Quenyuan, I enjoyed eating King Crabs with you. In addition, I am grateful to Dr. Choplin. Neil, it was a delight working with you on the imaging courses at the American Academy of Ophthalmology.

Paul Mulder, bedankt voor de tijd die jij hebt genomen om mij wegwijs te maken in de statistiek. Ik begrijp nu dat er geen absolute waarheid is.

Irene Notting, Lizzy Adeler, Merel Boas, Gijs Tangelder en Maartje de Graaf die ik mede heb begeleid tijdens hun keuzeonderzoek op de afdeling Perimetrie dank ik voor de plezierige samenwerking.

De directie, medische staf en arts-assistenten van Het Oogziekenhuis hebben zich tijdens mijn hele promotieonderzoek geïnteresseerd getoond in mijn resultaten. Mijn dank hiervoor.

Speciale dank gaat uit naar alle mensen die vrijwillig mee hebben gedaan aan het onderzoek op de afdeling Perimetrie. Zonder hen was het onderzoek niet mogelijk geweest.

Ramon van de Ven, dank je wel voor je vriendschap. Het is een eer dat jij mijn paranimf wilt zijn.

Ik dank mijn ouders, Nico en Virginie Reus-van den Bergh, en mijn zussen, Meynouw en Bregtje, voor hun nooit aflatende interesse in mijn promotieonderzoek. Pap en mam, jullie onvoorwaardelijke steun en begrip heb ik enorm gewaardeerd.

Tot slot is een promotie niet alleen een wetenschappelijke maar ook een persoonlijke ontwikkeling. In beide ben ik met veel liefde gestimuleerd door mijn vrouw Ellen. Lieve Ellen, ik dank je voor jouw steun en de ruimte die je mij gaf om dit project succesvol af te ronden.

Nic Reus







# Curriculum Vitae

---

**N**icolaas Johannes Reus werd geboren op 30 september 1975 te Uithoorn. Hij behaalde zijn VWO examen in 1993 aan het Geert Groote College te Deventer (thans: Etty Hillesum Lyceum). In hetzelfde jaar startte hij zijn studie Geneeskunde aan de Erasmus Universiteit Rotterdam (EUR). Tijdens zijn studie werkte hij als student-assistent op de afdeling Anatomie van de EUR (Prof.dr. J. Voogd, afdelingshoofd; thans: Department of Neuroscience, prof.dr. C.I. de Zeeuw, afdelingshoofd). Op deze afdeling werkte hij tevens mee aan verscheidene onderzoeksprojecten onder supervisie van dr. T.J.H. Ruigrok. Daarnaast was hij werkzaam in het studententeam van de afdeling Algemene Heelkunde, Academisch Ziekenhuis Dijkzigt te Rotterdam (thans: Erasmus MC). In 1997 deed hij onderzoek op de afdeling Physiology and Neuroscience van New York University Medical Center, Verenigde Staten van Amerika bij dr. J.I. Simpson (prof.dr. R. Llinás, afdelingshoofd).

Nadat hij in 2000 zijn artsexamen behaalde startte hij in Het Oogziekenhuis Rotterdam onder leiding van dr. H.G. Lemij het onderzoek dat beschreven is in dit proefschrift. Van juli 2004 tot en met december 2004 werkte hij als assistent-geneeskundige niet-in-opleiding (AGNIO) in Het Oogziekenhuis Rotterdam. Sinds december 2004 is hij in opleiding tot oogarts in dit instituut (prof.dr. J.C. van Meurs, opleider).



